

**SYNTHESIS AND CHARACTERIZATION OF UNDOPED
AND IRON DOPED ZINC SULFIDE THIN FILMS BY
CHEMICAL BATH DEPOSITION TECHNIQUE**

by

Kazi Zahanara Islam

Student ID: 0417142514F

Session: April 2017

MASTER OF SCIENCE



Department of Physics

BANGLADESH UNIVERSITY OF ENGINEERING AND TECHNOLOGY

DHAKA-1000, BANGLADESH

July, 2019

SYNTHESIS AND CHARACTERIZATION OF UNDOPED AND IRON DOPED ZINC SULFIDE THIN FILMS BY CHEMICAL BATH DEPOSITION TECHNIQUE

Kazi Zahanara Islam

*A Dissertation Submitted to the Department of Physics, Bangladesh University of
Engineering and Technology in Partial Fulfilment of the Requirement for the Degree of
Master of Science in Physics*



Department of Physics

BANGLADESH UNIVERSITY OF ENGINEERING AND TECHNOLOGY

DHAKA-1000, BANGLADESH

July, 2019

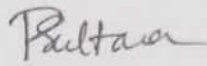
DEPARTMENT OF PHYSICS




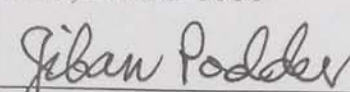
CERTIFICATION OF THESIS


The thesis titled “SYNTHESIS AND CHARACTERIZATION OF UNDOPED AND IRON DOPED ZINC SULFIDE THIN FILMS BY CHEMICAL BATH DEPOSITION TECHNIQUE” submitted by **Kazi Zahanara Islam**, Roll No.:0417142514F, Session: April/2017, has been accepted as satisfactory in partial fulfillment of the requirement for the degree of **Masters of Science (M. Sc.)** in Physics on 10 July, 2019.

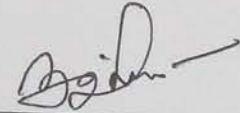
BOARD OF EXAMINERS

1. 

Dr. Parvin Sultana
Assistant Professor, Department of Physics
BUET, Dhaka-1000
Chairman
(Supervisor)
2. 

Dr. Md. Forhad Mina
Professor & Head, Department of Physics
BUET, Dhaka-1000
Member
(Ex-Officio)
3. 

Dr. Jiban Podder
Professor, Department of Physics
BUET, Dhaka-1000
Member
4. 

Dr. Mohammad Jellur Rahman
Associate Professor, Department of Physics
BUET, Dhaka-1000
Member
5. 

Dr. A. B. M. Obaidul Islam
Professor, Department of Physics
University of Dhaka, Dhaka-1000
Member
(External)

CANDIDATE'S DECLARATION

It is declared that this thesis or any part of it has not been submitted elsewhere for the award of any degree or diploma.

Kazi Zahanara Islam

To
My Mother Kazi Selena Islam
My Brother Kazi Tojammel Hosen
Who sacrificed a lot for me.

ACKNOWLEDGEMENT

All praise for Allah who has created us and given a greatest status among his all creations. I express very much gratefulness to the Almighty Allah, who gives me the strength, courage, patience and ability to fulfill this research work. I have been extremely fortunate in my life to be surrounded by so many loving and inspiring people whose friendship, companionship and support has been a gift to my life. They have each shaped me personally and professionally in unique ways, I am forever grateful for their presence in my side. Expressing my gratitude for their roles in my life in these few pages is the smallest thing I could do to treasure them.

Firstly, I would like to express my sincere appreciation to my supervisor Dr. Parvin Sultana for her wonderful guidance and tremendous support during my M. Sc. study and research. I especially wish to thank her for the generosity she showed with her time. It seemed I could knock on her door any time I needed to discuss anything, and she was always willing to talk. She is a wonderful advisor who helped me go through all the difficulties that I encountered in my study, research, and even life. She is a materials scientist. It is my great honor to be her student. What I learned from her will benefit my whole life.

I am thankful to Prof. Dr. Md. Forhad Mina, Head, Department of Physics, BUET for his instructive discussions, helpful suggestions, best wishes and cordial supports to carry out this work.

I wish to express my gratefulness to Prof. Dr. Md. Abu Hashan Bhuiyan for his constructive criticism, stimulating encouragement and various help. His advice and suggestions helped shape this work in many ways. I also would like to thank all the teachers of the Dept of Physics, BUET: Prof. Dr. Md. Feroz Alam Khan, Prof. Dr. A.K.M. Akther Hossain, Prof. Dr. Md. Mostak Hossain, Mrs. Fahima Khanam, Prof. Dr. Jibbon Poddar, Prof. Dr. Md. Rafi Uddin, Prof. Dr. Mohammad Abdul Basith, Dr. Afia Begum, Dr. Mohammad Jellur Rahman, Dr. Md. Rakibul Islam, Dr. Mohammad Abu Sayem Karal, Dr. Muhammed Samir Ullah, Mr. Md. Mehdi Masud , Mrs. Mehnaz Sharmin and all other teachers of department of Physics, BUET for their inspiration and constructive suggestions. I would also like to convey my thanks to the staffs of the department of Physics, BUET for their co-operation.

I would like to give special thanks to my friends Md. Golam Azam, Borhanul Asfia, Mrinmoi Mondol, Md. Mehdi Hasan Sohag and all the members of Material Science 2 Research Laboratory for their heartfelt cooperation and kind help throughout the study.

Finally, my parents, Kazi Selena Islam & Kazi Mezanul Islam and my brother Kazi Tojammel Hosen: it is indeed difficult for me to write words that sufficient to express my love for you. I will always remain indebted to you for your unconditional love and support. I would also like to acknowledge my family members, my sincerest gratitude for all they have done. I could not wish for a more supportive, loving family, and for them I am deeply thankful and blessed. I express my heartfelt gratitude to my parents and other family members for their constant support, encouragement, sacrifices and love during this research work.

I acknowledge with thanks to the Bangladesh University of Engineering and Technology for providing financial support to this thesis work.

The Author

Kazi Zahanara Islam

CONTENTS

Page No.

CANDIDATE'S DECLARATION	i
DEDICATION	ii
ACKNOWLEDGEMENTS	iv
ABSTRACT	xiii
LIST OF FIGURES	viii
LIST OF TABLES	xii

CHAPTER 1

GENERAL INTRODUCTION

1.1	Introduction	2
1.2	Review of earlier research works	3
1.3	The reason behind working with ZnS:Fe	7
1.4	Aim of the present work	7
1.5	Outline of the thesis	8
	References	9

CHAPTER 2

MATERIALS AND THIN FILMS DEPOSITION TECHNIQUES

2.1	Zinc sulfide	12
2.2	Properties of zinc sulfide	12
2.3	Phases of zinc sulfide	13
2.4	Properties of iron	13
2.5	Applications of zinc sulfide	14
2.6	Thin film deposition techniques	15
2.6.1	Physical deposition techniques	15
2.6.1.1	Thermal or vacuum evaporation method	16
2.6.1.2	Pulsed laser deposition	17
2.6.1.3	Sputtering deposition	18
2.6.2	Chemical deposition techniques	19

2.6.2.1	Chemical vapor deposition	19
2.6.2.2	Spin coating	20
2.6.2.3	Spray pyrolysis method	21
2.6.2.4	Chemical bath deposition	22
2.6.2.5	Sol-gel technique	23
2.7	Thin film formation stages	24
2.7.1	Volmer-weber condensation	25
2.8	Nucleation	26
2.8.1	Homogeneous nucleation	26
2.8.2	Heterogeneous nucleation	28
2.9	Thin film growth	29
2.9.1	Island stage	30
2.9.2	Coalescence stage	31
2.9.3	Channel stage	31
2.9.4	Continuous film stage	32
2.10	Influence of various thin film deposition parameters	32
	References	34

CHAPTER 3

THIN FILM CHARACTERIZATION TECHNIQUES

3.1	Surface morphology	37
3.1.1	Scanning electron microscope	37
3.2	Elemental analysis	40
3.2.1	Energy dispersive X-ray spectroscopy	40
3.3	Structural characterization	41
3.3.1	X-ray diffraction	41
3.4	Optical characterization	44
3.4.1	Beer-Lambert law	44
3.4.2	Derivation of Beer-Lambert law	45

3.4.3	Electronic transition	46
3.5	Thickness measurement of thin film	52
3.6	Electrical characterization	54
3.6.1	Direct method	55
3.6.2	Two Point Probe method	55
3.6.3	Four point probe method	56
3.6.4	Ven der pauw method	57
3.7	Vibrating sample magnetometer	59
3.7.1	Hysteresis loop	61
	References	63

CHAPTER 4

EXPERIMENTAL DETAILS

4.1	Introduction	65
4.2	Chemical bath deposition (CBD)	65
4.3	Experimental set-up	65
4.4	Experimental flow chart	68
4.5	Sample preparation	69
4.5.1	Substrate cleaning	69
4.5.2	Chemicals used for thin film deposition	70
4.5.3	Thin film deposition	71
4.7	Principle of CBD technique	72
4.8	Reaction mechanism	72
	References	75

CHAPTER 5

RESULTS AND DISSCUSSION

5.1	Surface morphology	77
-----	--------------------	----

5.2	Elemental analysis	80
5.3	Structural analysis	82
5.4	Optical analysis	84
5.4.1	Transmittance	84
5.4.2	Absorbance	85
5.4.3	Absorption coefficient	86
5.4.4	Optical band gap	86
5.4.5	Refractive index	88
5.4.6	Extinction coefficient	89
5.5	Thickness measurement	89
5.6	Electrical property	90
5.6.1	I-V characteristics	90
5.6.2	Resistivity and conductivity	91
5.7	Magnetic property	93
	References	95

CHAPTER 6

SUMMARY AND CONCLUSION

6.1	Summary	98
6.2	Conclusion	98
6.3	Scopes for further works	99

List of Figures

Figure No.	Figure Caption	Page No.
1.1	XRD patterns of ZnS annealed thin films prepared (a) improved method (b) original method; as-deposited films prepared by (c) improved method;(d) original method	4
1.2	SEM images of ZnS thin films. (a) not annealing; (b) 200°C 1 h; (c) 300°C 1 h	4
1.3	XRD pattern of sprayed ZnS films grown at temperature 400, 490 and 530 °C	5
1.4	(a) XRD pattern (b) M-H curves of undoped and Fe-doped nanoparticles	6
1.5	M-H curve of undoped and Fe doped ZnS thin films	7
2.1	Schematic diagram of thermal evaporation system	16
2.2	Schematic diagram of pulsed laser deposition system	17
2.3	Schematic diagram of sputter deposition system	18
2.4	Schematic diagram of chemical vapor deposition system	20
2.5	Schematic diagram of spin coating deposition system	20
2.6	Schematic diagram of spray pyrolysis deposition system	21
2.7	Schematic diagram of chemical bath deposition system	22
2.8	Schematic diagram of sol-gel deposition technique	23
2.9	Schematic diagram of thin film formation process	24
2.10	Three different modes of film growth	25
2.11	Free energy diagram for nucleation explaining the existence of a critical nucleus	27
2.12	Contact angle and interfacial tension	29
2.13	Different stages of film growth	30
2.14	The mechanism of formation of island stage during thin film growth	30
2.15	Electron micrograph shows the change in shape of islands during and after coalescence(a) at zero(b) after 1 to 2 sec. (c) after 60 sec.	31
2.16	Schematic diagram of channel stage	32

2.17	Schematic diagram of a continuous film stage	32
3.1	Schematic diagram of an electron microscope	38
3.2	Schematic diagram of a scanning electron microscope	39
3.3	Principle of EDX analysis	41
3.4	Bragg's law of X-ray diffraction	42
3.5	Absorption of light by a sample	46
3.6	Vibrational and rotational energy	47
3.7	Possible electronic transition	48
3.8	Schematic presentation of direct and indirect transition between valance and conduction band	49
3.9	Refraction of light at the interface between two media of different refractive indices	50
3.10	Interferometer arrangement for producing reflection Fizeau fringes of equal thickness	53
3.11	Substrate holder of interferometer	54
3.12	Four-point probe resistivity test circuit	56
3.13	Ven der pawn method	58
3.14	(a) Arbitrary point consideration (b) considering symmetry line	59
3.15	Schematic diagram vibrating sample magnetometer characterization arrangement	60
3.16	Schematic diagram of a hysteresis loop	61
4.1	Schematic diagram of chemical bath deposition system	66
4.2	Locally fabricated chemical bath deposition unit at the Dept. of Physics, BUET	67
4.3	(a) Close view of a heat chamber, (b) Lid of the reaction vessel	68
4.4	Soaked glass substrates into acid solution	69
4.5	(a) Ultrasonic cleaner and (b) its inner view	70
4.6	Pure and Fe doped ZnS thin film deposition by CBD technique	71
4.7	Various method of thin film deposition on CBD technique	73
5.1	FESEM images of (a) Pure ZnS, (b) 5, (c) 7, (d) 9, and (e) 10 at. % Fe doped ZnS thin films (annealed at 550°C) at 50k magnification	78

5.2	Histograms of (a) Pure ZnS and ZnS:Fe thin films doped with (b) 5 wt.%, (c) 7 wt.%, (d) 9 wt.% and (e) 10 wt.% Fe annealed at 550 °C (50K magnification)	79
5.3	EDX spectra of (a) Pure ZnS, (b) 5, (c) 7, (d) 9, and (e) 10 at. % Fe doped ZnS thin films annealed at 550°C	81
5.4	X-ray diffraction patterns of Pure ZnS and Fe doped ZnS thin films annealed at 550°C (a) Pure ZnS, (b) 5, (c) 7, and (d) 9 at. % Fe doped ZnS thin films	82
5.5	Variation of transmittance with wavelength for pure ZnS and ZnS:Fe thin films	84
5.6	Variation of absorbance with wavelength for pure ZnS and ZnS:Fe thin films	85
5.7	Variation of absorption coefficient with wavelength for pure ZnS and ZnS:Fe thin films	86
5.8	Variation of bandgap energy with wavelength for pure ZnS and ZnS:Fe thin films	87
5.9	Variation of reflective index with wavelength for pure ZnS and ZnS:Fe thin films	88
5.10	Variation of extinction coefficient with wavelength for pure ZnS and ZnS:Fe thin films	89
5.11	Variation of thickness with different Fe doping percentage	90
5.12	I-V characteristic curve of pure and Fe doped ZnS thin films	91
5.13	Variation of resistivity with Fe Doping at. %	92
5.14	Variation of conductivity with Fe Doping at. %	92
5.17	M-H Curve for Different Fe Doping Percentages	93

List of the Tables

Table No.	Table Caption	Page No.
2.1	Application areas of ZnS Thin Films	14
4.1	Chemical used for the synthesis of ZnS and ZnS:Fe	70
5.1	Average Particle Size	80
5.2	Quantitative analysis of the elements of the films	82
5.3	Structural Parameters of Pure and Fe Doped ZnS Thin Films	83
5.4	Band gap energy and refractive index of ZnS and ZnS:Fe thin films	88
5.5	Thickness of ZnS and ZnS:Fe thin films	90
5.6	Electrical measurements of ZnS and ZnS:Fe	93

ABSTRACT

Pure and Iron (Fe) doped Zinc Sulfide thin films have been prepared by chemical bath deposition (CBD) method on a glass substrate at 85°C temperature using non-toxic complexing agents. The molar concentration of Fe was varied from 0 to 15 at. % to form Fe doped ZnS (ZnS:Fe) thin films. The influence of Fe doping concentration on the structural, optical, electrical and magnetic properties of ZnS thin films was studied. Field emission scanning electron microscopy (FESEM) was used to study the surface morphology of pure and Fe doped ZnS thin films. The FESEM images showed that the glass substrate nicely covered by uniform spherical grains. The surface morphology changed from spherical ZnS grains to more compact thin layer of film and grain size were increased with the increase of Fe concentration. Energy dispersive X-ray (EDX) confirmed the presence of zinc, sulfur and iron. Quantitative analysis showed that at. % of Fe increases with the increase of Fe concentration in ZnS:Fe thin films. X-ray diffraction patterns of ZnS and ZnS:Fe annealed (at 550°C) showed polycrystalline zinc blend type of crystal structure with preferential orientation along (111) plane. The average crystal size of the thin films is approximately 31 nm. Transmittance and absorbance of ZnS and ZnS:Fe thin films were studied through UV-visible spectroscopy and optical bandgap, refractive index and extinction coefficient were calculated. The transmittance of pure ZnS was 60 % in the visible wavelength region and doped films had higher optical transparency compared to pure ZnS films and increased up-to 90 % for the concentration of 9 at. % Fe. Thickness of the films varied from 160 nm to 230 nm. The direct optical bandgap varied from 3.50 to 3.77 eV. Electrical resistivity of pure and Fe doped ZnS thin films were measured at room temperature by four-point probe method. The electrical resistivity was decreased with increasing Fe concentration and minimum value of resistivity was 3.7×10^2 ohm-cm. Activation energy of ZnS and ZnS:Fe thin films were obtained between 0.27 to 0.31 eV. The magnetic properties of ZnS:Fe thin films was studied through Vibrating Sample Magnetometer (VSM). From the VSM analysis, 9 at. % ZnS:Fe thin film exhibited room temperature weak ferromagnetism.

***GENERAL
INTRODUCTION***

CHAPTER 1

GENERAL INTRODUCTION

1.1 Introduction

Today the whole world works through electricity. Even the world hardly depending on it. That is why, it's becomes more challenging for the scientific community to produce fluent supply of electrical energy. At present we use fossil fuels (i.e. coal, liquefied petroleum, oil, natural gas) and nuclear resources as a source of energy to produce electricity. These sources of energy are non-renewable and can be pollutant for the environment. Burning of fossil fuels releases a huge amount of CO₂ per year, resulting in environmental problems such as greenhouse effect and global warming. Burning of unrefined coal also results in acid rain, which is directly responsible for large area forest and wildlife devastation besides soil pollution. On the other hand, USA and most European countries has terminated nuclear power programs due to the lack of long-term waste disposal strategy and incidents at several nuclear power plants. That's why, it is very much important to find out alternative renewable power sources. Potential renewable power sources are biomass, geothermal energy, hydroelectricity, ocean, thermal energy, wind energy, the direct conversion of sunlight into electricity by the photovoltaic effect etc. The sun is a massive source of energy that can be converted into electrical energy using solar cells. Hence, the direct conversion of sunlight is the most promising and the best alternative option that facilitates blue response in the shorter wavelength region. A variety of materials especially semiconductor materials in the form of a pn junction can potentially be used for the photovoltaic energy conversion. II-VI semiconducting material appeal abundant consideration because of their wide direct optical bandgap and promising applications in optoelectronics. They can be used to prepare different layers of thin film solar cell (such as window layer, buffer layer, absorber layer etc.). Nanostructured semiconducting materials gather much consideration due to the unique properties that cannot be obtained from their bulk counterpart. Materials in the nano region can display innovative optical, electronic, magnetic, chemical, and structural properties due to the quantum size effect and surface effect. These properties might find many important technological applications. As the properties of nanostructured materials depending on their size and morphology, it is important to find new ways to control the size and morphology. The controlled synthesis of materials from few micrometers to several nanometer as a thin layer on various material is known as thin film. It plays an important part in the development and study of materials through new and exceptional properties. Since thin films can be deposited onto low cost substrates

at relatively low temperature and thin film-based technologies are potentially cheaper than silicon-based technologies, it is receiving much attention presently.

Metal chalcogenide II-VI semiconducting thin films are currently attracting considerable research interest for the fabrication of large area photodiode arrays, solar selective coatings, solar cells, light emitting diodes, antireflection coatings etc. Among various metal chalcogenides ZnS, CdS, ZnO, CdTe etc. are the primary candidates because of their favorable electronic and optical properties for optoelectronic applications [1,2,3]. ZnS is a commercially important II-VI semiconducting thin films having a wide and direct optical band gap. Due to its larger band gap and n-type conductivity, ZnS is a potential alternative to CdS as a buffer layer in thin film solar cells. CdS thin films are widely used as a buffer layer on thin film solar cells to obtain high conversion efficiency [4]. But CdS is toxic and causes environmental pollution. That is why researchers are searching for Cd free buffer material. One of the promising candidates is ZnS. ZnS has a wider energy bandgap than CdS, which results in transmission of more high energy photons from the blue ultraviolet region to the junction. Consequently, the blue response of the cells is enhanced. ZnS thin film as a potential buffer material can be synthesized by various techniques such as: spin coating, sol-gel, spray pyrolysis, chemical vapor deposition, chemical bath deposition (CBD), rf-sputtering etc. [5-10]. Among these methods chemical bath deposition (CBD) is economical and simple technique for large area deposition compared to other high vacuum and high temperature methods. CBD technique can be used to prepare different layers of thin film solar cells and high efficiencies up to 18.6% have already been achieved with the corresponding CIGS – based solar cells [11-13].

The properties of zinc sulfide (ZnS) thin films can be further improved by using apposite dopant. Besides, transition metal doped ZnS thin films exhibit room temperature ferromagnetism [14] and efficient catalytic activity can be achieved if the photocatalytic material possesses ferromagnetic property [15]. In order to activate shorter wavelength region, various transition metal ions can be used as dopant. Therefore, the aim of the present research is the synthesis of pure and iron (Fe) doped ZnS thin films (ZnS:Fe) from non-toxic precursor solution by CBD technique and study their different properties.

1.2 Review of the earlier research works

Lots of work has been done on pure ZnS and transitional metal doped ZnS thin films using number of techniques by many researchers. But very few works have been done on Fe doped ZnS by CBD technique using environmentally benign precursor as well as complexing agents. Some of the earlier works are given below:

Long et al. [16] studied the effects of preheating the substrates on the properties of ZnS thin films using non-toxic complexing agents by CBD technique. From XRD pattern they found that preheating of the substrates has an obvious effect on solution reaction mechanism which helps to form ZnS thin films with improved crystallinity and average particle size was decreased as shown in Fig. 1.1. They reported that more compact, uniform surface morphology with smaller grains were well covered throughout the preheated substrate. The transmission spectrum showed an average transmittance of about 82.2%. They found the optical band gap of 3.67 eV.

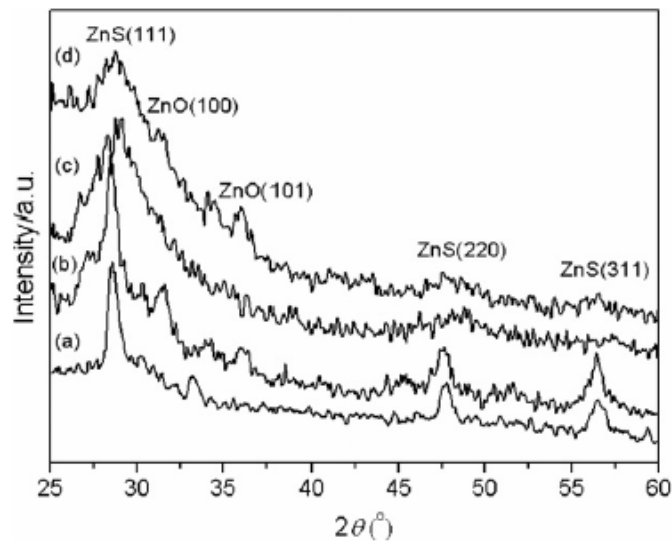


Figure 1.1: XRD patterns of annealed ZnS thin films prepared by (a) improved method, and (b) original method; as-deposited films prepared by (c) improved method; (d) original method [16]

Limei et al. [17] studied the structural, morphological, optical and electrical properties of ZnS thin films grown by CBD method.

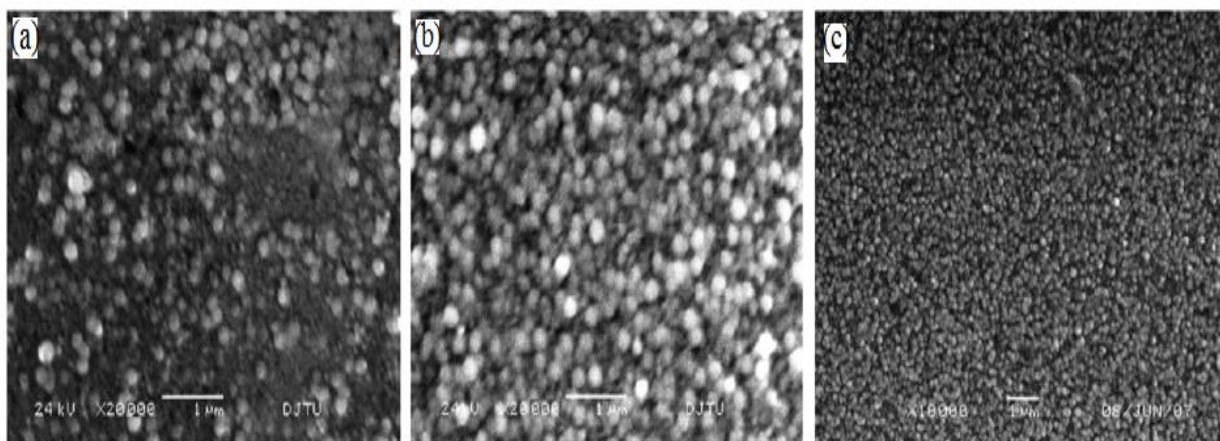


Figure 1.2: SEM images of ZnS thin films (a) as-deposited, and annealed at (b) 200°C, (c) 300°C for 1 hour [17]

They analyzed the effect of annealing temperature on the properties of the films. They found that as deposited films were amorphous and the crystallinity is improved after annealing the samples. The surface morphological studies revealed spherical and homogeneous grains all over the surface of the film but after annealing the grains grew up and surface became dense and flat as shown in Fig. 1.2.

Chowdhury et al. [18] investigated the growth parameters of cadmium sulfide (CdS) thin films deposited on glass/conducting glass substrates using low-cost CBD method. It has been confirmed by X-ray diffraction measurement that the deposited layers are mainly consisting of CdS phase. The PEC measurements indicated that the deposited CdS layer is n-type in electrical conduction. The optical study showed that the band gap is 2.42 eV for as-deposited film and 2.27 eV for annealed film. Surface morphology showed that the formation of pinhole free and smooth surface of CdS films of nanosized grains. The electrical resistivity is observed in the order of $10^4 \Omega \text{ cm}$ and decreases as temperature increases.

Dedova et al. [7] investigated the influence of compositions molar ratio and deposition temperature on phase composition, structural and morphological properties of ZnS thin films by spray pyrolysis technique. They found that equimolar solutions result in slightly Zn-rich composition and smaller crystallites.

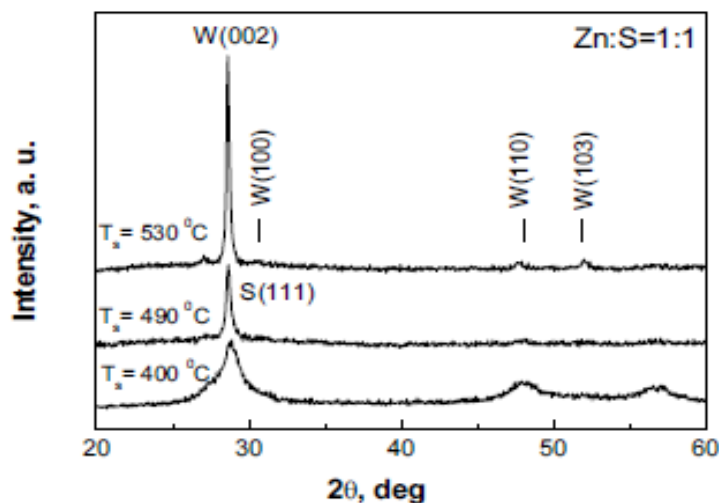


Figure 1.3: XRD pattern of sprayed ZnS films grown at temperature 400, 490 and 530 °C [7]

Cheng et al. [19] investigated the effect of tri-sodium citrate as a complexing agent on ZnS thin films by CBD method. They found that the concentration of tri-sodium citrate has a significant influence on the crystallinity and orientation of the ZnS thin films. X-ray diffraction pattern

showed that tri-sodium citrate improves crystallinity of the films. The transparency of the films increases to 70%. The SEM micrograph showed that the films were highly compact with nano structured grains of about 100 nm.

Kumar et al. [20] studied the structural, optical and magnetic properties of Fe doped ZnS (ZnS:Fe) nanoparticles synthesized by low temperature solvothermal technique.

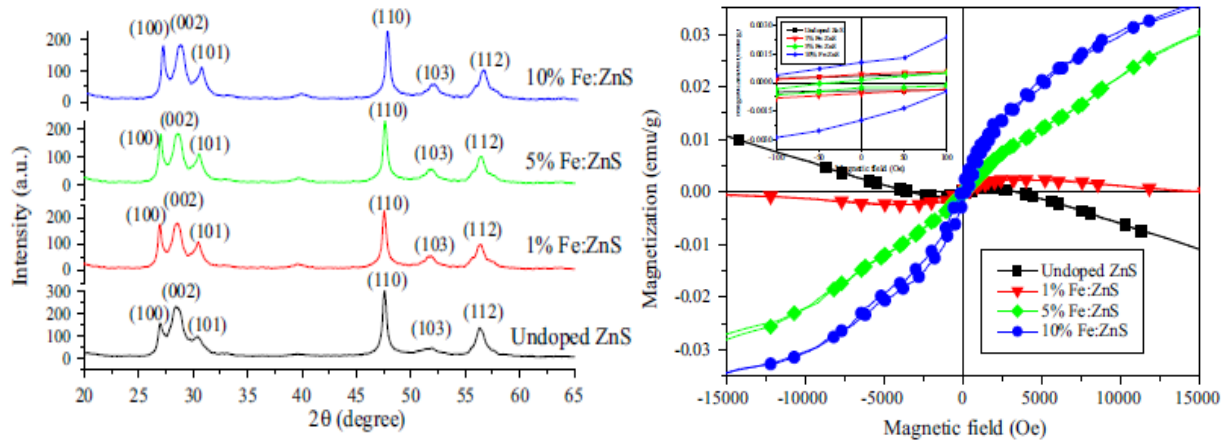


Figure 1.4: (a) XRD pattern, and (b) M-H curves of undoped and Fe-doped nanoparticles [20]

The XRD pattern revealed the wurtzite structure of the films and slight shift of the peaks confirmed the doping of Fe in ZnS lattice. The M-H curve analysis indicated ferromagnetic behavior with resolved hysteresis loops having small saturation magnetization where pure ZnS shows diamagnetic behavior. They also found weak ferromagnetic or paramagnetic behavior at 5 % ZnS:Fe thin film showed in Fig. 1.4.

Dixit et al. [15] studied the photocatalytic properties of Fe doped ZnS nanoparticles synthesized by wet chemical synthesis method. They found that 5% ZnS:Fe nanoparticles showed optimum photocatalytic activity. They also found that balance among distribution, location and oxidation states of dopant ions, levels of defects, crystallinity and charge carrier density were significant in achieving the optimum performance from the materials as photocatalyst.

Akhtar et al. [14] investigated the ferromagnetic and half metallic property of Fe doped ZnS thin film grown by chemical bath deposition technique. The morphological analysis showed cluster of spherical nanoparticles for all Fe doping concentration but different in size. They found undoped ZnS was diamagnetic whereas all the ZnS:Fe thin films showed room temperature ferromagnetism

as shown in Fig. 1.5. They also performed theoretical investigations that were consistent to the experimental data in all aspects in addition to the observation of half-metallicity in iron doped ZnS clusters.

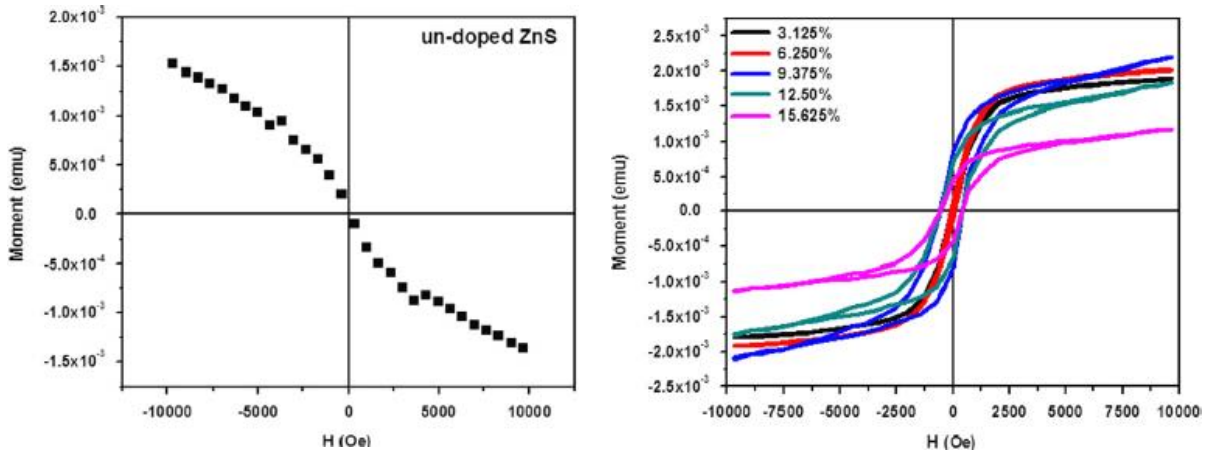


Figure 1.5: M-H curve of undoped and Fe doped ZnS thin films

1.3 The reason behind working with ZnS:Fe thin films

Some reasons are discussed below for selecting Fe doped ZnS thin films:

- Preparation of ZnS:Fe thin films by CBD technique using non-toxic complexing agents at ambient temperature and normal atmospheric pressure is advantageous from both ecological and economical view point.
- Pure ZnS and ZnS:Fe thin films are environmentally benign and it can be used as a Cd free buffer layer in thin film solar cell.
- ZnS:Fe thin film has wide direct bandgap which results in the transition of high energy photons to the junction and could enhance the response of the photovoltaic cell.
- It is expected that resistivity of the ZnS:Fe thin film will be less than pure ZnS thin films and free charge carrier concentration will be increased with increasing Fe concentration.
- Fe avoids the creation of recombination centers for photogenerated electron-hole pairs which could enhance photocatalytic activity.

1.4 Aim of the present work

The main objectives of the present work are as follows:

- Preparation of ZnS and ZnS:Fe thin films at different Fe concentration by chemical bath deposition (CBD) method using non-toxic complexing agents.

- ❑ Investigation of the surface morphology of thin films through Field Emission Scanning Electron Microscopy (FESEM) and the chemical composition of the deposited films will be studied by Energy Dispersive X-ray (EDX) analysis.
- ❑ Crystal structure of the deposited film will be studied by X-ray Diffraction (XRD) pattern.
- ❑ Transmittance, absorbance, optical absorption coefficient, optical band gap, refractive index etc. will be determined by UV-visible spectroscopy.
- ❑ DC electrical conductivity of the deposited films will be determined by linear four-point probe method.
- ❑ Investigation of the magnetic properties of the deposited films by Vibrating Sample Magnetometer (VSM).

1.5 Outline of the thesis

The thesis is organized as follows: The general introduction of the thin films with related literature review is in *Chapter 01*. Various thin film deposition techniques and materials are discussed in *Chapter 02*. The theoretical principles of various thin film characterization techniques are discussed in *Chapter 03*. In *Chapter 04*, experimental parts have been described in detail. Experimental results and its possible discussion are presented in *Chapter 05*. Finally, the summary and conclusion of the present work and scopes for future works are discussed in *Chapter 06*.

References

- [1] Borah, J. P., Barman, J., and Sarma, K. C., “Structural and optical properties of ZnS nanoparticles”, *Chalcogenide Lett.*, vol. 5(9), pp. 201-208, 2008.
- [2] Zaman, M. B., Chandel, T., Dehury K., and Rajaram, P., “Synthesis and characterization of spin-coated ZnS thin films”, *AIP conference Proceedings*, Vol. 100066, pp. 1-4 (1953).
- [3] Hichou, A. El., Addou, M., Bubendorff, J. L., Ebothe, J., Idrissi, B. El., and Troyon, M., “Microstructure and cathodoluminescence study of sprayed Al and Sn doped ZnS thin films”, *Semicond. Sci. Technol.*, vol. 19(2), pp. 230-235, 2004.
- [4] Ramanathan, K., Contreras, M. A., Perkins, C. L., Asher, S., Hasoon, F. S., Keane, J., Young, D., Romero, M., Metzger, W., Noufi, R., Ward, J., and Duda, A., “Properties of 19_2% efficiency ZnO/CdS/CuInGaSe₂ thin-film solar cells”, *Prog. Photovolt. Res. Appl.*, vol. 11, pp. 225-230, 2003.
- [5] Shriven, L. E., “Physics and applications of dip coating and spin coating”, *Mater. Res. Society*, vol. 121, pp. 717, 1988.
- [6] Murali, K.R., “Preparation of sol-gel dip coating ZnO thin film”, *J. Phys. Chem. Solids*, vol. 98, pp. 2293-2296, 2007.
- [7] Dedova, T., Krunk, M., and Gromyko, I., “Effect of Zn: S molar ratio in solution on the properties of ZnS thin films and the formation of ZnS nanorods by spray pyrolysis”, *Phys. Status Solidi A*, vol. 211, pp. 514–521, 2005.
- [8] Estaves, L. M., Oliveira, H. A., and Passos, F. B., “Carbon nanotube as catalyst support in chemical vapor deposition reaction: A review”, *J. Indu. Eng. Chem.*, vol. 65, pp. 112, 2018.
- [9] Shin, S. W., Agawane, G. L., Gang, M. G., Moholkar, A. V., Moon, J. H., Kim, J. H., and Lee, J. Y., “Preparation and characterization of chemical bath deposited ZnS thin films: effect of different complexing agents”, *J. Alloys Compd.*, vol. 526, pp. 25-30, 2012.
- [10] Mukherjee, C., Rajiv, K., Gupta, P., Sinha, A. K., and Abhinandan, L., “Growth and characterization of high quality ZnS thin films by RF sputtering”, *AIP Conf. Proceedings*, vol. 1451, pp. 203, 2012.
- [11] Neghavi, N., “From CdS to Zn(S, O, OH): A better understanding of chemical bath deposition parameters and cells properties using electrodeposited CuIn(S, Se)₂ and evaporated Cu(In, Ga)Se₂ absorbers”, *In 21st European Photovoltaic Solar Energy conference*, pp. 1843-1848 (2006).

- [12] Ennaoui, A., “New chemical route for the deposition of ZnS buffer layers: Cd-free CuInS₂-based thin film based solar cells with efficiencies above 11%”, *In 2nd European Photovoltaic Solar Energy Conference Barcelona*, (2005).
- [13] Contreras, M. A., Nakada, T., Hongo, M., Pudov, O. A., and Sites, J. R., “ZnO/ZnS(O, OH)/Cu(In,Ge)Se₂/Mo solar cell with 18.6% efficiency”, *3rd WCPEC*, (2003).
- [14] Akhtar, M. S., Malik, M. A., Alghamdi, Y. G., Ahmad, K. S., Riaz, S., and Naseem, S., “Chemical bath deposition of Fe-doped ZnS thin films: investigations of their ferromagnetic and half-metallic properties”, *Mater. Sci. Semicond. Process.*, vol. 39, pp. 283–291, 2015.
- [15] Dixit, N., Vaghasia, J. V., Sarkar, S. S. M., Chavda, M., Agrawal, N., and Soni, H. P., “Photocatalytic activity of Fe doped ZnS nanoparticles and carrier mediated ferromagnetism”, *J. Environ. Chem. Eng.*, vol. 3, pp. 1691–1701, 2015.
- [16] Long, F., Wang, W., Cui, Z., Fan, L., Zou, Z., and Jai, T., “An improved method for chemical bath deposition of ZnS thin films”, *Chem. Phys. Letts.*, vol. 462, pp. 84-87, 2008.
- [17] Limei, Z., Yuzhi, and X., and Jianfeng, L., “Study on ZnS thin films prepared by chemical bath deposition”, *J. Environ. Sci. Supple.*, pp. 76-79, 2009.
- [18] Chowdhury, R. I., Hossen, M. A., Mustafa, G., Hussain, S., Rahman, S. N., Farhad, S. F. U, Murata, K., Tambo, T., and Islam A. B. M. O., “Characterization of chemically deposited Cadmium Sulfide thin films”, *International Journal of Modern Physics B.*, vol. 24(30), 5901–5911, 2010.
- [19] Cheng, j., Fan, D. B., Wang, H., Liu, B. W., Zhang, Y. C., and Yan, H., “Chemical bath deposition of crystallite ZnS thin films”, *Semicond. Sci. Technol.*, vol. 18, pp. 676-679, 2003.
- [20] Kumar, S., and Verma, N. K., “Structural, optical and magnetic investigations on Fe doped ZnS nanoparticles”, *J. Mater. Sci.- Mater. Electron.*, vol. 26, pp. 2754–2759, 2015.

***MATERIALS AND THIN FILM
DEPOSITION TECHNIQUES***

CHAPTER 2

MATERIALS AND THIN FILM DEPOSITION TECHNIQUES

In this chapter, basic properties and applications of ZnS are discussed in brief. In this work, Fe has been used as the dopant material. So, it is important to know the basic properties of Fe and its oxides compound. There is a short discussion on Fe in this chapter. Basic principles of various techniques are also been discussed later.

2.1 Zinc sulfide

ZnS is an important wide direct bandgap semiconductor of II–VI class. Its band gap energy (E_g) of 3.68 eV at room temperature which makes it transparent to practically all wavelengths in the UV-visible region. It is well known that semiconductor nanocrystals exhibit quantum confinement effect when their size becomes comparable to or smaller than the Bohr radius of excitons [1]. This results in large separation of the energy levels of the ZnS semiconductor and the effective band gap increases. Hence nanoscale semiconductors show interesting properties and tuning of the band gap is possible by controlling their sizes in the nano regime.

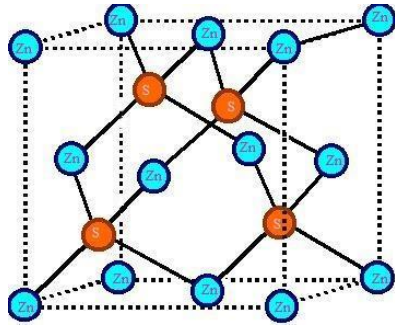
2.2 Properties of zinc sulfide

Zinc Sulfide (ZnS) is a metal chalcogenide semiconductor. The basic properties of ZnS are as follows:

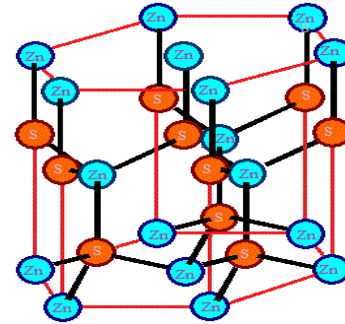
Name of the properties	Value/ Type
Chemical Name	Zinc Sulfide
Chemical Formula	ZnS
Molar Mass	97.474 g/mol
Density	4.090 g/cm ³
Color	White
Appearance	Crystalline Solid
Melting point	1850 °C
Crystal Structure	Cubic or Hexagonal
Semiconductor Type	n-type Semiconductor
Band Gap	3.54 eV for Cubic, 3.91 eV for Hexagonal
Refractive Index	2.3677
Std. Enthalpy of Formation $\Delta_f H_{298}$	204.6 kJ. / mol

2.3 Phases of zinc sulfide

ZnS exists in two main crystalline phases i.e. cubic and hexagonal, and this dualism is an example of polymorphism. Cubic phase of ZnS is more stable and known as zinc blende. The hexagonal phase is known as mineral wurtzite. The transition from the zinc blende to wurtzite form occurs at around 1020° C. The coordination geometry at Zn and S is tetrahedral for both phases.



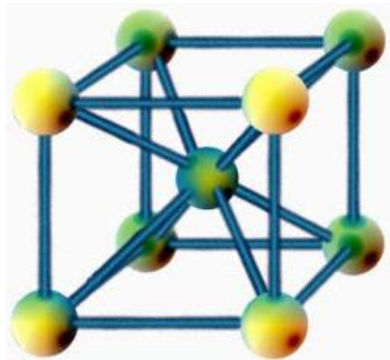
Cubic structure of ZnS



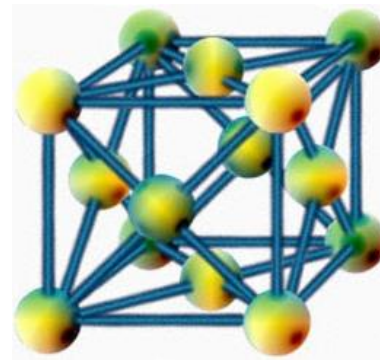
Wurtzite structure of ZnS

2.4 Properties of iron

Iron is a chemical element with the chemical symbol Fe and atomic number 26. Fe is a group VII element in the periodic table with electronic configuration $1s^2 2s^2 2p^6 3s^2 3p^6 4s^2 3d^6$. It is the fourth-most abundant element in the earth's crust and exists in four distinct crystalline forms. The 3d orbital has one electron pair and rest of the electrons are unpaired. This will give rise to a spin angular momentum of $\frac{1}{2}$ which can result in a net magnetic moment.



bcc (α -Iron)



fcc (γ -Iron)

Two common oxidation states with the magnetic properties of iron oxides make it suitable for numerous applications. Fe is an example of allotropy and has at least four allotropic forms i.e. α , γ , δ , and ϵ . It exists in a wide range of oxidation states from -2 to +7 and the most reactive metal of this group in the periodic table. Fe is a magnetic material and its magnetic ordering changes from paramagnetic to ferromagnetic. The basic properties of Fe are as follows:

Name of the Properties	Value/ Type
Atomic Number	26
Atomic Mass	55.845
Phase	Solid
Crystal Structure	Octahedral
Density	7.874 g/cm ³
Melting Point	1538 °C
Boiling Point	2862°C
Atomic Radius	0.126 nm
Ionic Radius	0.092 nm
Electrical Conductivity	96.1 nΩ-m
Magnetic Ordering	Ferromagnetic
Curie Point	1316 °C

The ionic radius of Zn²⁺ and Fe²⁺ is quite close i.e. 0.74 Å and 0.77 Å respectively. Therefore, Fe can be a suitable dopant of ZnS. Because close ionic radius helps Fe²⁺ to substitute or penetrate ZnS lattice.

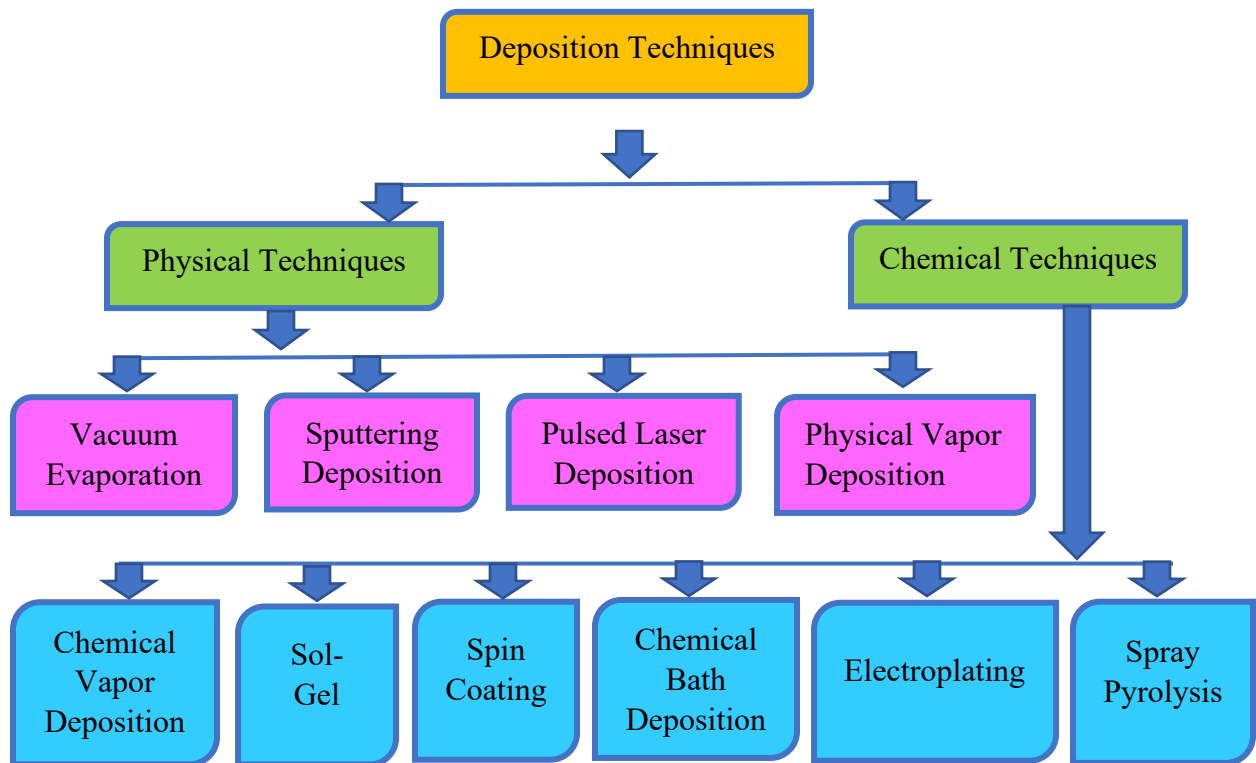
2.5 Applications of zinc sulfide

Table 2.1: Application areas of ZnS thin films

Properties category	Typical applications
Optical	<ul style="list-style-type: none"> • Antireflection & highly reflecting coatings • Photosensitive coating of “analog” film for the old camera
Optoelectronics	<ul style="list-style-type: none"> • Photo detectors • Image transmission • Optical memories
Electronics	<ul style="list-style-type: none"> • Active thin film elements (Transistors, Diodes) • Passive thin film elements (Resistors, Condensers, Interconnects) • Integrated circuits (VLSI, Very Large-Scale Integrated Circuit)
Engineering	<ul style="list-style-type: none"> • Self-supporting coatings of metals for rocket nozzles, crucibles, pipes etc. • Protection against high temperature corrosion • Hard coatings for cutting tool
Sensor	<ul style="list-style-type: none"> • Data acquisition in aggressive environments and media telemetry • Biological sensors
Alternative Energies	<ul style="list-style-type: none"> • Solar collectors and solar cells • Thermal management of architectural glasses and foils

2.6 Thin film deposition techniques

Thin film deposition is the process of adding a thin layer of material on a substrate which has order from few microns to several nanometer. This is a technique used for depositing a thin film of desired material onto a substrate or onto earlier deposited layers. Most deposition techniques allow layer thickness to be controlled within a few tens' micron, and some allow single layers of atoms to be deposited at a time. But the structure of the film on nanometer or micrometer scale can affect the properties of thin film [2]. The properties of thin films depend on the method of deposition. The required properties can be obtained by choosing proper method of thin films deposition. Thin film deposition method can be broadly classified as physical and chemical techniques. Through controlling the parameters thin films can be deposited by several physical and chemical techniques [3]. In this section, a brief description of some commonly used deposition techniques for thin films on a variety of commercially available substrates will be described. The following flow chart represents the classification of thin film deposition techniques.



2.6.1 Physical deposition techniques

In physical methods, the film material is moved from a target source to the substrate with some form of energy. This deposition uses mechanical, electrochemical or thermodynamic means to produce a thin film of solid. The material to be deposited is placed in an energetic, entropic

environment, so that the particles of the material escape its surface. The whole system is kept in a vacuum deposition chamber, to allow the particles to travel as freely as possible.

2.6.1.1 Thermal or vacuum evaporation method

Thermal evaporation involves heating a solid material inside a high vacuum chamber, taking it to a temperature which produces some vapor pressure. To raise a vapor cloud inside the chamber a relatively low vapor pressure is required. This evaporated material constitutes a vapor stream, which traverses the chamber and heat the substrate, sticking to it as a coating or film.

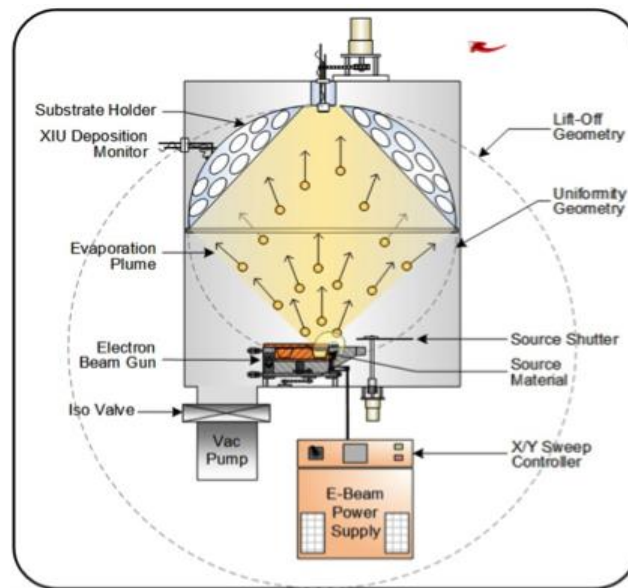


Figure 2.1: Schematic diagram of thermal evaporation system [4]

Thermal evaporation may be performed directly or indirectly by variety of physical methods.

Several varieties are:

- Resistive heating
- Exploding wire techniques
- Flash evaporation
- Arc evaporation
- Laser evaporation
- R.F. heating
- Electron bombardment

In this process, the deposited material is heated to its melting point usually located at the bottom of the chamber. Thermal evaporation system design and method can adjust a number of parameters

such as thickness, uniformity, adhesion, strength, stress, grain size, optical or electrical properties etc. Although one of the oldest methods used for depositing thin film: thermal evaporation or vacuum evaporation is still widely used in the laboratory and industry for depositing metal and metal alloys [4].

2.6.1.2 Pulsed laser deposition

Pulsed laser deposition is a thin film deposition technique where a high-power pulsed laser beam is focused inside a high vacuum chamber to evaporate material from a target of the desired composition and deposited as thin film on a substrate. The laser pulse is absorbed by the target and energy is converted to electronic excitation and later on thermal, chemical and mechanical energy which result in evaporation, ablation and plasma formation

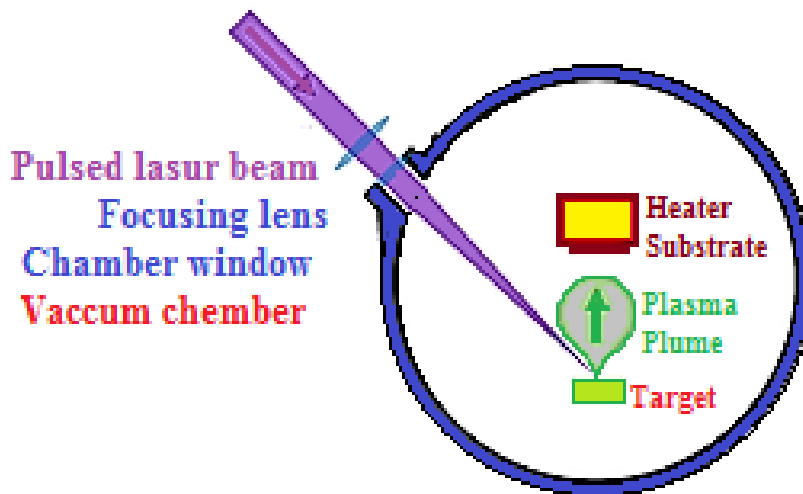


Figure 2.2: Schematic diagram of pulsed laser deposition system [5]

The ejected species expand into the surrounding vacuum in the form of a plasma plume which contains many energetic species including atoms, molecules, electrons, ions and particles before deposition on the typically hot substrate [5]. This Process mainly goes through four individual stages. Each of these steps is important for the crystallinity, uniformity and stoichiometry of the thin film. They are as follows:

- Laser absorption on the target, ablation of the target material and creation of a plasma
- Plasma plume expansion
- Deposition of the ablated material
- Nucleation and growth

There are some aspects that influence the deposition rate. They are as follows:

- ❑ Target material
- ❑ Pulse energy of laser
- ❑ Distance between target and substrate
- ❑ Type of gas and pressure on the chamber

2.6.1.3 Sputtering deposition

Sputtering is a process whereby atoms are ejected from a solid target material due to the bombardment of the target by energetic ions. Sputter deposition is a method of depositing thin film by sputtering materials from a target which is then deposited onto a substrate. Atoms can be ejected from the target by momentum exchange between the sputtering ions and the target atoms due to collision. The average number of atoms ejected from the target per incident ion is called the sputter yield. The sputter yield from the target is thereby one of the main parameters for sputtering deposition of thin films and depends on the ion incident angle, the energy of the ions, the mass of the ions and target atoms, and the surface binding energy of the atoms in the target. Sputtered atoms and ions ejected from the target have a wide energy distribution whereas the sputtered ions can ballistically fly from the target on straight lines and impact energetically on the substrate or vacuum chamber [6].

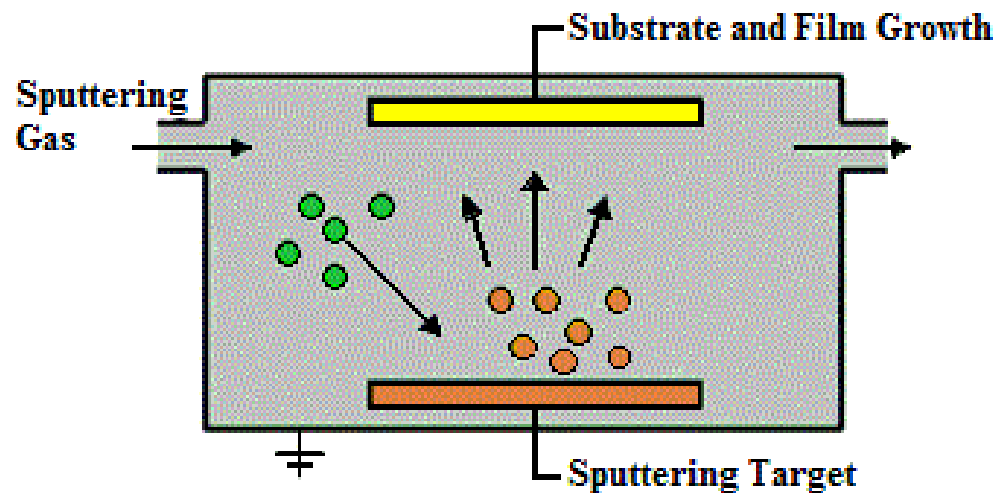


Figure 2.3: Schematic diagram of sputtering deposition system [6]

However, the sputtered ions could act as moderator or a necessary growth reactant. Typically, an inert gas is used for sputtering i.e. Argon or Xenon. There is a number of sputtering deposition method such as-

- ❑ Reactive sputtering
- ❑ Ion-beam sputtering
- ❑ Ion-assisted sputtering
- ❑ Gas flow sputtering
- ❑ High-power impulse magnetron sputtering
- ❑ High-target-utilization sputtering

The most promising advantage of this technique is to sputter and deposit element, alloys and compounds.

2.6.2 Chemical deposition techniques

In chemical deposition process, liquid precursor undergoes a chemical change at a solid surface, leaving a solid layer. This process relies on a chemical reaction with vapor species controlling the film constituent that are incident on a substrate to produce a film of the desired composition. Thin films from chemical deposition tend to be conformal instead of directional. Chemical deposition processes exploit the creation of solid materials directly from chemical reactions in gas and/or liquid compositions and with the substrate material. We describe briefly some of the commonly used chemical methods for depositing large area thin film on a commercially available substrate.

2.6.2.1 Chemical vapor deposition

The deposition of films from chemical reaction or gaseous phases by thermal decomposition on a substrate surface at high temperature is known as the chemical vapor deposition. This technique is cast-off for the preparation of various inorganic as well as organic compounds. The basic principle involves decompositions or partial dissociation of the vapor phase species in a neutral atmosphere and the deposition of the product [7].

Sometimes a carrier gas is also introduced either to control the rate of reaction or to prevent undesired reactions at the prevailing elevated temperature. An appropriate control of the rate of flow of the gaseous species, temperature and pressure of the reaction chamber lead to the formation of required deposition. It is a basic tool of manufacturing product such as- sunglasses, potato-chip bags and is fundamental to the production of much of today's electronics. It is also a technique subjected to constant refining and expansion, pushing materials research in new directions such as the production of large-scale sheets of graphene, or the development of solar cells that could be "printed" onto a sheet of paper or plastic.

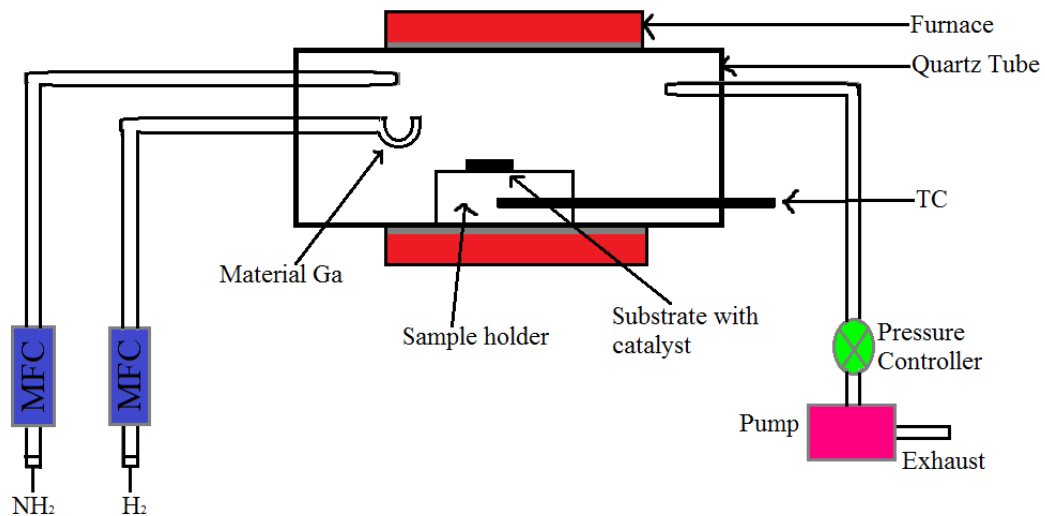


Figure 2.4: Schematic diagram of chemical vapor deposition system

2.6.2.2 Spin coating

Spin coating is used for several decades for the application of thin films. It is a procedure used to apply uniform thin films on flat surface.

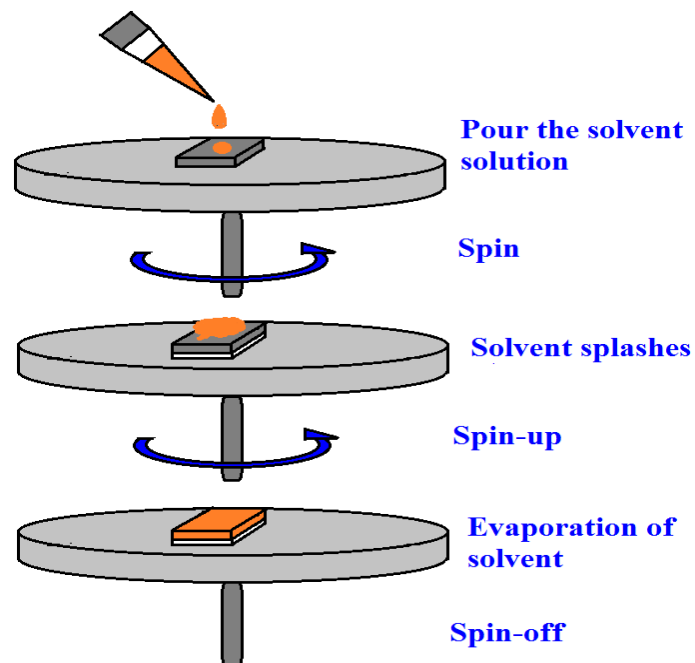


Figure 2.5: Schematic diagram of spin coating deposition system

Spin coating involves acceleration of a liquid puddle on a rotating substrate [8]. Usually small amount of coating material is applied onto the center of the substrate and then spinning the

substrate at high speed in order to spread the coating material by centrifugal force. A machine used for spin coating is called spin coater. Rotator is continued until the desired thickness of the film achieved. The applied solvent is usually volatile and simultaneously evaporates. The higher the angular speed of spinning, the thinner the deposited film. The thickness of the film also depends on the viscosity, concentration of the solution and the solvent [9].

2.6.2.3 Spray pyrolysis method

Spray pyrolysis is a powerful technique to synthesize a wide variety of high purity commercially homogeneous ceramic powder.

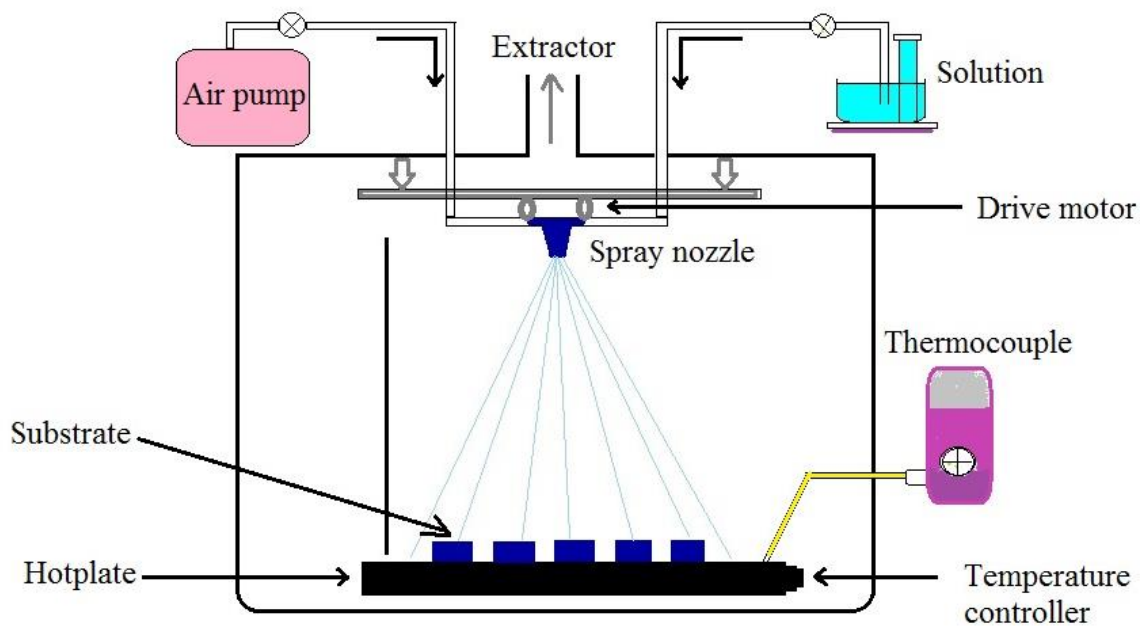


Figure 2.6: Schematic diagram of spray pyrolysis deposition system

Even multi-layered films can be easily prepared using this technique. The method involves spraying a solution usually in aqueous, containing soluble of the constituent atoms of the desired compound to a heated substrate. Every sprayed droplet reaching the substrate undergoes pyrolysis decomposition forms a single crystallite or a cluster of crystallites of the products. Different parameters like volume of the solution sprayed, substrate temperature, solution and flow rates concentration of the solution, distance between the substrate and spray nozzle have to be optimized to get a homogeneous uniform thickness and good quality of the film. Hydrolysis and pyrolysis are the main chemical reactions involved in this process.

2.6.2.4 Chemical bath deposition (CBD)

The basic principle involves in the synthesis of thin films by the CBD method is the controlled release precipitation of the desired compound from a solution of its constituents. The ionic product must exceed the solubility product, thus the formation of thin films on substrates by ion by ion condensation.

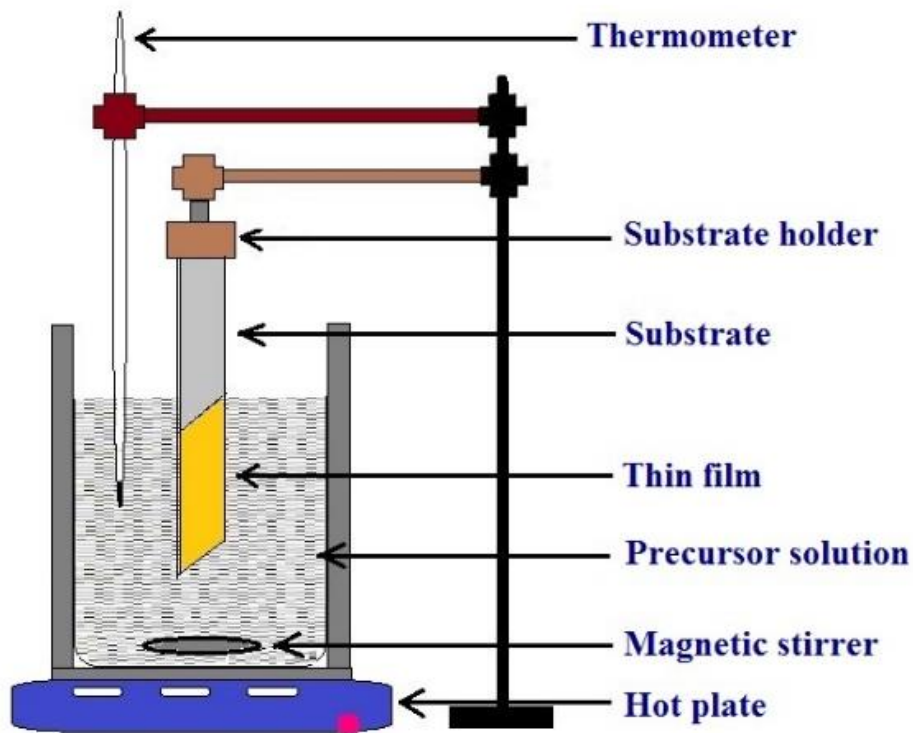


Figure 2.7: Schematic diagram of chemical bath deposition system

This process is used for large area deposition or continuous deposition. In this process, the substrate is immersed into a precursor solution container. Deposition of thin film onto the substrate through this technique involve two steps i.e. nucleation and particle growth. These two steps depend on some parameters which controls the particle growth on the substrate surface such as duration of deposition, composition and temperature of the solution, pH of the solution, molarity of concentration, topographical and chemical nature of the substrate [10,11]. Very small change of these parameters affects the properties of the thin film broadly. Chemical Bath Deposition is relatively a simple process but it produced stable, adherent, uniform and hard films with good reproducibility. It can be used to synthesize wide variety of metal chalcogenide thin films on

various substrates. CBD is one of the most commonly used techniques to prepare different layers of thin film solar cells.

2.6.2.5 Sol-Gel technique

Sol-gel technique is a wet chemical route for the synthesis of colloidal dispersion of oxides which can be altered to powder, fiber, thin film and monoliths [12]. This technique is mostly used for fabricating metal oxide. This process involves conversion of monomer into a colloidal solution called “sol” that acts as the precursor for an integrated network (or “gel”) of either discrete particles or network polymers. Sol-gel coating is a process of preparation of single or multi component oxide coating which may be glass, glass ceramic or crystalline ceramic depending on the process. Also, the nanomaterial used in modern ceramic and device technology required high purity and enable to control the composition and structure. The sol-gel deposition technique is one of the stimulating techniques since it has many advantages i.e. [13]

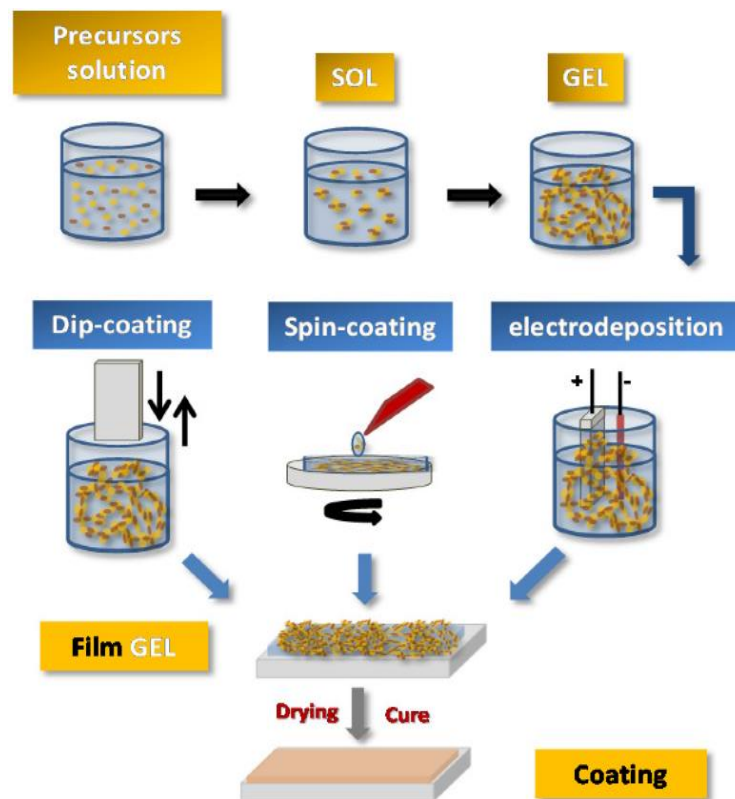


Figure 2.8: Schematic diagram of sol-gel deposition technique [13]

- i. The reactants for sol-gel process can be conveniently purified by distillation and crystallization

- ii. Organic and inorganic salts can be added to adjust the microstructure or to improve the structural, optical and electrical properties of oxide films
- iii. All strong materials are mixed at molecular level in the solution so that a high degree of homogeneity of the film can be expected
- iv. The sol-gel technique is almost exclusively applied for fabrication of transparent layers with a high degree of planarity and surface quality

2.7 Thin film formation stages

Thin film science has grown world wide a major research area. The importance of coatings and synthesis of new materials for industry caused in a tremendous increase of innovative thin film processing technologies. The property of a thin film strongly depended on their structure. So, it is important to know the factors that govern the structure of the film. The typical thin film deposition process consists of three major steps which are: [14]

- a) Production of the appropriate atomic, molecular, or ionic species.
- b) Transport the produced species to the substrate through a medium.
- c) To form a solid deposition, condensation is occurred either directly or via a chemical and/or electro chemical reaction

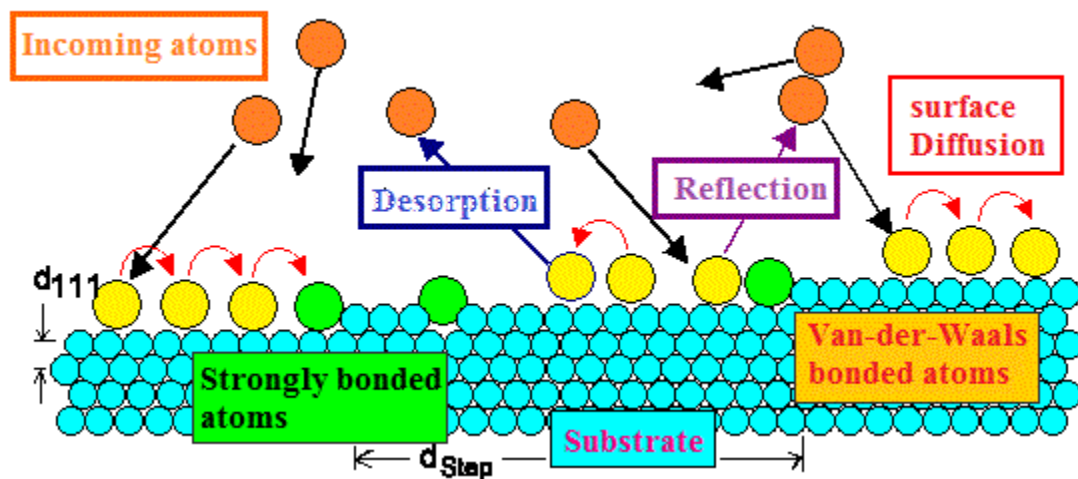


Figure 2.9: Schematic diagram of thin film formation process

Thin film is equipped by deposition of the desired materials (metals, semiconductors, insulators, dielectric etc.) atom by atom on a substrate by phase transition. Sufficient time interval between the two successive deposition of atoms and also layers are required so that these can occupy the minimum potential energy configuration. In thermodynamic stable films, all atoms will take up

positions and orientation energetically compatible with the neighboring atoms of the substrate or to the previously deposited layers, and then the effect of substrate or the initial layers will diminish gradually.

Thin film condensation can be distinguished by three mechanisms, depending on the strength of interaction between the atoms of the growing film and substrate. These three major steps are:

- A three-dimensional nucleation forming, growth and coalescence of islands (Volmer-Weber mechanism)
- The layer by layer growth (Vander Merwe mechanism)
- Absorption of mono layer and subsequent nucleation on the top of this layer (Stranski-Krastanov mechanism) (Venables, 1993)

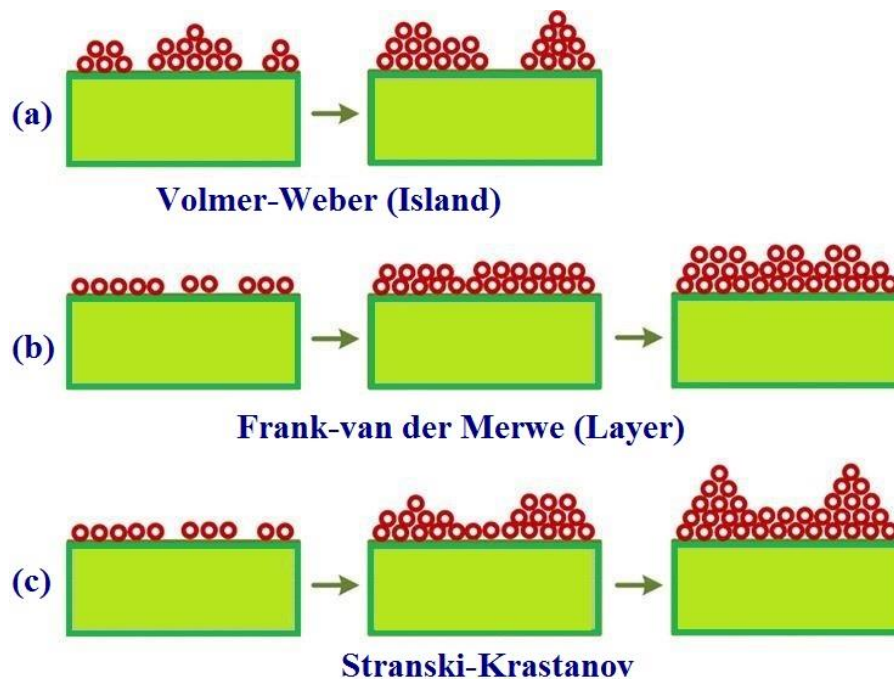


Figure 2.10: Three different modes of film growth

In most cases, mechanism (a) takes place and here we are going to describe this mechanism in brief. Schematic diagram of the three different growth modes is shown in Fig. 2.10.

2.7.1 Volmer-weber condensation

Much research on the mechanism of the thin film growth has been done with evaporated films; extensive information on initial growth has been published by D. W. Pashley and his co-workers [15]. The structural behavior and properties of the films depend on the growth process. Thin film

is most commonly prepared by the condensation of atoms from the vapor phase of a material, i.e. the transformation of a gas into a liquid or solid. The condensation of vapor atom is determined by its interaction with the impinged surface in the following manner:

The impinging atom is attracted to the surface by the instantaneous dipole and quadruple moments of the surface atoms. As a result, the atoms losses its velocity component normal to the surface in a short time, provide the incident kinetic energy is not too high. The vapor atoms are then physically absorbed (called adatom), but it may or may not be completely thermally equilibrium. It may move over the surface and its own kinetic energy parallel to the surface. The adatom has a finite stay or residence time on the surface during which it may interact with other adatoms to form a stable cluster and be chemically absorbed, with the release of the heat condensation. If not absorbed, the adatoms evaporated or desorbs into vapor phase. Therefore, thermodynamically, the only requirement for condensation to occur is that partial pressure of the thin film material in the gas phase be equal or larger than its vapor pressure in the condensed phase at that temperature.

The ‘Condensation’ and “Striking” coefficient is the probability that an impinging atom will be incorporated into the substrate. It is measured by the ratio of the amount of the material condensed on a surface to the total amount of impinged. In fact, the striking coefficient is so small that condensation is not observed by the ordinary techniques. On the other hand, the striking coefficient is found to be strongly dependent on the total time during which the substrate was subjected to the impingement, and also on the substrate temperature. A non-unity striking coefficient is usually explained in terms of monomer re-evaporation forms the areas of the substrate which are outside, the capture zones around each stable nucleus [15,16].

2.8 Nucleation

The first stage in the process of depositing thin film on substrates is the formation of absorbed monomers of one or more atoms which is the second phase under the action of forces similar to surface tension, or capillarity combine to form small clusters. There are two types of nucleation occurs during the formation of thin film:

- i. Homogeneous nucleation
- ii. Heterogeneous nucleation

2.8.1 Homogeneous nucleation

The classical theories of nucleation suppose that the clusters are formed by an additional mechanism until the critical size is reached. The classical theory of nucleation is based on a condensation of a vapor to liquid, and can be extended to crystallization from melts and solutions.

The change of the free energies associated with the process of homogeneous nucleation may be considered as follows,

$$\Delta G = \Delta G_s + \Delta G_v = 4\pi r^2 \sigma + \frac{4}{3} \pi r^3 \Delta G_v \quad (2.1)$$

Where ΔG_s is the excess free energy between the surface of the particle and the bulk. ΔG_v is excess free energy between a very large particle and the solute in solution [17]. For homogeneous nucleation the volume free energy for supercooling can be expressed by:

$$\Delta G_v = \frac{\Delta H_f \Delta T}{T_o} \quad (2.2)$$

The two terms on the right-hand side of equation (2.1) have an opposite effect on the system and they depend differently on the radius of the nucleus r . Therefore, the free energy of formation ΔG passes through a maximum value ΔG_{cryt} , which corresponds to the nucleus critical size. From Fig. 2.11 it can be seen that ΔG_s is a positive quantity, proportional to r^2 . ΔG_v is a negative quantity proportional to r^3 .

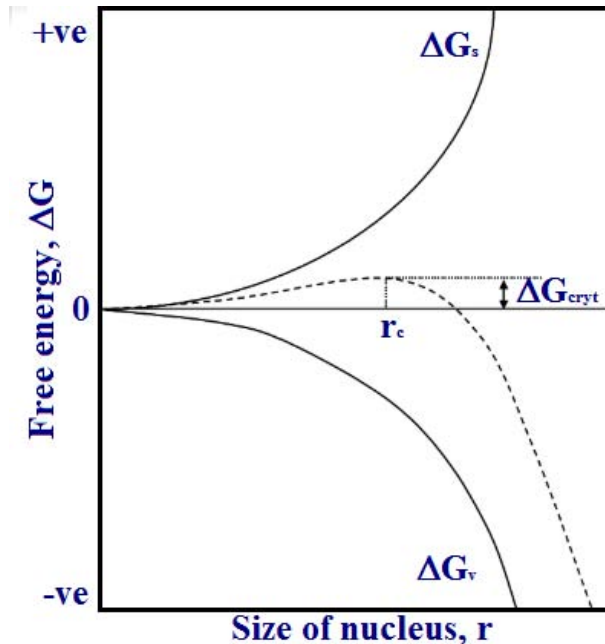


Figure 2.11: Free energy diagram for nucleation explaining the existence of a critical nucleus. With respect to r the critical size for a spherical nucleus can be obtained from equation 2.1 as follows:

$$\frac{d\Delta G}{dr} = 8\pi r\sigma + 4\pi r^2\Delta G_v = 0 \quad (2.3)$$

Or

$$r_c = \frac{-2\sigma}{\Delta G_v} \quad (2.4)$$

The r_c represents the minimal size of a nucleus which needs to be gained before the new phase is formed. If the cluster size is smaller than the critical size, they can easily be dissolved back in the liquid or evaporate. From Fig. 2.11 it can be seen that nuclei with sizes larger r_c will reduce the energy necessary to get a stable nucleus which can continuously grow into crystals. Combining the equations 2.1 and 2.4 it leads to,

$$\Delta G_{crys} = \frac{16\pi\sigma^3}{3(\Delta G_v)^2} = \frac{4\pi\sigma r_c^2}{3} \quad (2.5)$$

The nucleation rate can be expressed as follows:

$$J = A \exp\left[\frac{-16\pi\sigma^3 v^2}{3k^3 T^3 (\ln S)^2}\right] \quad (2.6)$$

The nucleation process is strongly depending on the interfacial tension. This is one of the most difficult parameters concerning the measurements, when trying to calculate nuclei critical size.

2.8.2 Heterogeneous Nucleation

It has been known for many years that different heterogeneities, motes, inclusions, etc. can encourage phase transformations (by reducing formation energies), mainly condensation and crystallization.

Nucleation in heterogeneous systems normally occurs at lower supersaturations compared with homogeneous nucleation Fig. 2.11. Therefore, a correction factor is needed which, must be less than a unit and can be explained as follows:

$$\Delta G_{het} = f\Delta G_{hom} \quad (2.7)$$

Where

$$f = \frac{(2 + \cos \theta)(1 - \cos \theta)^2}{4} \quad (2.8)$$

where θ is the contact angle between liquid and solid surface. The contact angle θ is determined by Young's relation

$$\cos \theta = \frac{\sigma_{sl} - \sigma_{cs}}{\sigma_{cl}} \quad (2.9)$$

Where σ_{sl} is the solid-liquid interfacial tension, σ_{cs} is crystal-solid interfacial tension and σ_{cl} crystal-liquid interfacial tension.

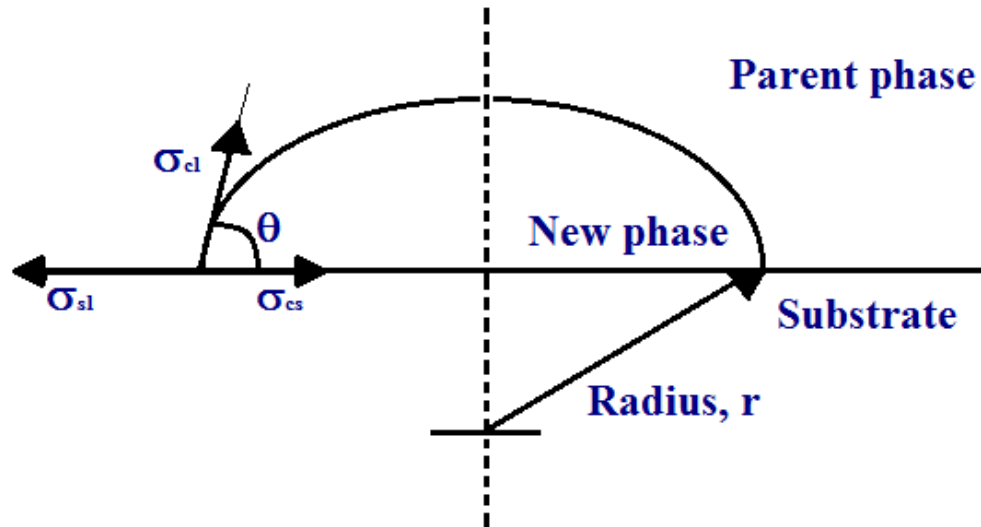


Figure 2.12: Contact angle and interfacial tension

It is assumed that a free liquid drop automatically takes the shape that minimizes the free energy of the entire system [18]. A surface with cluster contact angle of zero is known as wetting while a surface with cluster contact of more than 90° is known as non-wetting. When the contact angle is between 0° to 90° a system is known as partially wetting. A surface will also be known as hydrophilic if liquid wets the surface and as hydrophobic if a water cluster has a contact angle greater than 30° on the surface. In general, there appears to be only a limited number of places at which nuclei can form. Nuclei are always formed on a surface Fig. 2.12.

2.9 Thin film growth

The final and conclusion stage of thin film formation is growth. Growth states to a constructive change in size or maturation frequently a period of time. The prediction of nucleation theories in general have been found to be true even through relatively crude experimentations, but for quantitative comparison sophisticated techniques are needed. However, the remark revealed different stages of thin film growth leading to a continuous film [19]. These stages are:

- i. Island stage
- ii. Coalescence stage

- iii. Channel stage
- iv. Continuous film stage

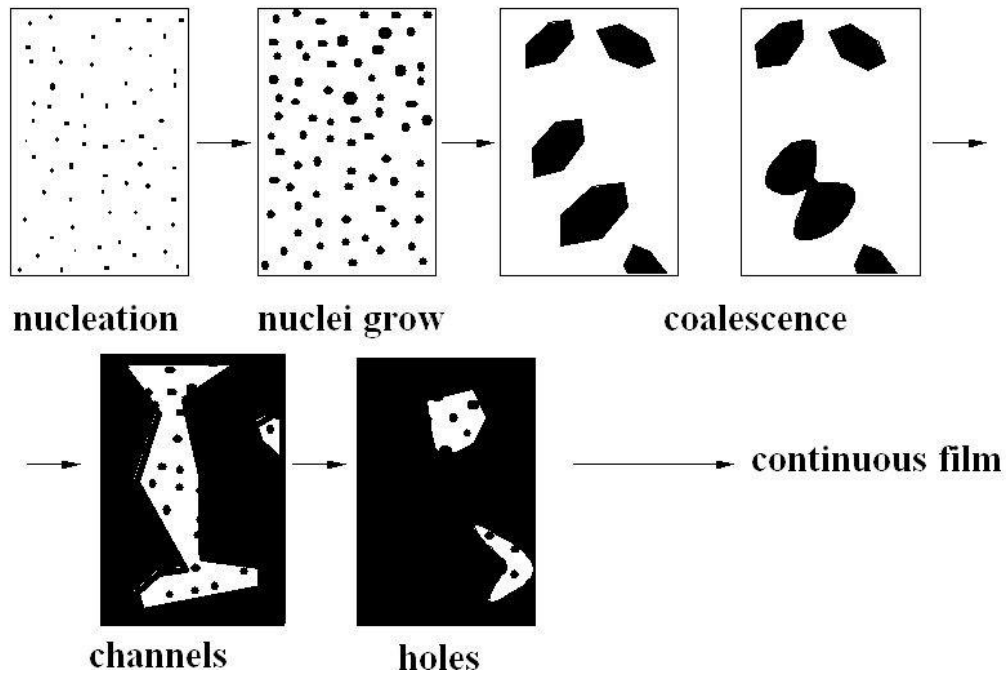


Figure 2.13: Different stages of thin film growth [19]

2.9.1 Island stage

When a substrate under impingement of condenses monomer is observed in the electron microscope, the first evidence of condensation is a sudden burst of nuclei of fairly uniform size. Growth of nuclei is three dimensional, but the growth parallel to the substrate is greater than that normal to it.

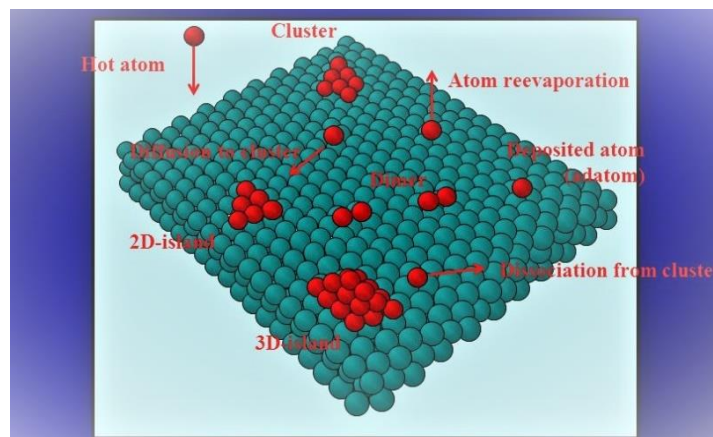


Figure 2.14: The mechanism of formation of island stage during thin film growth

This is probably because growth occurs largely by the surface diffusion of monomers on the substrate, rather the direct impingement from the vapor phase. The island structure formation tendency amplified by,

- i. At high substrate temperature
- ii. At low boiling point of film material
- iii. At low deposition rate
- iv. At weak bonding energy between film material and substrate
- v. At high surface energy of film material and
- vi. At low surface energy of the substrate

2.9.2 Coalescence stage

The island increases their size by further deposition and come closer to each other. Through the coalescence of smaller ones, the large ones appear to grow. The coalescence occurs in less than 0.1s for the small nuclei.

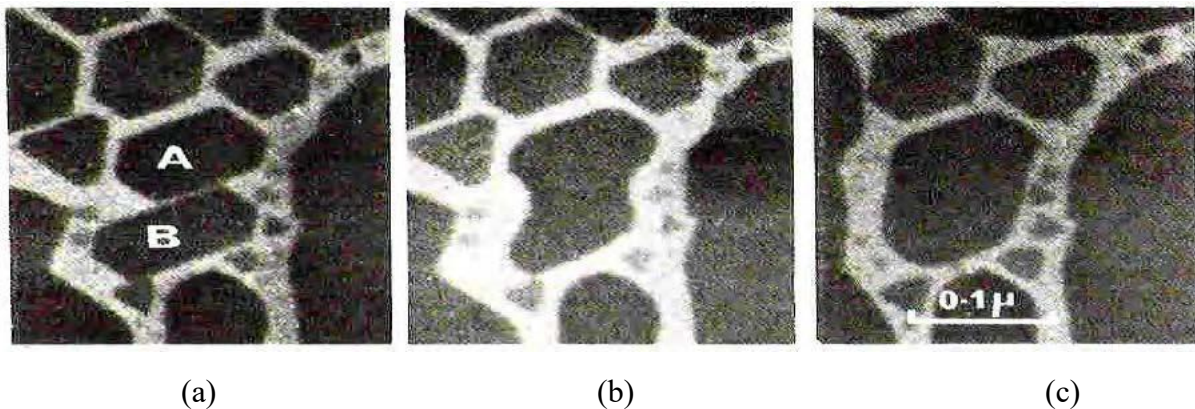


Figure 2.15: Electron micrograph shows the change in shape of islands during and after Coalescence (a) at zero (b) after 1 to 2 sec. (c) after 60 sec. [19]

2.9.3 The channel stage

When larger island grows together, they have channel of interconnected holes of exposed substrate in the form of network on the substrate. As deposition continues, secondary nucleation occurs in these channels and forms the last stage of nucleation.

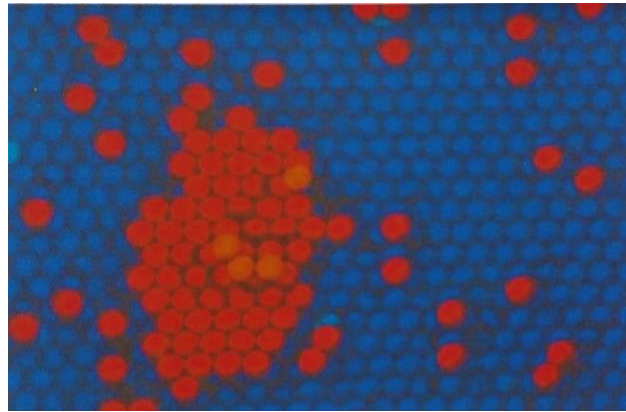


Figure 2.16: Schematic diagram of channel stage

2.9.4 Continuous film stage

This is the final stage of film growth. This is slowly filling the empty channels which requires a considerable amount of deposition. These empty channels filled with secondary nucleation, growth and coalescence. Through this way a continuous film is formed.

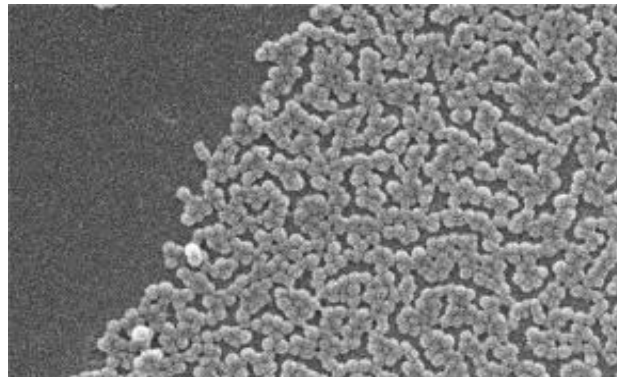


Figure 2.17: Schematic diagram of a continuous film stage

2.10 Influence of various thin film deposition parameters

The physical properties of thin films depend on some important factors. These factors are important because thin films are characterized through the properties such as thickness, smoothness, crystallite orientation and multilayer aspects. Moreover, for high quality thin films uniform crystallite structure, nominal stoichiometry, well oriented crystallites and high film density as well as smooth film surface are necessary. These properties of thin films change significantly with the very small change of the factors.

i. The nature of the substrates

Specific applications require different substrate materials that offer an acceptable cooperation for the purpose imminent. Ideally, the substrate should give mechanical support but should not interact with the film except to provide sufficient adhesion, and in many cases, the provision of a template

for atomic ordering. In practice, however, the substrate exerts considerable influence on film characteristics. The search for viable substrate materials is an active area of research [3]. Before selecting a particular substrate, the lattice parameter should be considered so that it matches to the lattice parameter of the growing films. Otherwise structural mismatches create mechanical fracture in the film.

ii. Substrate temperature

During deposition the temperature of the substrate affects the properties of the film. At low temperature polycrystalline films are formed on both vitreous and crystalline substrates with high densities of structural imperfection. On the other hand, at high temperature oriented single crystal films are formed on crystalline substrates.

iii. Post-deposition annealing

Annealing is known as heat treatment because the films are heated to a higher temperature and cooling it back to room temperature. The benefit of annealing is to improve crystallinity of the films. The annealing temperature is related to the properties of deposited films. Even the post-annealing process removes some defects of the films and its plays an important role in the mobility of the atoms.

iv. Vacuum pressure and inertness of the reaction chamber

If the deposition chamber is not vacuum and inert then the evaporated atoms cannot be reached at the surface of the substrate. They interact with the gases within the reaction chamber and scattered inside it. So that sufficient low pressure and inertness is necessary for the deposition of thin film on substrate.

v. Film thickness and deposition Rate

The film thickness is depending on the growth rate and deposition duration proportionally. If the growth rate increases, the film thickness also increases having the same deposition time. Even the temperature at which epitaxy occurs is dependent on the deposition rate.

vi. Temperature of evaporation source

If the temperature of evaporation source increased uniformly, then the film is expected to be uniform. Else, it may not be uniform owing to sudden increase in temperature.

vii. Complexing agents

The concentration of the metal ions is controlled by the concentration of the complexing agent. The metal ion concentration decreases with concentration of the complexing ions. Even complexing agents has an impact on crystallinity of deposited film. Otherwise, other parameters such as deposition rate, thickness etc. may be affected.

References

- [1] Nemeec, P., Simurda, M., Nemeec, I., Formanek, P., Sprinzl, O., Trojanek, F., and Maly, P., *Phys. Stat. Sol. (a)*, vol. 205, pp. 2324-2329, 2008.
- [2] Ohring, M. (2002) *Material Science of thin films*. Academic Press, San Diego, CA, 2nd edition.
- [3] Chopra, K.L. (1969) *Thin Film Phenomena*. McGraw Hill, New York.
- [4] Brown, R., Maissel, L. I. and Glang, R. (1970) *Handbook of Thin Film Technology*. McGraw Hill, New York.
- [5] Aziz, M. J., “Film growth mechanism in pulsed laser deposition” *Appl. Phys. A: Mater. Sci. Proc.*, vol. 93(3), pp. 579-587, 2008.
- [6] Mukherjee, C., Rajiv, K., Gupta, P., Sinha, A. K., and Abhinandan, L., “Growth and characterization of high quality ZnS thin films by RF sputtering”, *AIP Conf. Proceedings*, vol. 1451, pp. 203, 2012.
- [7] Estaves, L. M., Oliveira, H. A., and Passos, F. B., “Carbon nanotube as catalyst support in chemical vapor deposition reaction: A review”, *J. Indu. Eng. Chem.*, vol. 65, pp.112, 2018.
- [8] Balzarotti, R., Cristiani, C., and Francis, L. F., “Spin-coating deposition on complex geometry substrate: Influence of operative parameters”, *Surf. Coat. Tech.*, vol. 330, pp. 1-9, 2017.
- [9] Shriven, L. E., “Physics and applications of dip coating and spin coating”, *Mater. Res. Society*, vol. 121, pp. 717, 1988.
- [10] Shin, S. W., Agawane, G. L., Gang, M. G., Moholkar, A. V., Moon, J. H., Kim, J. H., and Lee, J. Y., “Preparation and characterization of chemical bath deposition ZnS thin films: effect of different complexing agents”, *J. Alloys Compd.*, vol. 526, pp. 25-30, 2012.
- [11] Karimi, A., Sohrabi, B., and Vaezi, M. R., “Highly transparent flexible and hydrophilic ZnS thin film is prepared by facile and environmentally friendly chemical bath deposition method”, *Thin Solid Films*, vol. 651, pp. 97-110, 2018.
- [12] Murali, K.R., “Preparation of sol-gel dip coating ZnO thin film”, *J. Phys. Chem. Solids*, vol. 98, pp. 2293-2296, 2007.
- [13] Zhang, C., “High quality oriented ZnO film grown by sol-gel process assisted with ZnO seed layer”, *J. Phys, Chem. Solids*, vol. 71, pp. 364-369, 2010.
- [14] Hartnangle, H. L., Dawar, A. L., Jani, A. K., and Jagadis, C., “Semiconducting transparent thin films”, CRC Press, Bristol, (1995).

- [15] Zhang, Z., and Lagally, M. G., “Atomistic processes in the early stage of thin film growth”, *Science*, vol. 276, pp. 377-383, 1997.
- [16] Chopra, K. L., “Nucleation, growth and structure of films”, *Thin Film Phenomena*, McGraw Hill, New York, pp. 110-137, 1969.
- [17] Waugh M. R., “Characterization of transparent conducting thin film”, University Collage, London, 2011.
- [18] Tolman, R.C., “The effect of droplet size on surface tension”, *J. Chem. Phys.*, vol. 17, pp. 118, 1949.
- [19] Jensen, and Havlin, P., “A fractal model for the first stage of thin film growth” *Fractals*, vol. 4(3), pp.321-329, 1996.
- [20] Ratsch, C., and Venables, J.A., “Nucleation theory and the early stage of thin film growth”, *J. Vac. Sci. Technol. A*, vol. 21(5), pp. 99-109, 2003

THIN FILM CHARACTERIZATION TECHNIQUES

CHAPTER 3

THIN FILM CHARACTERIZATION TECHNIQUES

The deposited ZnS and Fe doped ZnS thin films are characterized for their surface morphological, structural, optical, electrical and magnetic properties. Scanning electron microscopy (SEM) is used to identify the surface morphology and energy dispersive X-ray (EDX) spectroscopy is used for the compositional study of the films. The nature and structural properties are studied from X-ray diffraction (XRD) of the film. The optical parameters are analyzed from the transmittance and absorbance spectrum obtained from UV-Visible spectrophotometer. The four-point probe technique is used for measuring electrical conductivity of the films. Vibrating Sample magnetometer (VSM) is used to study the magnetic property of the prepared films.

The principle, functioning and importance of each technique are described momentarily in this chapter with associated theory.

3.1 Surface morphology

Surface morphology is an advance form of high-resolution imaging that uses sophisticated microscopes to capture images of the samples and a split of image analyzing that cannot be seen through naked eye. Such images are captured from the bare surface of the samples, products and objects.

3.1.2 Scanning electron microscope

The scanning electron microscope is a sophisticated microscope that generates a variety of signals at the surface of solid specimens using a focused beam of high energy electrons. The signal of electron –sample interaction reveals information about the sample such as external morphology (texture), chemical composition, crystalline structure and orientation of the materials making up the sample. In scanning electron microscope, electrons are used instead of light to form an image of various objects such as featured metal compound, foreign particles, thin films electronic component, polymer, biological samples etc. The shorter wave length of electron allows image magnification from 0 to 100,000X, compared to about 2,000X for conventional optical microscopy.

In SEM, an electron beam is scanned across a sample surface. The electron beam is produced from a thermal emission source, such as a field emission cathode or a heated tungsten filament. The electron beam is generating a number of different types of signals; i.e. secondary electron, back scattered electrons, characteristics X-rays, light emitted from the area of the specimen where the electron beam is impinging, absorbed current and transmitted electrons.

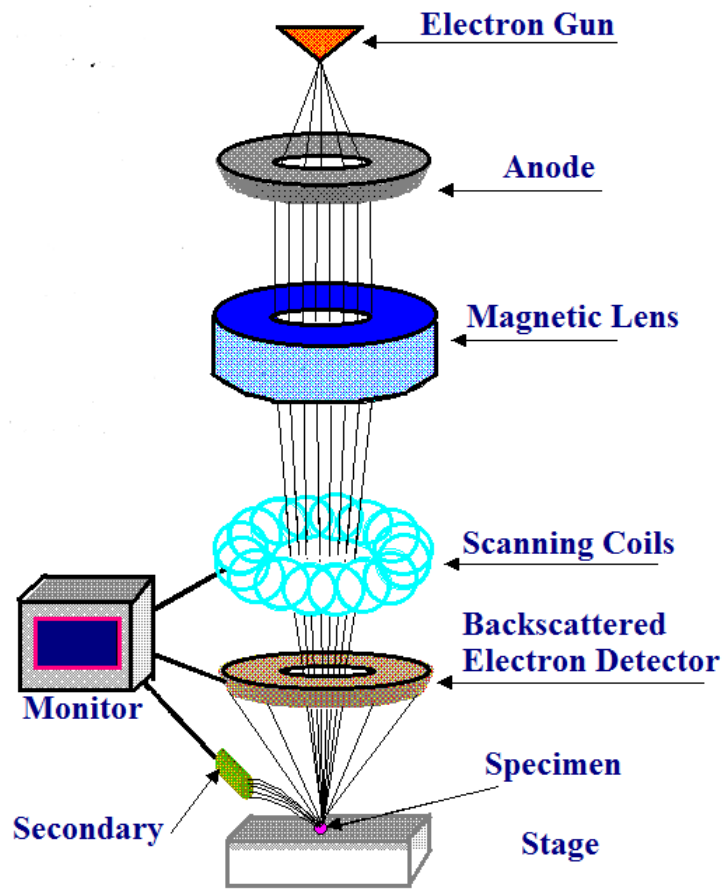


Figure 3.1: Schematic diagram of an electron microscope

In secondary electron imaging, the secondary electrons are emitted from very close to the specimen surface. Therefore, it can produce very high-resolution images of a sample surface and revealing details less than 1nm in size. Back-scattered electrons are beam electrons to be reflected from the sample by elastic scattering. They appear from deeper locations within the specimen and, accordingly, the resolution of these images is less than secondary electron images. On the other hand, back scattered electrons are often used in analytical SEM, along with the spectra made from the characteristic X-rays, because the intensity of the back scattered electron is strongly related to the atomic number (Z) of the specimen. Back scattered electron images can provide information about the distribution, but not the identity of different elements in the sample. The characteristic X-rays are emitted when the electron beam removes an inner shell electron from the sample, causing a higher-energy electron to fill the shell and release energy. The energy or wavelength of these characteristic X-rays can be measured by Energy-dispersive X-ray spectroscopy or Wavelength-dispersive X-ray spectroscopy and used to identify and measure the abundance of elements in the sample and map their distribution.

Due to the very narrow electron beam, SEM micrographs have a large depth of field yielding a characteristic three-dimensional appearance useful for understanding the surface structure of a sample. A wide range of magnifications is possible, from about 10 times to more than 500,000 times, about 250 times the magnification limit of the best optical microscopes.

The electron beam, has an energy ranging from 0.2 keV to 40 keV, is focused through one or two condenser lenses to a spot about 0.4 nm to 5 nm in diameter. The beam passes through pairs of scanning coils or pairs of deflector plates in the electron column, typically in the final lens, which deflect the beam in the x and y axes so that it scans in a raster fashion over a rectangular area of the sample surface.

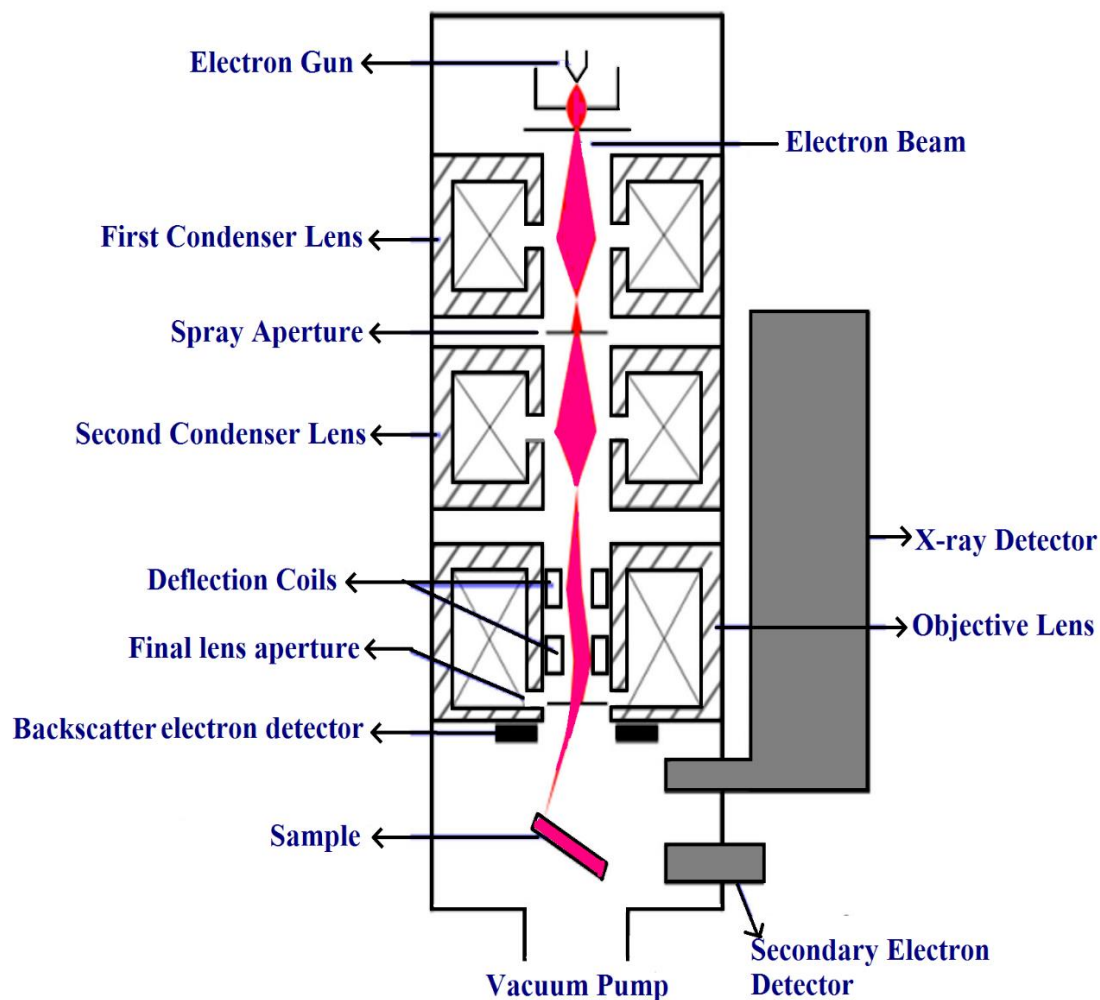


Figure 3.2: Schematic diagram of a scanning electron microscope

When the primary electron beam interacts with the sample, the electrons lose energy by repeated random scattering and absorption within a teardrop-shaped volume of the specimen known as the interaction volume, which extends from less than 100 nm to approximately 5 μm into the

surface. The size of the interaction volume depends on the electron's landing energy, the atomic number of the specimen and the specimen's density. The energy exchange between the electron beam and the sample results in the reflection of high-energy electrons by elastic scattering, emission of secondary electrons by inelastic scattering and the emission of electromagnetic radiation, each of which can be detected by specialized detectors. The beam current absorbed by the specimen can also be detected and used to create images of the distribution of specimen current. To amplify the signals electronic amplifiers of various types are used, which are displayed as variations in brightness on a computer monitor. Each pixel of video is synchronized with the position of the beam on the specimen in the microscope, and the significant image is appearing on computer monitor, therefore, a distribution map of the intensity of the signal being emitted from the scanned area of the specimen. In modern mechanism, the images are digitally captured and displayed on the computer monitor and also saved to a computer's hard disc.

A thermal field emission gun scanning electron microscope of model JEOL JSM- 7600F has been used in this research work to investigated the surface morphology of the films.

3.2 Elemental analysis

Elemental analysis is a process where a sample of some material is analyzed for its elemental and sometimes isotopic composition. This analysis performed through Energy Dispersive X-ray Spectroscopy (EDX).

3.2.1 Energy dispersive X-ray spectroscopy

Energy Dispersive X-ray Spectroscopy (EDX or XEDS), is also called energy dispersive X-ray analysis (EDXA) or energy dispersive X-ray micro analysis (EDXMA), usually used for the elemental analysis or chemical characterization of a sample. It works on the interaction of some source of X-ray and a specimen. A high-energy beam of charged particles such as electrons or protons, or a beam of X-rays, which focused into the sample being studied to stimulate the emission of characteristic X-ray from a specimen. The fundamental principle of this characterization is that each and every element has a unique atomic structure which allowing a unique set of peaks on its electromagnetic emission spectrum. Normally, an atom has unexcited or ground state electrons in discrete energy levels or electron shells bound to the nucleus. The incident beam may excite an electron from an inner shell and ejecting it from the shell while creating an electron hole. An electron from higher energy shell fills the hole and then the difference in energy between the higher and lower energy shell may release in the form of an X-ray.

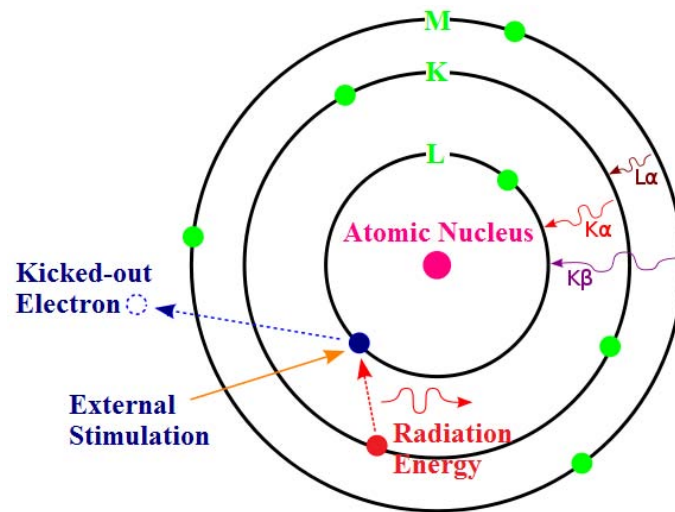


Figure 3.3: Principle of EDX analysis

EDS is also used to measure multi-layer coating thickness of metallic coatings and analysis of various alloys. The accuracy of this quantitative analysis of sample composition is affected by various factors. An EDX not only identifies the element corresponding to each of its peaks, but also the type of X-rays emitted by an electron in the L-shell electrons going to the K-shell is identified as a K-alpha peak. The peak corresponding to X-rays emitted by M-Shell electrons going to the K-Shell is identified as K-beta peak.

3.3 Structural characterization

The term structural encloses a variety of concepts, which describes on various scales, the arrangement of the building blocks materials. On an atomic scale, one deals with crystals structure, which is defined by the crystallographic data of the unit cell. These data contain the shape and dimension of the unit cell and the atomic position within its Bravais structure. They are obtained by diffraction experiment.

3.3.1 X-ray diffraction

X-ray diffraction (XRD) one of the oldest and effective technique for determining the structure of crystalline materials. It has long been used to address numerous issues related to the crystal structure of solids, including lattice constant and geometry, identification of unknown materials, orientation of single crystals, preferred orientation of polycrystals defects, stresses etc. It provides extensive information about the crystal structure whether the sample is single crystal or polycrystal, either with a random orientation or with a preferential orientation with respect to the film plane. X-rays are the electromagnetic waves and its wavelength $\sim 1-100 \text{ \AA}$. The wavelength of an X-ray is thus of the same order of magnitude as the lattice constant of crystals.

When X-rays are incident on a crystal surface, they are reflected from it.

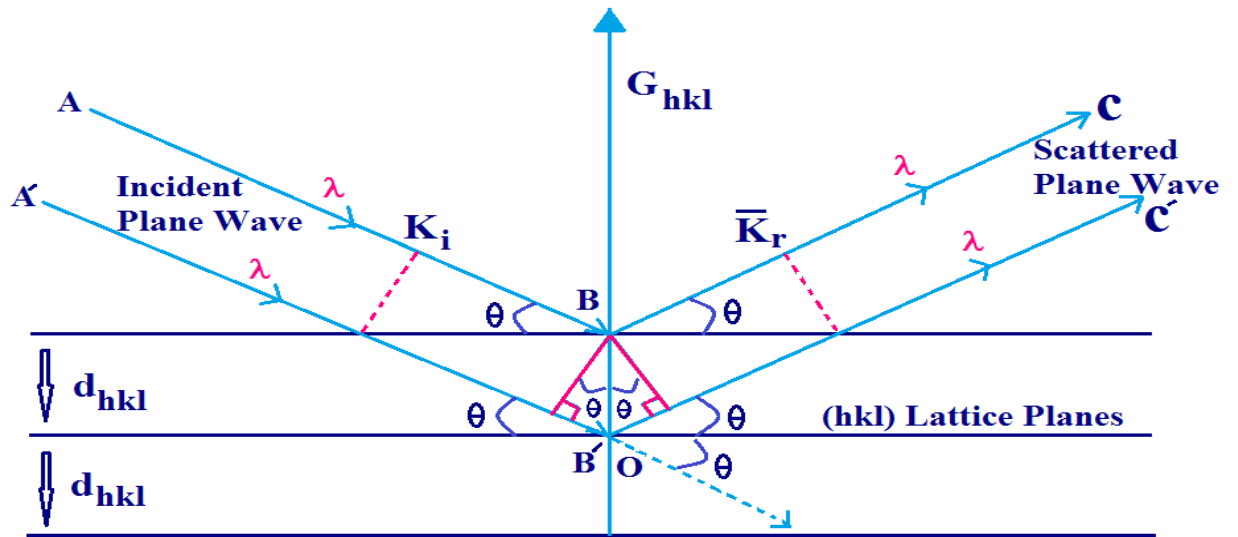


Figure 3.4: Bragg's law of X-ray diffraction

The reflection obeys Bragg's law as follows:

$$2d \sin \theta = n\lambda \quad (3.1)$$

where d is the distance between crystal plane, θ is the X-ray incident angle λ ; is the wavelength of the X-ray and n is the order of diffraction. Bragg's law also suggests that the diffraction is only possible when the following boundary condition is satisfied,

$$\lambda \leq 2d \quad (3.2)$$

Thin surface films, up to about 1000 Å thick, can be investigated using X-ray diffraction. Thicker films can be characterized by reflection high-energy electron diffraction (RHEED). Analysis of the diffraction patterns obtained by these techniques and comparison with standard ASTM data can reveal the existence of different crystallographic phases in the film, their relative abundance, lattice parameters and any preferred orientations. The interplanar spacing for the cubic system is given by,

$$d_{hkl} = \frac{a}{\sqrt{h^2+k^2+l^2}} \quad (3.3)$$

From the width of the diffraction line, it is possible to estimate the average grain size in the film [2]. The X-ray line broadening is commonly used to determine the crystallite size, which is given by

$$D = \frac{k\lambda}{\Delta \cos \theta} \quad (3.4)$$

Where D is the average grain size, λ is the wavelength of the radiation used as the primary beam of $\text{CuK}\alpha$ ($\lambda = 1.54178 \text{ \AA}$), θ is the peak position in degree and Δ is the full width at half maximum (FWHM) of the peak in radian. The dimensionless shape factor K has a typical value of about 0.9, but varies with the actual shape of the crystallite [3].

Using values, the set of lattice planes (h k l) are identified from standard data and the lattice parameters are calculated using the relations. The lattice parameter of cubic lattice can be determined by using the relation,

$$\frac{1}{d^2} = \frac{h^2 + k^2 + l^2}{a^2} \quad (3.5)$$

Where h, k and l are the incident of the crystal planes; d is the inter spacing and β is the full-width half maximum. The origin of the strain in thin film is related to misfit, which in turn depends upon deposition condition. The strain developed in the film is known as micro-strain (ϵ) and it is calculated using the relation, [4]

$$\epsilon = \frac{\beta \cos \theta}{4} \quad (3.6)$$

Dislocation is an imperfection in a crystal associated with the mis-registry of the lattice in one part of the crystal with that in another part. Unlike vacancies and interstitial atoms, dislocations are not equilibrium imperfection, i.e. thermodynamic considerations are insufficient to account for their existence in the observed densities. The dislocation density δ is the dislocation lines per unit area of the crystal, can also be evaluated from the crystallite size 'D' using the formula [5],

$$\delta = \frac{1}{D^2} \quad (3.7)$$

3.4 Optical characterization

The optical property of a semiconductor investigated from the observable facts namely transmission, reflection, absorption, refraction, polarization and interference etc.

From these facts it is possible to calculate optical acquaintances such as: absorption coefficient (α), refractive index (n), direct and indirect band gap, extinction coefficient (k) and optical conductivity (σ_{opt}), real and imaginary part of dielectric constant etc. The pure ZnS and Fe:ZnS thin films absorbance and transmittance were measured by using a double beam UV-Vis spectrophotometer (Shimadzu Corporation, UV-2600, Japan) in the wavelength range of 300-1000 nm at room temperature. The samples were placing in the incident beam and raw glass substrate in the reference beam of the instrument for the measurement. The transmission spectra were recorded for the pure ZnS and ZnS:Fe thin films from 5 to 15 at. %. The optical properties of films have been studied extensively because of their applications in various optical and optoelectronic devices. Optical properties of a solid originate from its interactions with electromagnetic waves and are manifested in optical frequencies. The effect of such interaction in the audio frequency region results in the dielectric behavior, optical frequencies and optical behavior.

3.4.1 Beer-Lambert law

The Beer-Lambert law (or Beer's law) is the linear relationship between absorbance and concentration of an absorbing species [6]. The general Beer-Lambert law is usually written as:

$$A = \alpha bc \quad (3.8)$$

Where A is the measured absorbance, $\alpha(\lambda)$ is a wavelength-dependent absorbance coefficient, b is the path length, and c is the analyzed concentration. When molarity is the unite of concentration, the Beer-Lambert law is written as,

$$A = \epsilon cb \quad (3.9)$$

Where ϵ is the wavelength-dependent molar absorptive coefficient and its unit is $M^{-1}cm^{-1}$. Experimental measurements are usually made in terms of transmittance (T) and is defined as,

$$T = \frac{I}{I_0} \quad (3.10)$$

Where, I_0 is the initial light intensity and I is the intensity of light when it passes through the sample. The relation between A and T is,

$$A = -\log T = -\log \left(\frac{I}{I_0} \right) \quad (3.11)$$

3.4.2 Derivation of Beer-Lambert law

The Beer-Lambert law can be derived from an approximation for the absorption coefficient for a molecule by approximating the molecule by a solid disk, whose cross-sectional area is σ , represents the effective area seen by a photon of frequency ν . If the frequency of the light is far from resonance, the area is approximately 0 and if ν is close to resonance the area is a maximum. Taking an infinitesimal slab, dz , of sample Fig. 3.5.

I_0 is the intensity of light that entering the sample at $z = 0$, I_z , is the intensity of light entering the infinitesimal slab at z , dI is the intensity absorbed in the slab, and I is the intensity of light leaving the sample. Then, the total solid area on the slab due to the absorbers will be $\sigma N A dz$. Then the fraction of photons that absorbed will be $\sigma N A dz/A$ so,

$$\frac{dI}{I_z} = -\sigma N dz \quad (3.12)$$

Integrating this equation from $z=0$ to $z=b$ gives,

$$\begin{aligned} \ln I - \ln I_0 &= -\sigma N b \\ -\ln \left(\frac{I}{I_0} \right) &= \sigma N b \end{aligned}$$

Since N (molecules/cm³) \times (1 mole/ 6.023×10^{23} molecules) \times 1000 cm³/liter = c (moles/liter) and $2.30 \log(x) = \ln(x)$ then,

$$\begin{aligned} -\log \left(\frac{I_0}{I} \right) &= -\sigma \left(\frac{6.023 \times 10^{20}}{2.303} \right) cb \\ \text{or, } \log \left(\frac{I_0}{I} \right) &= A = \epsilon cb \end{aligned} \quad (3.13)$$

Where, $\epsilon = \sigma \left(\frac{6.023 \times 10^{20}}{2.303} \right) = \sigma (2.61 \times 10^{20})$ and ϵ is a constant of proportionality, called the absorptivity.

The equation can be written as,

$$I = I_0 e^{-\alpha d} \quad (3.14)$$

Here,

$$\alpha = \frac{2.303A}{d} \quad (3.15)$$

Where, α is the absorption coefficient, A is the absorbance, and d is the thickness of the material.

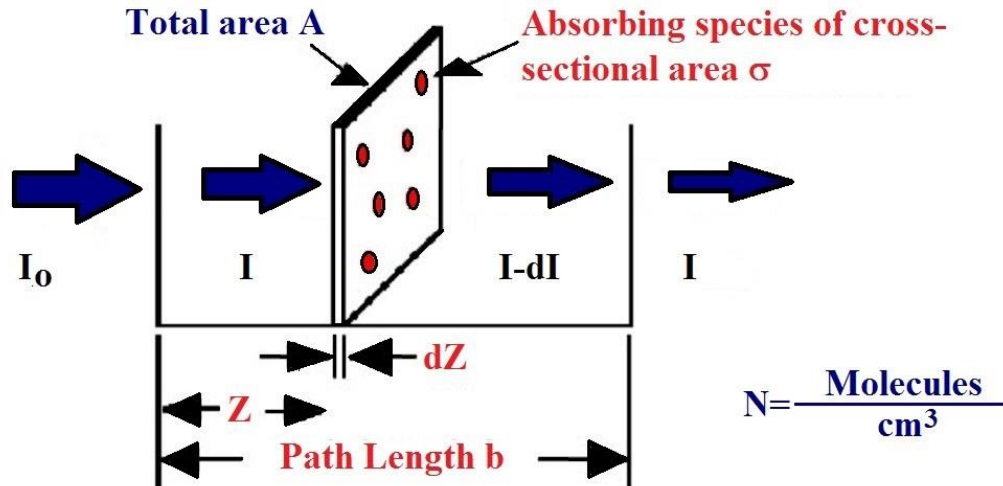


Figure 3.5: Absorption of light by a sample [5]

3.4.3 Electronic Transition

The absorption of UV or visible radiation corresponds to the excitation of outer electrons. There are three types of electronic transition which can be considered:

1. Transitions involving π , σ and n electrons
2. Transitions involving charge transfer electrons
3. Transitions involving d and f electrons

When an atom or molecule absorbs energy, electrons are promoted from their ground state to an excited state. In a molecule, an atom can rotate and vibrate with respect to each other. These rotation and vibrations also have discrete energy levels, which can be considered as being packed on top of each electronic level Fig. 3.6.

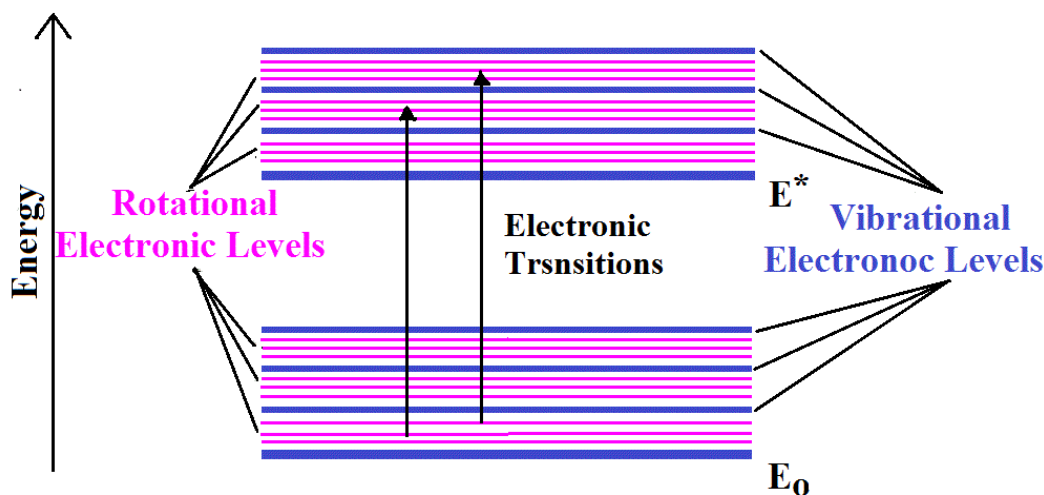


Figure 3.6: Vibrational and rotational energy

Absorbing species containing π , σ and n electrons

Absorption of ultraviolet and visible light radiation in organic molecules is restricted for certain functional groups (chromospheres) that containing valence electrons of low excitation energy. The spectrum of a molecule containing these chromospheres is complex. This is because the superposition of rotational and vibrational transitions on the electronic transitions gives a combination of overlapping lines. This appears as continuous absorption band. Possible electronic transitions of π , σ and n electrons are showed in Fig. 3.7.

$\sigma \rightarrow \sigma^*$ Transition

An electron in a bonding σ orbital is excited to the corresponding antibonding σ^* orbital. The energy required is large. For example, methane (which has only C-H bonds, and can only undergo $\sigma \rightarrow \sigma^*$ transitions) shows an absorbance maximum at 125 nm. Absorption maxima due to $\sigma \rightarrow \sigma^*$ transition is not seen in typical UV-Vis. Spectra (200-700 nm).

$n \rightarrow \sigma^*$ Transition

Saturated compounds containing atoms with lone pairs (non-bonding electrons) are capable of $n \rightarrow \sigma^*$ transitions. These transitions usually need less energy than $\sigma \rightarrow \sigma^*$ transitions. They can be initiated by light whose wavelength is in the range 150-250 nm. The number of organic functional groups with $n \rightarrow \sigma^*$ peaks in the UV region is small.

$n \rightarrow \sigma^*$ and $\pi \rightarrow \pi^*$ Transition

Most absorption spectroscopy of organic compounds is based on transitions of n or π electrons to the π^* excited state. This is because the absorption peaks for these transitions fall in an

experimentally convenient region of the spectrum (200-700nm). These transitions need an unsaturated group in the molecule to provide the π electrons.

Molar absorptivity from $n \rightarrow \sigma^*$ transitions are relatively low, and range from 10 to 100 $\text{L}^{-1} \text{mol}^{-1} \text{cm}^{-1}$. $\pi \rightarrow \pi^*$ transitions normally give molar absorptivity between 1000 and 10,000 $\text{L}^{-1} \text{mol}^{-1} \text{cm}^{-1}$. The solvent in which the absorbing species is dissolved also has an effect on the spectrum of the species. Peaks resulting from $n \rightarrow n^*$ transitions are shifted to shorter wavelengths (blue shift) with increasing solvent polarity. This arises from increase of the lone pair, which lowers the energy of the n orbital. Often, the reverse i.e. red shift is seen for $\pi \rightarrow \pi^*$ transitions. This is caused by attractive polarization forces between the solvent and the absorber, which lower the energy levels of both the excited and unexcited states. This effect is greater for the excited state, and so the energy difference between the excited and unexcited states is slightly reduced—resulting in a small red shift. This effect is also influencing $n \rightarrow \pi^*$ transitions but is overshadowed by the blue shift resulting from the increase of lone pairs.

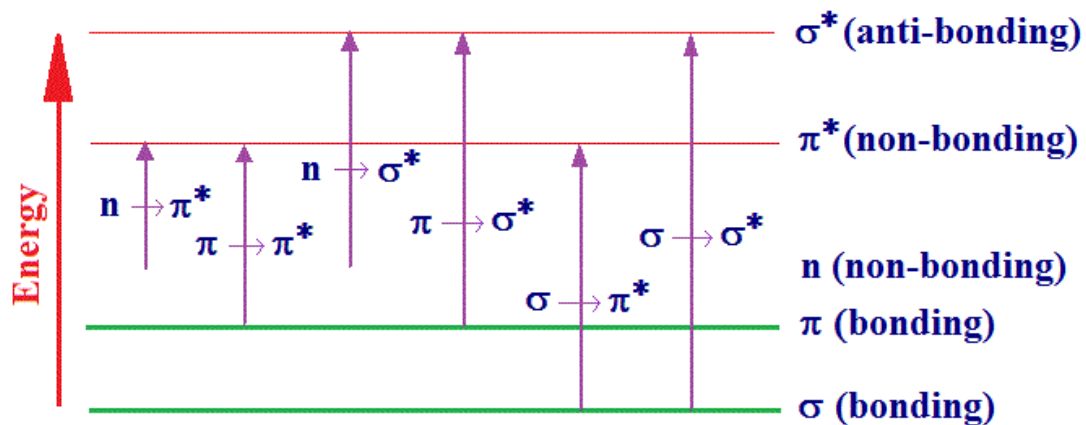


Figure 3.7: Possible electronic transition

i. Direct and indirect optical transition

Bandgap is an energy range where no electron states exist. In solid state physics, band gap is also called an energy gap. For insulators and semiconductors, the band gap usually refers to the energy difference between the top of the valence band and the bottom of the conduction band. It is the energy mandatory to promote a valence electron bound to an atom to become a conduction electron, which is free to move within the crystal lattice and provide as a charge carrier to conduct electric current.

For semiconductor materials, the band gap is of two types, a direct band gap or an indirect band gap. The minimal-energy state in the conduction band and the maximal-energy state in the valence

band are each characterized by a certain crystal momentum (k-vector) in the Brillouin zone. If the k-vectors are the same, it is called a “direct gap”. If they are different, it is called an “indirect gap”. The direct and indirect band gap of a material can be determined from the “Tauc” relation. The relation is given below,

$$\alpha h\nu = A(h\nu - E_g)^n \quad (3.16)$$

Where $h\nu$ is the energy of absorbed light, A is a constant or Tauc parameter depending upon the transition probability for direct transitions, $n=1/2$ and $n=2$ for indirect transition. E_g is optical band gap [7].

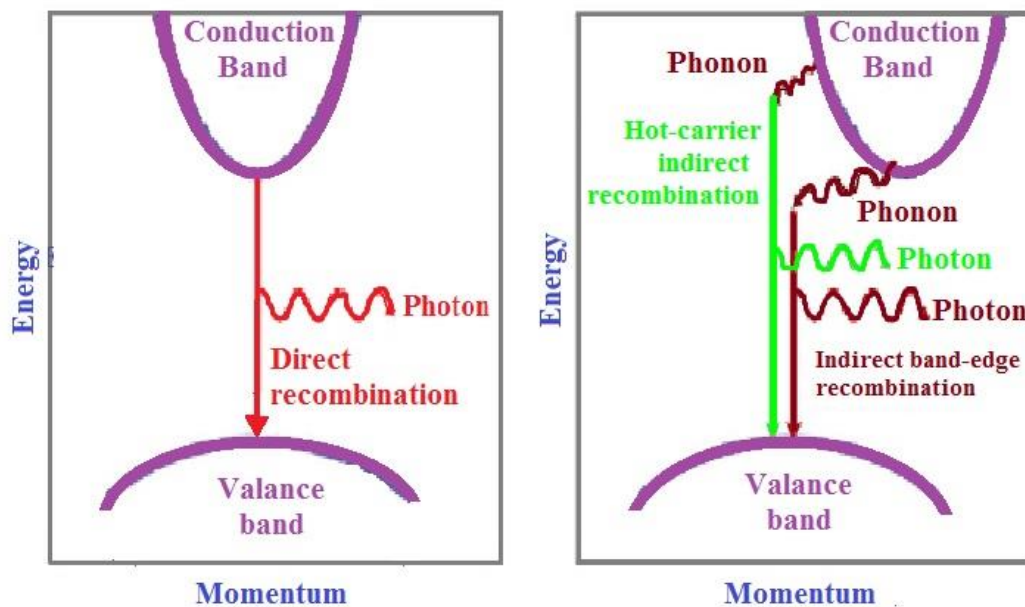


Figure 3.8: Schematic presentation of direct and indirect transition between valence and conduction band

ii. Refractive index and extinction coefficient

Refractive index is one of the most important optical constants of a material, which in general depends on the wavelength of the electromagnetic wave, through a relationship called dispersion. In optics it is a dimensionless number which describes how light propagates through any medium. It is defined as,

$$n = \frac{c}{v} \quad (3.17)$$

Here, n is the refractive index, c is the speed of light and v is the phase velocity of light in the medium. Refraction of light at the interface of two media of different refractive indexes n_1 and n_2 , shown in the Fig. 3.8.

The real part is usually the refractive index (n) and the imaginary part is called the extinction coefficient (k). In this section, n and k will be presented in detail along with some common dispersion relations. The refractive index is the ratio of velocity of light (c) in vacuum to its velocity v in the medium, $n=c/v$. Using the Maxwell's equation's, one obtains the well-known Maxwell's formula for refractive index of the substance as $n = \sqrt{\epsilon\mu_r}$ where ϵ is the static dielectric constant or relative permittivity and μ_r the relative permeability. As $\mu_r = 1$ for nonmagnetic substance, one gets, $n = \sqrt{\epsilon}$, which is very useful in relating the dielectric properties to optical properties of materials at any particular frequency of interest. As ϵ depends on the wavelength of light, n also depends on the wavelength of light, and this dependence is called dispersion. In addition to dispersion, an electromagnetic wave propagating through a medium experience's attenuation, which means it loses its energy, due to various loss mechanisms such as generation of phonons, photo generation, free carrier absorption, scattering, etc.

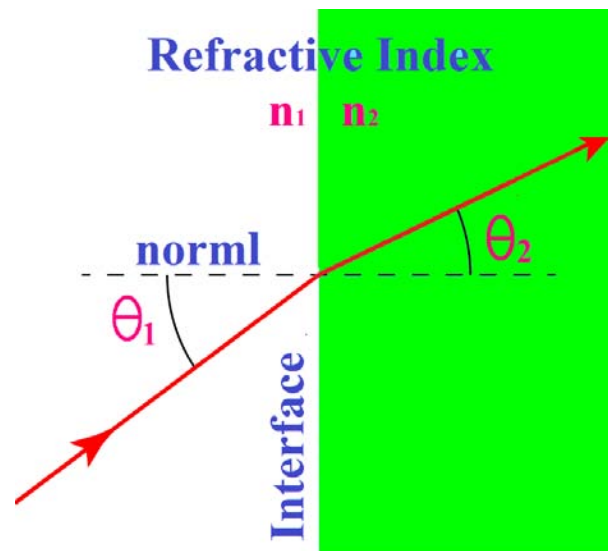


Figure 3.9: Refraction of light at the interface between two media of different refractive indices. In such materials, the refractive index becomes a complex function of the frequency of the light wave. The complex refractive index, denoted by n^* , with real part n , and imaginary part k , called the extinction coefficient, is related to the complex relative permittivity (ϵ) by:

$$n^* = n - jk = \sqrt{\epsilon} = \sqrt{(\epsilon_r - j\epsilon_i)} \quad (3.18)$$

Where ϵ_r and ϵ_i , are the real and imaginary parts of ϵ respectively. Equation gives

$$n^2 - k^2 = \epsilon_r \text{ and } 2nk = \epsilon_i \quad (3.19)$$

In explicit terms, n and k can be obtained as:

$$n = \sqrt{\frac{1}{2} [\sqrt{(\epsilon_r^2 + \epsilon_i^2)} + \epsilon_r]} \quad (3.20)$$

$$k = \sqrt{\frac{1}{2} [\sqrt{(\epsilon_r^2 + \epsilon_i^2)}]} \quad (3.21)$$

The optical constants n and k can be determined by measuring the reflectance from the surface of a material as a function of polarization and the angle of incidence. For normal incidence, the reflection coefficient, r , is obtained as

$$r = \frac{(1 - n^*)}{(1 + n^*)} = \frac{1 - n + jk}{1 + n + jk} \quad (3.22)$$

The reflectance R is then defined by

$$R = |r|^2 = |(1 - n + jk)/(1 + n + jk)|^2 = \{(1 - n)^2 + k^2\}/\{(1 + n)^2 + k^2\} \quad (3.23)$$

And refractive index can be calculated by using following equation

$$n = \left(\frac{1 + R}{1 - R} \right) + \sqrt{\frac{4R}{(1 - R)^2} - k^2} \quad (3.24)$$

Notice that whenever k is large, for example over a range of wavelength, the absorption is strong, and the reflectance is almost united. The light is then reflected and any light in the medium is highly attenuated. Extinction coefficient can be determined from the relation as follows,

$$k = \frac{\alpha\lambda}{4\pi} \quad (3.25)$$

Optical conductivity of thin films is calculated by using the following equation,

$$\sigma_{opt} = \frac{\alpha nc}{4\pi} \quad (3.26)$$

Where, c is the speed of light in vacuum [8].

iii. Absorption coefficient

When a semiconductor is illuminated by a light, a photon strikes the surface, a fraction of photons is reflected and the remaining photons enter the semiconductor. Some of these are absorbed within the semiconductor and the remainder transmitted into the semiconductor. The absorption of radiation by any medium occurs through the excitation of electrons and photons. For semiconductor, it is convention to consider several types of absorption arising from

- I. Electronic transitions within energy band
- II. Electronic transition between different energy bands
- III. Electronic transitions to localized states of impurity atoms
- IV. Lattice vibrations
- V. Vibrations of impurity atoms

In the fundamental absorption region, the transmission T is given by

$$T = A \exp\left(\frac{4\pi kt}{\lambda}\right) \quad (3.27)$$

Where 'A' is a constant, 'k' is the extinction co-efficient and 't' is the thickness. For $k^2 \ll n^2$ the principle variation of T occurs in the exponential term and pre-exponential term A. Therefore

$$T \approx \exp(\alpha t) \quad (3.28)$$

Where, $\alpha = 4\pi k/\lambda$, is the absorption co-efficient of the film. Thus, the value of absorption co-efficient may be calculated from the relation

$$\alpha = -\frac{\ln T}{t} \quad (3.29)$$

3.5 Thickness measurement of thin film

Film thickness is defined as the depth of the coating applied. This can be consisting of a single layer or multiple layers. Film thickness is also defined as the perpendicular distance between any point of the surface to the other end of the film. It is one of the most important parameters and has a significant role in the properties of thin film. Therefore, the film thickness should be measured very carefully to get the possible accurate value. There are several procedures for thin film thickness measurement, for instance, stylus profiler technique, weighting, X-ray fluorescence and multiple-beam interferometer technique [9].

Multiple-beam interferometer technique is employed for the measurement of thickness of the thin films. Currently, it is a well-developed and standard method [10]. In this method two reflecting surface are brought into close proximity to produce interference fringes. When two reflecting surfaces brought into close proximity, interference fringe are produced, the measurement of which make possible a direct determination of film thickness and surface topography with high accuracy. In this method two types of fringes are utilized for thickness measurement.

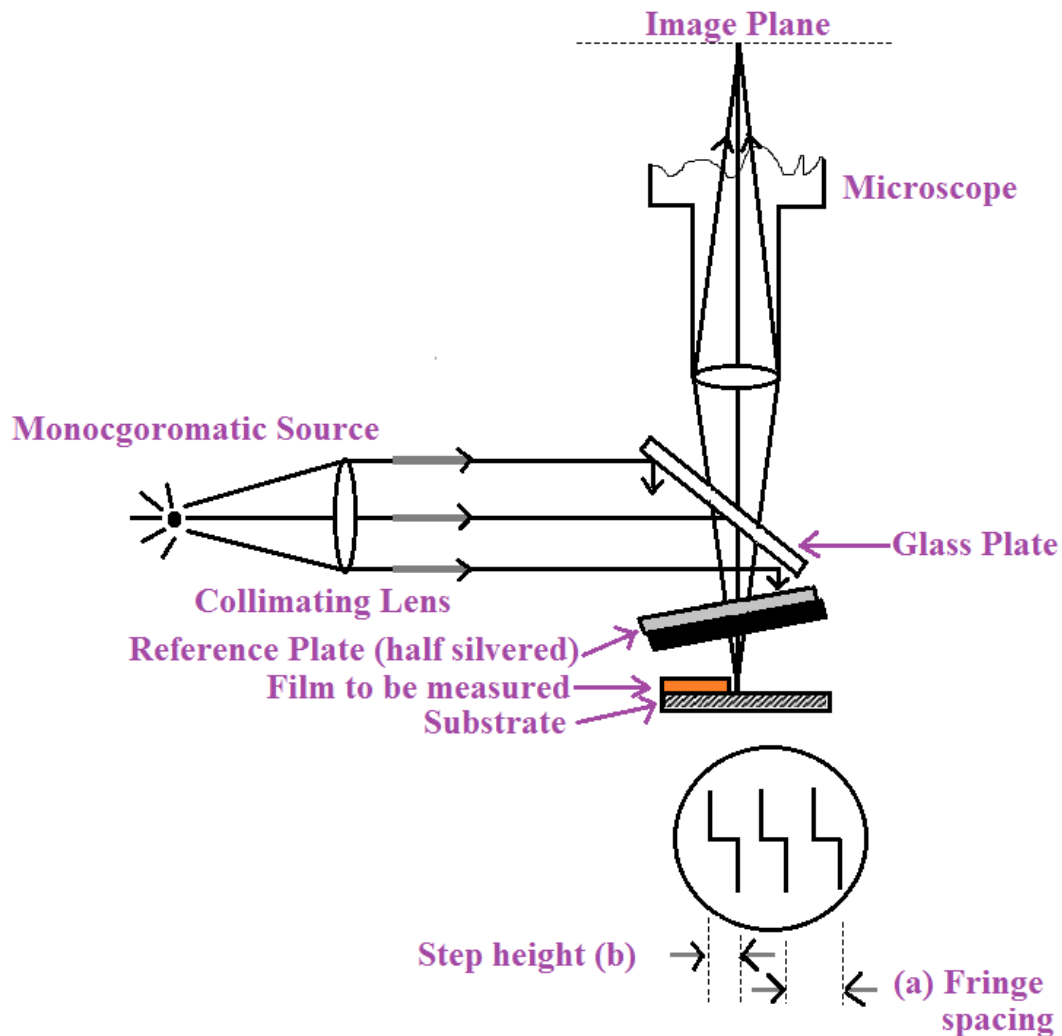


Figure 3.10: Interferometer arrangement for producing reflection Fizeau fringes of equal thickness

The first produces Fizeau fringes of equal thickness by using a monochromatic light source. The second produces fringes of equal chromatic order by using a light source. The second method is used for thinner films. In the present work Fizeau fringes method is used for thickness measurement. For the experimental arrangement a low power microscope, a monochromatic

source of light, a glass plate and an interferometer are required. To make the Fizeau fringes of equal thickness visible in a multiple beam interferometer formed by a thin absorbing film on a glass substrate, generally an auxiliary reflecting coating on the film surface is required. But if the experimental sample is transparent with a very smooth surface on such auxiliary coating is necessary.

The thin film sample is placed into a holder and another plane glass substrate placed over it Fig. 3.11. This is illuminated with a parallel monochromatic beam of light a fringe system is produced and is viewed with low power microscope. The fringe spacing and fringe displacement across the steps are measured and used to calculate the film thickness. The thickness of the film “d” can be determined through the relation,

$$d = \frac{\lambda}{2} \times \frac{b}{a} \quad (3.30)$$

Where,

λ =wavelength

b=step height

a=fringe spacing

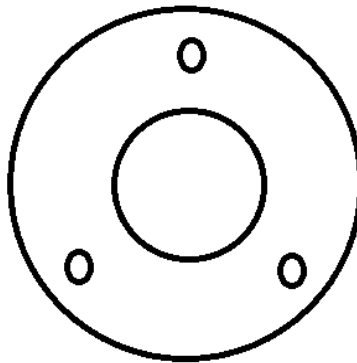


Figure 3.11: Substrate holder of interferometer

In general, the sodium light is used, for which $\lambda = 5893\text{\AA}$. Fig. 3.10 shows the schematic diagram of multiple beam interferometer thickness measurement method.

3.6 Electrical characterization

Electrical characterization of a semiconductor involves measurement of the resistivity (ρ). Various models and methods have been suggested to measure the electrical resistance (R) or resistivity (ρ) and ρ is the key physical property of all materials. There are four methods used for the measurement of resistivity such as:

- i. Direct method
- ii. Two probe method
- iii. Four probe method
- iv. Van der pauw method

Some of these methods are discussed in the following section.

3.6.1 Direct Method

The resistivity of a thin film can be measured easily by using direct method

$$\rho = R \frac{wt}{L} \quad (3.31)$$

Where, w and t are the breath and thickness of the sample. For simplicity, if we consider w=L, the above equation becomes,

$$\rho = Rt \quad (3.32)$$

Electrical conductivity of a material is reciprocal of resistivity of the material. Conductivity is denoted by σ and defined as,

$$\sigma = \frac{1}{\rho} \quad (3.33)$$

Measuring the resistance, R and thickness, t one can easily determine the resistivity and the conductivity.

3.6.2 Two Point Probe Method

This is the simplest method of measuring resistivity. In this method, voltage drop v across the sample and current through the sample I are measured. Then the resistivity is given us

$$\rho = \frac{vA}{IL} \quad (3.34)$$

When any two surface or wires come into physical contact with each other, the contact is never perfect. So that current experiences a significant resistance as it tries to flow from one contacting surface to the next. The resistance is simply referred as “contact resistance” and denote as R_c . The wire use to connect the sample also have finite resistance even the manner in which the voltmeter is connected to the two-prober measurement caused the potential drop.

So, if the resistance of the sample is R_s and the current in the circuit is I, the potential drop measured by the voltmeter is,

$$V = IR_c + IR_s + IR_c \quad (3.35)$$

The contact resistance term appears twice, because contacts have to be made on either side of the sample.

This probe measurement will not be very reliable or reproducible because they will depend so sensitively on the small sample of material at the electrode tips.

3.6.3 Four Point Probe Method

The most common way of measuring resistivity of a semiconductor material is by using a four-point co-linear probe with equal spacing. Two outer probes are used for sourcing current (I) and the two inner probes are used for measuring the voltage drop (V) across the surface of the sample.

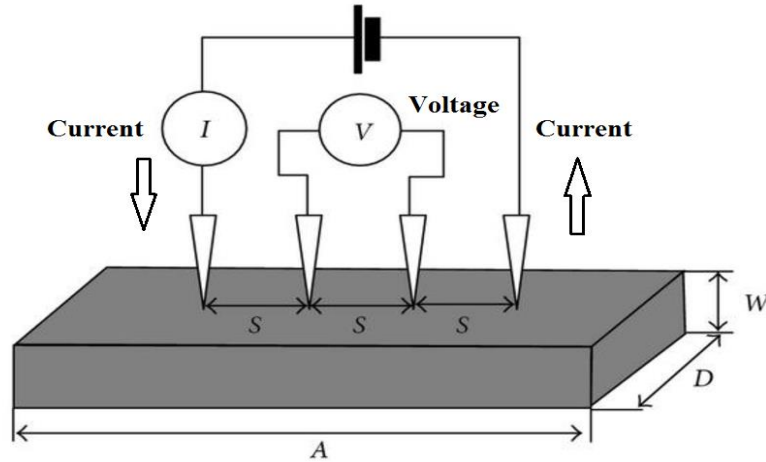


Figure 3.12: Four-point probe resistivity test circuit

Here the two inside current points represent the dipole.

The resistivity of a sample, relatively large compared to the probe spacing can be estimated from the following equation,

$$\rho = \frac{V}{I} \left[\frac{2\pi}{\frac{1}{s_1 + s_2} - \frac{1}{s_1 + s_2} - \frac{1}{s_2 + s_3}} \right] \quad (3.36)$$

Where, s_1 , s_2 and s_3 are the probe spacing, ρ is the resistivity in $\Omega\text{-cm}$. When the probes are equally spaced i.e., $s_1 = s_2 = s_3 = s$, then equation (3.36) becomes,

$$\rho = \frac{V}{I} 2\pi s \quad (3.37)$$

Here is the distance between all the four points is equal. 'I' is the current flowing through the sample, V is produced voltage across two inner points and s is the distance between the adjacent points [11,12].

But in case of thin metallic films, the electrical resistivity (ρ) of the film, whose length is much longer than its thickness can be expressed as,

$$\rho = \frac{\pi}{\ln 2} \frac{V}{I} \times d \quad \text{or} \quad \rho = 4.532 \left(\frac{V}{I}\right) \times d \quad (3.38)$$

Knowing the value of ρ and thickness of the films d , the sheet-resistance (surface resistance) can be determined [13] according to the following equation,

$$R_s = \frac{\rho}{d} \quad (3.39)$$

This technique has limitation, however for as more highly resistive materials are examined the point contact are incapable of supplying current that are high enough to make ΔV readily measurable. The necessary input resistance between the inner probes becomes very high. The practical upper limit of resistivity that can be measured by the four-probe technique is about $10^8 \Omega\text{m}$.

3.6.4 Van Der Pauw method

The van der pauw method is widely used in the semiconductor industry to determine the resistivity of sample because of its convenient [14]. This method is applicable when the sample fulfilled the following conditions:

- I. The contacts are on the circumference of the sample
- II. The contacts are sufficiently small
- III. The sample is homogeneous in thickness
- IV. The surface of the sample singly connected. i.e. the sample does not have isolated holes.

Most semiconductor samples satisfy these conditions, so that this convenient measurement method has been widely utilized.

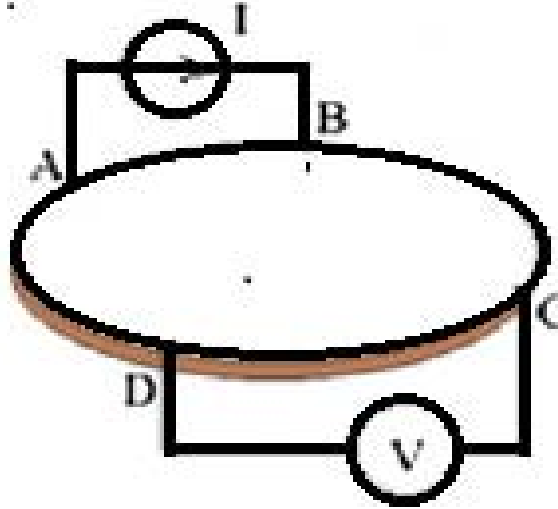


Figure 3.13: Ven der pawn method

Fig. 3.13 shows the experimental arrangements for measuring resistivity by using Van der pauw method. Consider an arbitrary shape completely free of holes sample and provide it with four small contacts. A, B, C and D, at arbitrary place on the periphery. Silver paste or indium was used to the contact. If a current I_{AB} applied to contact A and take it off at contact B. We measured the potential difference $V_p - V_o$ and define,

$$R_{AB,CD} = \frac{V_D - V_C}{I_{AB}} \quad (3.40)$$

Analogously we defined,

$$R_{BC,DA} = \frac{V_A - V_D}{I_{BC}} \quad (3.41)$$

Van der Pauw method is based on a simple relation between $R_{AB,CD}$ and $R_{BC,DA}$, i.e.

$$\exp\left(-\frac{\pi d}{\rho} R_{AB,CD}\right) + \exp\left(-\frac{\pi d}{\rho} R_{BC,AD}\right) = 1 \quad (3.42)$$

Where, d is the thickness of the sample and ρ is the resistivity. If d and resistance $R_{AB,CD}$ and $R_{BC,AD}$ are known then ρ is the only unknown quantity of the above equation yield.

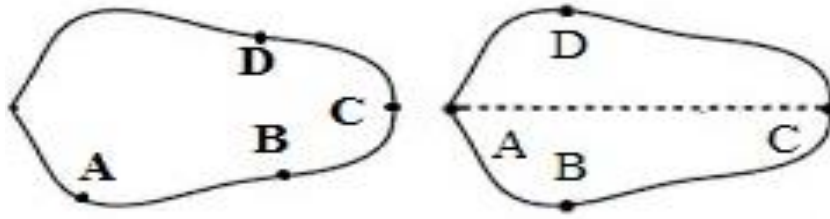


Figure 3.14: (a) Arbitrary point consideration (b) considering symmetry line

The situation is particularly easy if the sample possesses a line of symmetry. In that case, A and C are placed on the line of symmetry, while B and D are disposed symmetrically with respect to this line. Then

$$R_{BC,DA} = R_{AB,CD} \quad (3.43)$$

Which is seen in Fig. 3.14 (b). From the reciprocity theorem for passive four poles,

$$R_{BC,DA} = R_{DA,BC} \quad (3.44)$$

And it follows from symmetry that

$$R_{DA,BC} = R_{AB,CD} \quad (3.45)$$

Hence, we arrive at second equation: ρ can be obtained from first equation,

$$\rho = \frac{2\pi d}{\ln 2} R_{AB,CD} \quad (3.46)$$

3.7 Vibrating sample magnetometer

The vibrating sample magnetometer (VSM) works on Faraday's law of induction, which tells us a change in magnetic field will produce an electric field. This electric field can be measured and can tell us about the change in magnetic field. VSM is used to measure the magnetic behavior of magnetic material [15]. A 'VSM' operates by first placing the sample to be studied in a constant magnetic field. If the sample is magnetic, this constant magnetic field will magnetize the sample by aligning the magnetic domains, or the individual magnetic spin, with the field. The stronger the constant field, the larger will be the magnetization.

The magnetic dipole moment of the sample will create magnetic field around the sample, which is sometimes called magnetic stray field. As the sample is moved up and down, this magnetic stray field is changing as a function of time and can be sensed by a set of pick-up coils. The alternating

magnetic field will cause proportional electric field in the peak-up induction. This current will be proportional to the magnetization of the sample. The greater the magnetization, the greater induced current. The induced current is amplified by a transimpedance amplifier. By using controlling and monitoring software, the system can tell us how much the sample is magnetized and how it depends on the strength of the constant magnetic field.

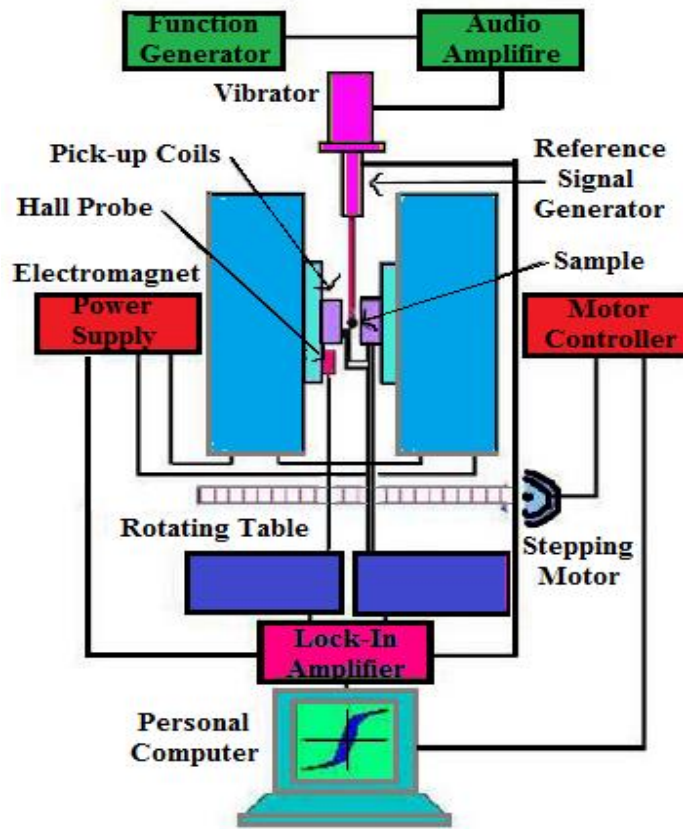


Figure 3.15: Vibrating sample magnetometer characterization arrangement

Components of vibrating sample magnetometer are as follows:

- i. Electromagnet
- ii. Power supply
- iii. Vibrating system
- iv. Signal generator
- v. Lock-in-amplifier
- vi. Hall probe
- vii. PID regulator
- viii. PC or XY recorder

Water cooled electromagnet, along with the power supply, generate constant magnetic field used to magnetized the sample. the sample holder rod attached to a transducer and the end of it hangs down in between the pole pieces. The transducer moves the sample up and down at a set frequency typically 85Hz. The sample rod can be rotated to archive the desired orientation of the sample to the constant magnetic field. There are also three knobs for controlling the x, y and z position of the sample. The sample producing an alternating current in the sensor coils at the same frequency as the vibration of the sample. The signal generator contains the information about the magnetization of the sample. The amplifier just amplifies the signal created by the sensor coil. The lock in amplifier is tuned to pick up only signals at the vibrating frequency.

Hall probe creates the magnetic field and PC or XY-recorder collect the data and can be graphed or plotted on the printer [16]. In this work, MicroSense EasyVSM Software Version 9.1Wa was used for analyzing magnetic property.

3.7.1 Hysteresis Loop

Hysteresis loop is a closed curve shows the variation of magnetic flux density of a ferromagnetic material with the external magnetic field producing it, when this field is changed through a complete cycle.

When a ferromagnetic material is magnetized in one direction, it will not relax back to zero magnetization when the imposed magnetizing field is removed. It must be driven back to zero by a field in the opposite direction. If an alternating magnetic field is applied to the material, its magnetization will trace out a loop called a hysteresis loop.

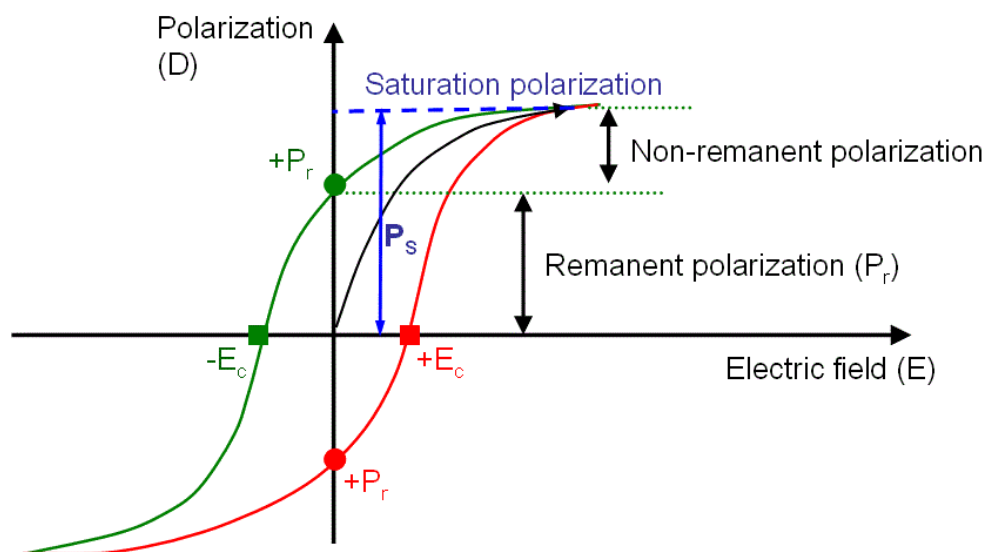


Figure 3.16: Schematic diagram of a hysteresis loop [16]

The lack of retractability of the magnetization curve is the property called hysteresis and it is related to the existence of magnetic domains in the material. Once the magnetic domains are reoriented, it takes some energy to turn them back again. This property of ferromagnetic materials is useful as a magnetic "memory". Some compositions of ferromagnetic materials will retain an imposed magnetization indefinitely and are useful as "permanent magnets". The magnetic memory aspects of iron and chromium oxides make them useful in audio tape recording and for the magnetic storage of data on computer disks. Magnetism is caused by the motion of electric charges. Every substance is made up of atoms. This makes the atoms in these substances strongly magnetic but they are not yet magnets. To become magnetized, another strongly magnetic substance must enter the magnetic field of an existing magnet. Also, the magnetism of metals and other materials are determined by the orbital and spin motions of the unpaired electrons and the way in which unpaired electrons align with each other.

References

- [1] Knag, S. J., Joung, Y. H., and Yoon, Y. S., “Effect of substrate temperature on structural, optical and electrical properties of ZnO thin films deposited by pulsed laser deposition”, *J.Matter. Sci.:Mater. Electron*, vol. 1, pp. 1073-1078, 2008.
- [2] Long, F., Wang, W., Cui, Z., Fan, L., Zou, Z., and Jai, T., “An improved method for chemical bath deposition of ZnS thin films”, *Chem. Phys. Letts.*, vol. 462, pp. 84-87, 2008.
- [3] Cullity, B. D. (1959) *Elements of X-ray Diffraction*, Addison-Wesley Publishing Company. Inc, U. S. A.
- [4] Zhao, Y., and Zhang, J., “Micro strain and grain size analysis from diffraction peak width and graphical derivation of high-pressure thermomechanics”, *J. Appl. Cryst.*, vol. 41, pp. 1095-1108, 2008.
- [5] Szekely, F., Groma, I., and Lendvai, J., “Characterization of self-similar dislocation structures by X-ray diffraction”, *Mater. Sci. Engi., A*, vol. 324, pp. 179-182, 2002.
- [6] Swinehart, D. F., “The Beer-lambert law”, *J. Che. Edu.*, vol. 39(7), pp. 333-335, 1962.
- [7] Davis, E.A., and Mott, N. F., “conduction in non-crystalline system, optical absorption and photoconductivity in amorphous semiconductor”, *Philos. Mag.*, vol. 22, pp. 903-922, 1970.
- [8] Singh, J., “Optical properties of condensed matter and application”, *Chichester: John Wiley & Sons*, 2006.
- [9] Tolanasky, S. (1948) *Multiple Beam Interferometry*. Oxford University Press, London.
- [10] Pliskin, W. A., and Stelvio, J. Z. (1970) *Thin Film Technology*. McGraw Hill New York.
- [11] Singh, Y., “Electrical resistivity measurement: a review”, *Int. J. Mod. Phys.: Conf. Series*, vol. 22, pp. 745-756, 2013.
- [12] Starrs, W. J., Kandasami, G., Jones, S., and Chrisp, R. M., “Electrode configurations for resistivity measurements on concrete”, *ACI Mater. J.*, vol. 106(3), pp. 258-264, 2009.
- [13] G. P. Panta, and D. P. Subed, “Electrical characterization of Aluminum (A) thin films measured by using four-point probe method”
- [14] Van Der Pauw, L. J., “A method of measuring specific resistivity and hall effect of discs of arbitrary shape”, *Philips. Res. Report.*, vol. 13(1), pp. 1-9, 1958.
- [15] Akhtar, M. S., Malik, M. A., Alghamdi, Y. G., Ahmad, K. S., Riaz, S., and Naseem, S., “Chemical bath deposition of Fe-doped ZnS thin films: investigations of their ferromagnetic and half-metallic properties”, *Mater. Sci. Semicond. Process.*, vol. 39, pp. 283-291, 2015.
- [16] http://physlab.org/wp-content/uploads/2016/03/Sproj_alamdar1.pdf.

EXPERIMENTAL DETAILS

CHAPTER 4

EXPERIMENTAL DETAILS

4.1 Introduction

Thin film technology is the basis of developments in solid state electronics. Chemical Bath Deposition (CBD) is one of the most commonly used techniques for the deposition of thin films from aqueous solution. In this work, ZnS and ZnS:Fe thin films are prepared by using a locally fabricated CBD unit. This chapter includes a brief discussion on the CBD system and various steps of preparation of ZnS and ZnS:Fe thin films on glass substrate by CBD technique.

4.2 Chemical bath deposition (CBD)

Chemical Bath Deposition is basically chemical deposition technique in which desired materials are deposited on a glass substrate through nucleation and particle growth. This technique has a number of advantages over conventional thin film deposition methods.

The main advantages of the CBD technique are:

- i. Low cost, low reaction temperature is required.
- ii. Suitable for large scale deposition.
- iii. No sophisticated instrument or high vacuum is required.
- iv. Possible to deposit binary, ternary semiconducting thin films.
- v. The material consumption is low and minimizes the loss.
- vi. The process is shown that facilitates better orientation of the crystallites with improved grain structure.
- vii. The method can be used to dopant a large number of metal chalcogenides.

In addition, this method is free from many inherent problems i.e. increased point defects concentrations, evaporation, decomposition of thin films etc. associated with high-temperature techniques.

4.3 Experimental set-up

CBD was first introduced in 1869. In 1989, CBD was used for solar control coatings [1]. CBD opened a new avenue for solar cell after getting efficiency of 11% reported by Kapur *et. al.* [2]. A schematic diagram of conventional CBD set-up is shown in the Fig. 4.1.

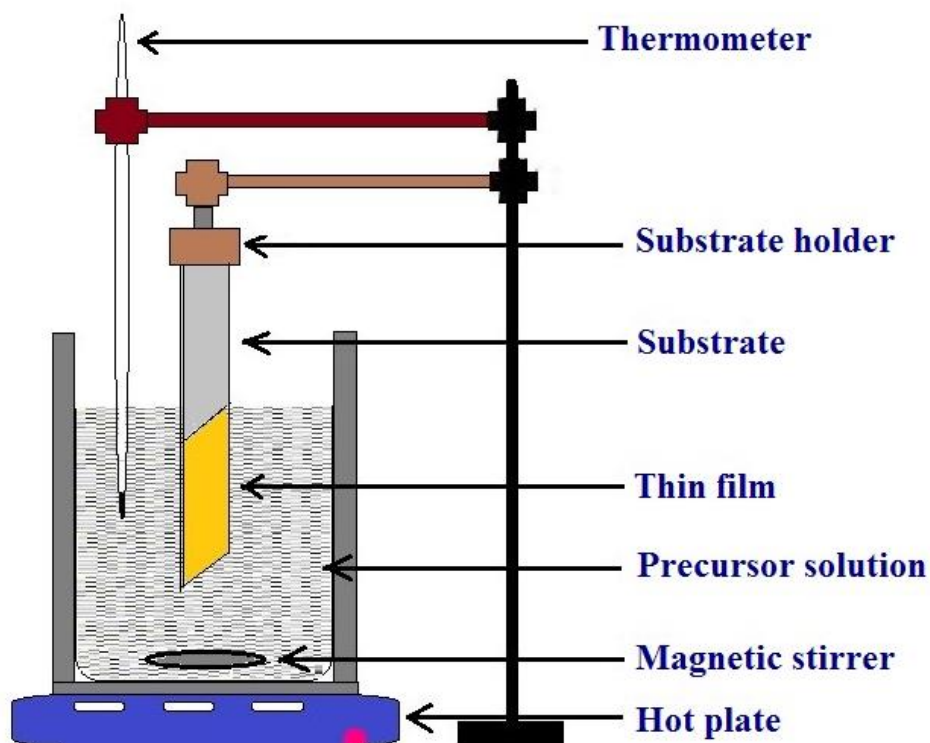


Figure 4.1: Schematic diagram of chemical bath deposition system

Different parts of this set up is as follows:

i. Hotplate and magnetic stirrer

Hotplate usually having two different unit i.e. temperature unite and stirring unit. These two units supply essential temperature and stirring speed for the deposition and make them constant throughout the procedure.

ii. Water bath

A quartz beaker containing water or paraffin oil is used as a bath. The reaction vessel was placed inside it to get homogenous temperature. Water bath was insulated with thermocouple in order to prevent the thermal loss to surroundings.

iii. Chemical bath

The chemical bath consists of a glass vessel containing the reaction mixture of precursor solutions and complexing agents in required amount. In this bath the whole reaction is carried on and deposition occurs on glass substrates emerged into the bath.

iv. Substrate

Microscopic soda lime glass substrates are used to deposit thin films. Substrate is emerged into the precursor solution during the desired deposition time. Thin film is formed at the substrate surface.

v. Substrate holder

Holder has two different points. One point holds the substrate to dipping it into the solution vertically and another point holds the temperature sensor to sensing the temperature of the bath.

In this research work, a modified CBD system is fabricated to maintain the required temperature and minimize the heat loss throughout the process. In this system, no water bath is used rather than the reaction vessel is directly placed inside the heat chamber where the solution is heated homogeneously from all sides. The system is designed in such a way that the heat loss from the chamber to the surroundings is negligible because the reaction vessel is completely inserted into the chamber and is covered by a lid to reduce the loss due to evaporation. On the lid, two rectangular holes are made to insert two substrates and two small circular holes for inserting a thermometer and adding ammonia to control the pH of the solution. The locally fabricated modified CBD system is shown on Fig. 4.2.



Figure 4.2: Locally fabricated chemical bath deposition unit at the Dept. of Physics, BUET

This set-up contains the following parts:

i. Heat chamber

The reaction vessel is put into the chamber showed in Fig. 4.3 (a). The capacity of the vessel is approximately 250 ml. The reaction bath fully inserted completely into the chamber. Consequently, the reaction bath heated from all side and the heat loss to the surroundings is negligible. The bath is covered with a lid which contains four holes as shown in figure 4.3 (b).

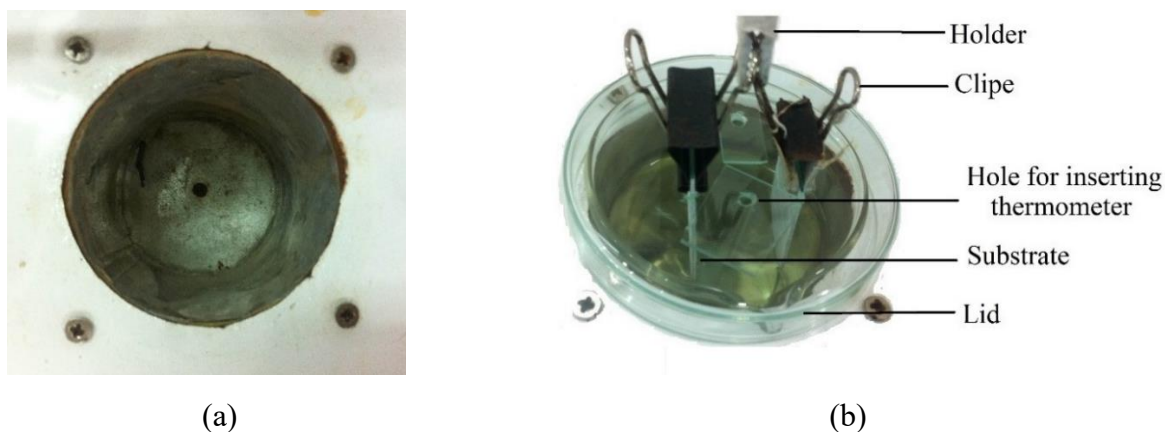


Figure 4.3: (a) Close view of a heat chamber, (b) Lid of the reaction vessel

ii. Button and regulator

There are four ‘ON’ and ‘OFF’ buttons for power, stirrer, heater and temperature. There are also two regulators for controlling the stirrer and heater.

iii. Monitor

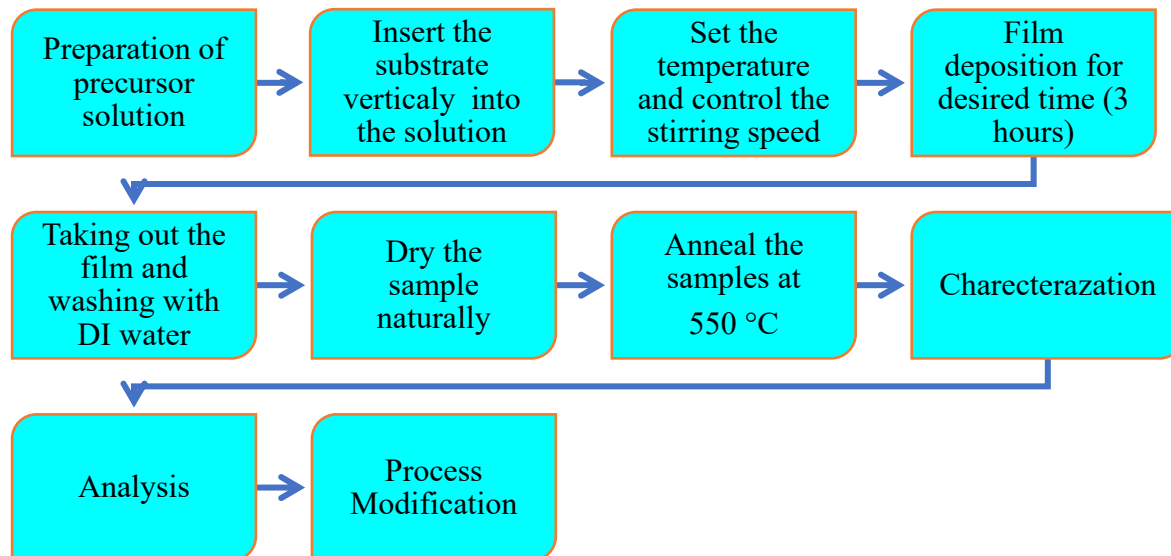
Monitor has two screens and four buttons. One of the screens shows the settled temperature and another screen shows the temperature of the vessel. Among the buttons one is called set which pressed before fixing the temperature of the chamber. Other buttons are used to change the temperature. There is a small green light under the set button which blink to indicate that the temperature is controlled automatically.

4.4 Experimental flow chart

Chemical bath deposition techniques (CBD) used in the present study is one of the useful solution growth method for the preparation of compound semiconductor.

The major steps of synthesis are shown in the flow chart:

Flow chart of thin film deposition



4.5 Sample preparation

In chemical bath deposition technique, sample preparation is a very sensitive work. It has some steps to follow i.e.

- i. Substrate cleaning process
- ii. Chemical measurement
- iii. Solution preparation and
- iv. Deposition

4.5.1 Substrate cleaning

The cleaning of the substrate has a great influence on the properties of the thin films deposited on to them. If the substrate is not cleaned properly, the quality of the film will be compromised i.e. non-uniformity and poor adhesion takes place.

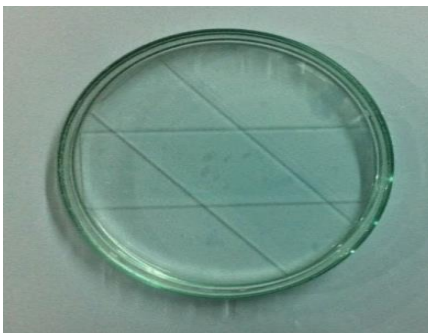


Figure 4.4: Soaked glass substrates into acid solution

Hence, much attention is paid on the cleaning of the substrate. The systematic procedure used for cleaning the substrate is given below:

- The substrates were initially washed with running tap water, wiped with acetone and cotton to remove the visible contaminations like dust particles.
- After cleaning with acid, the substrates are cleaned with ultrasonic cleaner in two steps. At first, the substrates kept into a petri dish and filled it with acetone, then clean it in ultrasonic bath for 10 minutes. After that rinse the substrate in DI water.

Again, keep the substrate into the ultrasonic bath containing DI water for 10 minutes, and dry it naturally.



(a)



(b)

Figure 4.5: (a) Ultrasonic cleaner and (b) its inner view

In the present work, non-conducting amorphous and approximately 100 % transmitting glass slides of $76 \times 22.5 \times 1.2$ mm (Sail Brand, CAT. No. 7101, China) has been used for deposition of pure and ZnS:Fe thin films.

4.5.2 Chemicals used for thin film deposition

All the chemicals used for the preparation of thin films were analytical grade. The materials selected for preparing undoped and Fe doped ZnS thin film are listed below:

Table 4.1: Chemical used for the synthesis of ZnS and ZnS:Fe thin films

Name of the chemicals	Chemical Formula	Molar Mass (gm/mol)	Character
Zinc-acetate	$Zn(CH_3COO)_2 \cdot 2H_2O$	219.50	Source of Zinc
Thiourea	$(NH_2)_2SC$	76.12	Source of Sulfur
Tartaric Acid	$COOH(CHOH)_2COOH$	150.087	Complexing agent
Tri-Sodium Citrate	$Na_3C_6H_5O_7$	258.06	Complexing agent
Ammonia solution	NH_4OH	35.04 (25%)	pH controller
Ferric (III) Chloride	$FeCl_3$	162.21	Dopant

4.5.3 Thin film deposition

After measuring all the required materials, reaction solution is prepared. It has some steps:

Solution preparation and deposition

Solution preparation is the most important part to deposit good quality films. Some steps were maintained to prepared sample solution. Firstly, 0.1M thiourea was mixed within 50 ml de-ionized water in a beaker and stirred for 20 minutes to make homogeneous solution. Then 0.1M zinc acetate mixed with 50 ml de-ionized water in another beaker and stirred for 20 minutes to make zinc acetate solution. 0.2M tartaric acid of 25 ml added to the zinc solution and stirred for 5 minutes. Again 25 ml of 0.2M tri sodium citrate is added to the mixed solution and stirred for 5 minutes. After that the previously prepared 50 ml thiourea solution was added to it and continuously stirred for 20 minutes to get approximately homogeneous clear solution. Finally, 50 ml of 0.1M ferric chloride solution is added to the mixture.

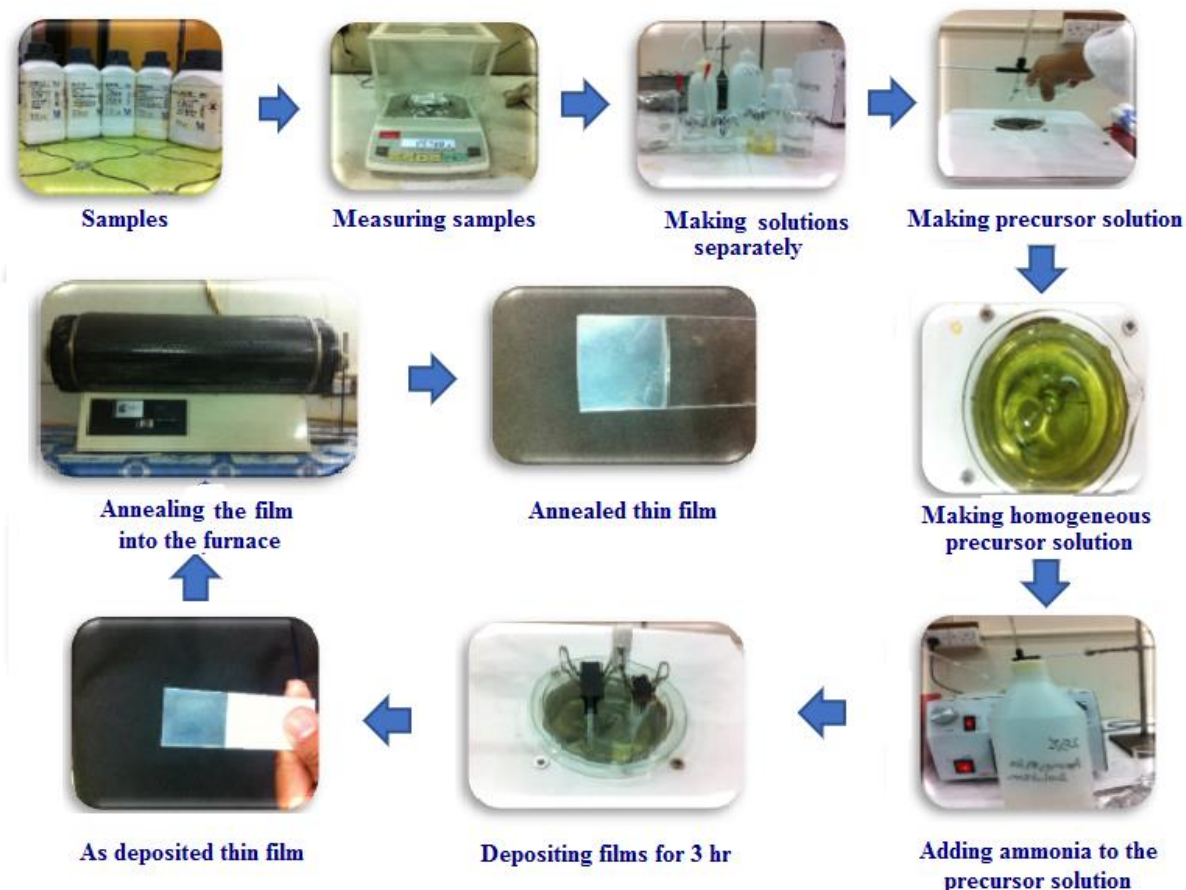


Figure 4.6: Pure and Fe doped ZnS thin film deposition by CBD technique

Then the reaction vessel was placed into the CBD system and continuously stirred. The pH value of the solution was kept 10 using ammonia solution to get alkaline medium which was confirmed using a pH indicator strip. The solution was heated to 85 °C with continuous stirring and

ultrasonically cleaned glass substrates were placed vertically inside the beaker containing the reaction bath. After, deposition for 3 hours, the samples were taken out and dried it naturally.

4.6 Principle of CBD technique

Chemical bath deposition technique is basically a chemical process. It has two steps: nucleation and particle growth. It is based on the formation of solid phase from precursor solution. A solution containing cation and anion sources with one or more chelating agent needs to be prepared. One of the major factors which govern the reaction mechanism and growth rate is the suitable complexing agents. It plays very important role in controlling the concentration of the metal ions. In CBD a wide range of substrates such as ebonite, iron, steel, porcelain and brass can be used apart from glass. The film thickness and chemical composition can be controlled by varying the deposition parameters such as temperature, precursor concentration, complexing agent, deposition duration and the pH of the solution. With appropriate control of the deposition parameters, definite composition of thin film can be obtained. The search for a suitable non-toxic complexing agent is also very essential to ensure environmental safety. The different stages of CBD are as follows:

- i. During the nucleation period, an initial mono layer of the metal chalcogenide is formed on the substrate.
- ii. During the growth phase, this monolayer acts as catalytic surface for the metal ions and chalcogenide ions.
- iii. When the film growth reaches a terminal phase, the film ceases to grow.
- iv. An optimum temperature-concentration combination needs to be obtained for getting maximum film thickness in a given duration of deposition.

4.7 Reaction mechanism

The growth of metal chalcogenide thin films mainly takes place via three different mechanisms depending on the concentration of the complexing agents in the reaction bath [3]. Three mechanisms are as follows:

i. Cluster by cluster process

When the reaction bath contains excess Zn^{2+} ions, then ions forms clusters and homogeneous precipitation takes place on the reaction bath. Therefore, deposited film exhibits layer grains, voids and rough surface.

ii. Mixed process

In general, both mechanisms exist simultaneously. Depending on the nucleation process, one mechanism dominates the others.

iii. Ion by ion process

When the reaction bath contains a sufficient amount of the complexing agents, then all the metal (cations) ions are bonded with anions and the deposition process follows a heterogeneous reaction to deposit the film on the substrate and the ions condense on the substrate surface.

The schematic illustration to describe three mechanisms are as follow:

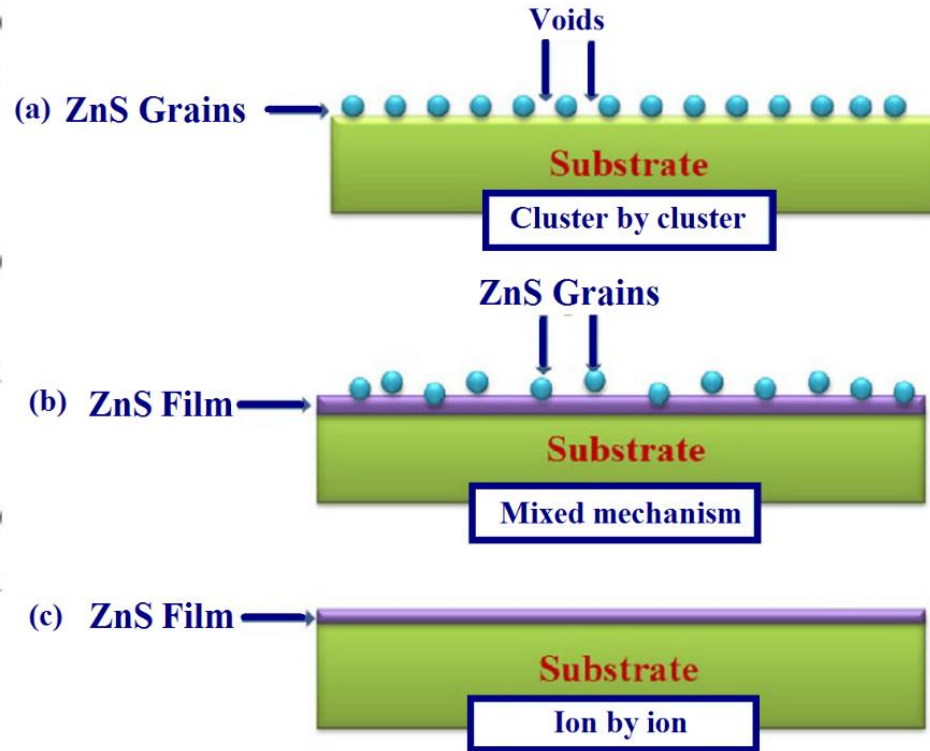
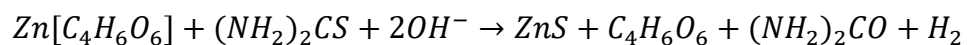
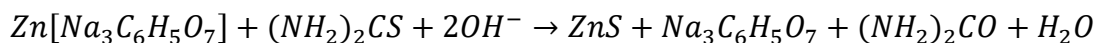
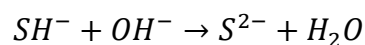
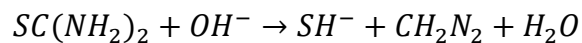
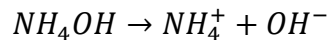
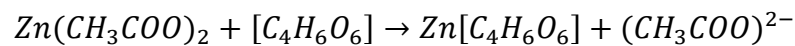
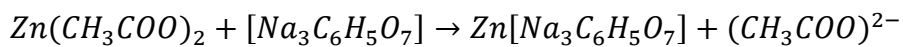


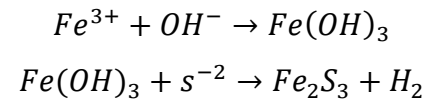
Figure 4.7: Different mechanisms for the thin film deposition using CBD technique [4]

The following equations represents the reactions occurs in the reaction bath [5]:



Mainly the complexing agents form complex ions with Zn^{2+} ions. These complex ions and sulfide ions migrate to the substrate surface and there they react to form ZnS through heterogeneous nucleation.

The possible chemical reactions to form Fe doped ZnS thin films



References

- [1] Nair, P. K., Nari, M. T. S., Femandez, A., and Ocampo, M., “Semiconductor thin films by chemical bath deposition for solar energy related applications”. *J. Phys. D Appl. Phys.* vol. 22, pp. 829, 1989.
- [2] Basal, B. M., and Kapur, V. K., “Semiconductor thin films by chemical bath deposition for solar energy related applications in Solar Energy Materials and Solar Cell”, *IEEE Trans. Electron. Dev.*, vol. 37, pp. 418, 1990.
- [3] Agawane, G. L., Shin, S. W., Moholkar, A. V., Gurav, K. V., Yun, J. H., Lee, J. Y., and Kim, J. H., “Effects of various parameters on structural and optical properties of CBD-grown ZnS thin films: a review”, *J. Alloys and Compounds*, vol. 535, pp. 53-61, 2012.
- [4] Sinha, T., Lihare, D., and Khare, A., “Effects of various parameters on structural and optical properties of CBD-grown ZnS thin films: a review”, *J. Electronic Materials*, 2017.
- [5] Long, F., Wang, W., Cui, Z., Fan, L., Zou, Z., and Jai, T., “An improved method for chemical bath deposition of ZnS thin films”, *Chem. Phys. Letts.*, vol. 462, pp. 84-87, 2008.
- [6] Cheng, j., Fan, D. B., Wang, H., Liu, B. W., Zhang, Y. C., and Yan, H., “Chemical bath deposition of crystallite ZnS thin films” *Semicond. Sci. Technol.*, vol. 18, pp. 676-679, 2003.

RESULTS AND DISCUSSION

CHAPTER 5

RESULTS AND DISCUSSION

Synthesized pure and iron (Fe) doped zinc sulfide (ZnS) thin films have been structurally, optically, electrically and magnetically characterized through various experiments. The results obtained from different experimental measurements are discussed in this chapter.

5.1 Surface Morphology

The surface morphology of pure and Fe doped ZnS (ZnS:Fe) thin films were studied by scanning electron microscope. The FESEM images are shown in Fig. 5.1 taken at 50k magnification. The FESEM micrograph reveal that the scanned areas are nicely covered with uniform spherical nanostructured thin film layer of films on the substrate surfaces for both pure ZnS and ZnS:Fe samples. In case of pure ZnS thin film, Fig. 5.1 (a), it is noticed that agglomeration of nano crystallites leads to the formation of spherical homogeneous grains, having an average particle size of ~ 25 nm onto the substrate surface. Although spherical grains are distributed uniformly, porosity is noticed throughout the scanned area. In the synthesis of ZnS thin films, two competitive growth processes are observed: homogeneous process and heterogeneous process. In homogeneous process ZnS precipitates in the bottom of the reaction bath. On the other hand, ZnS thin films deposited on the substrate in the heterogeneous process. To suppress the homogeneous growth, various deposition parameters would be controlled.

Various properties of thin films can also be tuned using dopant. Fig. 5.1 (b)-(e) shows SEM images for different wt. % of Fe dopant. The growth in all the cases is quite similar with pure ZnS up to 9 wt. % ZnS:Fe thin films due to the continuous nucleation and growth. For 5 wt. % of Fe doping, more compact thin layer of films with less porosity is observed and grain size is decreased but some cracks are noticed in various places. All films were annealed at high temperature of 550°C which may create cracks in the films. The lowest average grain size is 21 nm for 5 wt. % Fe doped ZnS thin film and increases gradually for (7-10) wt. % of ZnS:Fe thin films.

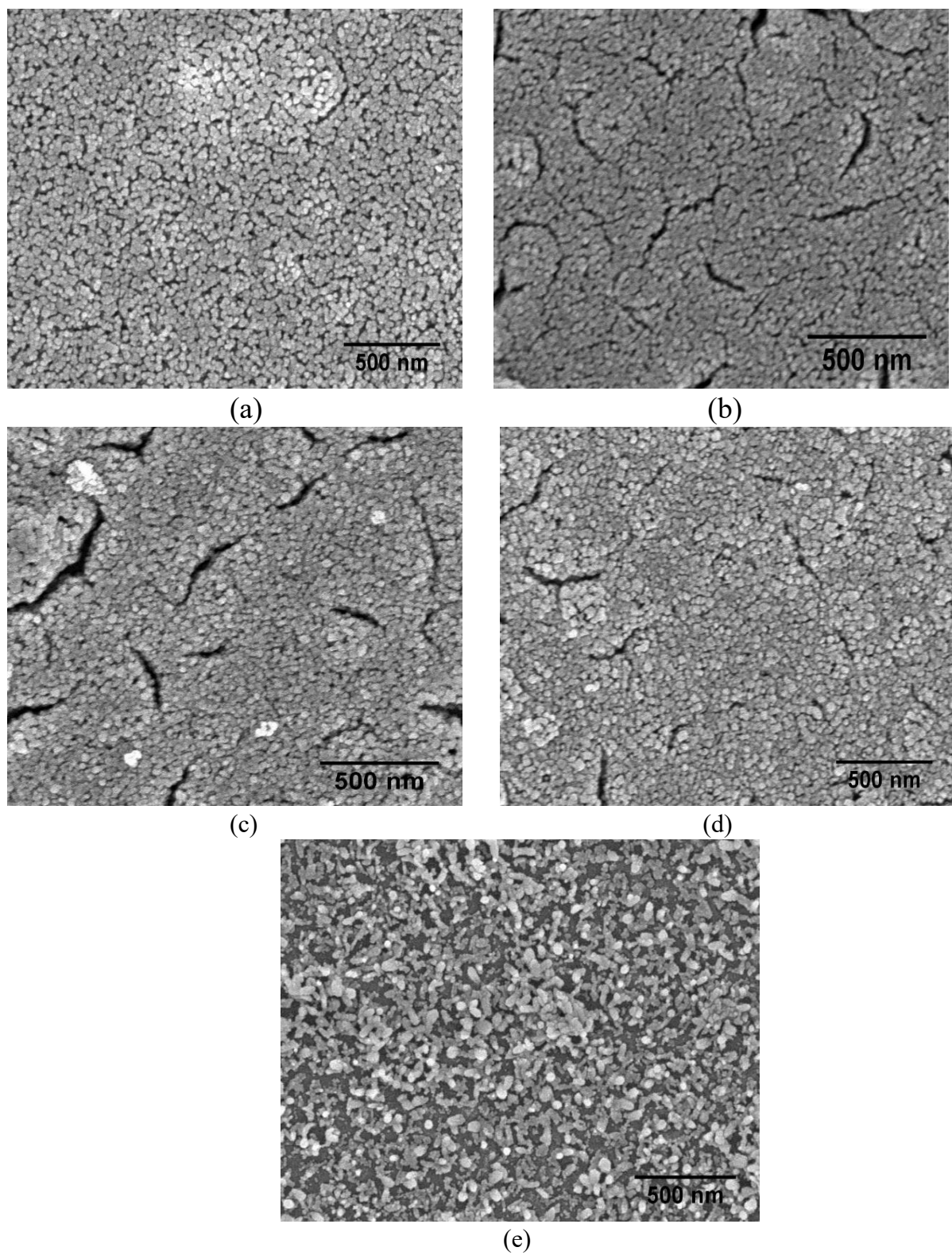


Figure 5.1: FESEM images of (a) Pure ZnS and ZnS:Fe thin films doped with (b) 5 wt.%, (c) 7 wt.%, (d) 9 wt.% and (e) 10 wt.% Fe annealed at 550 °C (50K magnification).

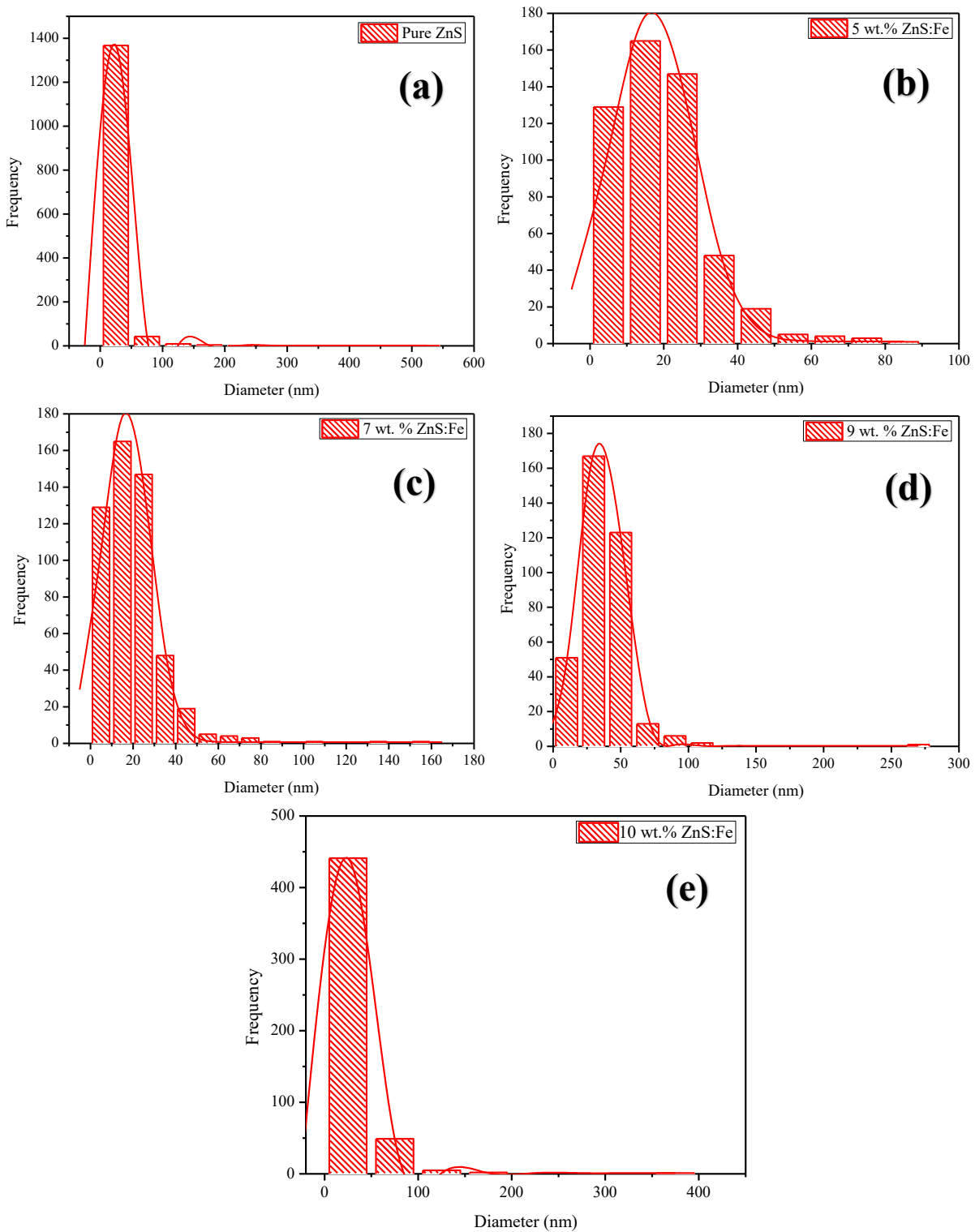


Figure 5.2: Histograms of (a) Pure ZnS and ZnS:Fe thin films doped with (b) 5 wt.%, (c) 7 wt.%, (d) 9 wt.% and (e) 10 wt.% Fe annealed at 550 °C (50K magnification)

In case of 9 wt. % Fe doped ZnS thin film, uniform compact morphology is observed and cracks are less prominent. In case of 10 wt. % of ZnS:Fe the crystallinity is decreased and grains are distributed randomly throughout the substrate.

Zn and Fe have different ionic radius that might causes the strain field or stress that disturb the grain growth. Also, the dopant act to pin the grain boundaries and therefore limit grain boundary mobility. On the other hand, dopant increases nucleation center. This is the reason why higher percentage of ZnS:Fe shows another layer above the mono layer.[1]

Fig. 5.2 showed the histograms for the FESEM images pure and ZnS:Fe thin films at 50 K magnification. The particles size is calculated from the histograms by using “ImageJ” software. The following equation is used:

$$\text{average crystal size} = X_c \pm \sigma$$

where X_c = average particle size from the Gaussian fit of the histogram and standard deviation $\sigma = W_c/2$, W_c found from Gaussian fit of the histogram. The results are listed in the Table 5.1 below:

Table 5.1: Variation of average particle sizes for pure ZnS and ZnS:Fe thin films

Composition	Average particle size (nm)
Pure ZnS	25±4
5 wt. % ZnS:Fe	21±8
7 wt. % ZnS:Fe	28±7
9 wt. % ZnS:Fe	27±3
10 wt. % ZnS:Fe	31±5

5.2 Elemental Analysis

The elemental analysis of pure and Fe doped ZnS thin films are performed by energy dispersive X-ray spectroscopy (EDX). The EDX spectra of pure and Fe doped ZnS thin films are shown in Fig. 5.3 and the quantitative analysis of the elements are presented in the Table 2. From Fig. 5.3(a) two peaks corresponding to Zn and S are observed in the spectra of ZnS thin films. Inferiority of sulfur is noticed for all the samples. This may be happened due to the fact that sulfur has a great aptitude towards oxygen. Therefore, it might compose SO₂ and then evaporated. Very small peak for Fe impurity in the EDX spectra [Fig. 5.3 (b)-(d)] is noticed.

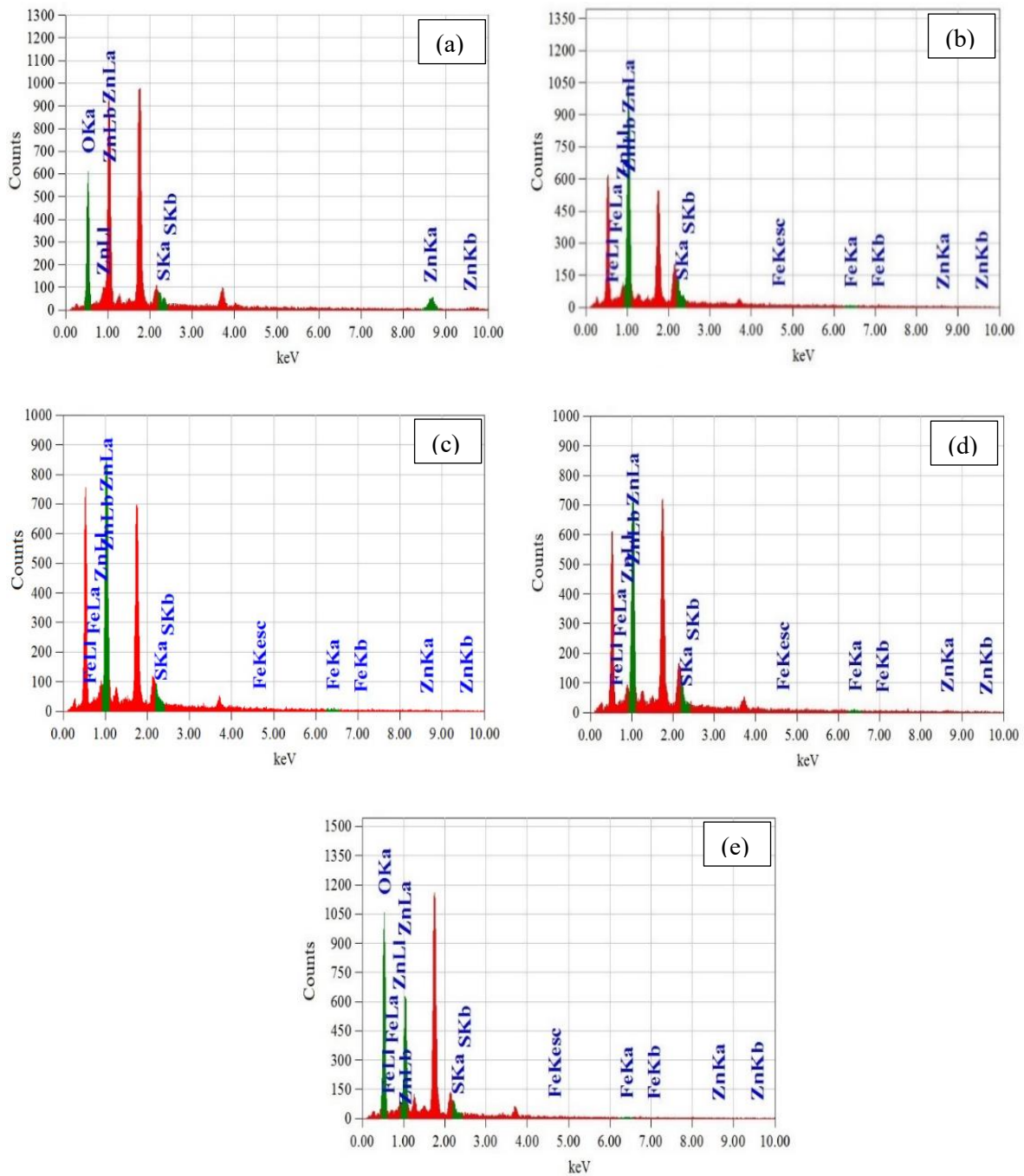


Figure 5.3: EDS spectra of (a) Pure ZnS and ZnS:Fe thin films doped with (b) 5 wt.%, (c) 7 wt.%, (d) 9 wt.% and (e) 10 wt.% Fe annealed at 550°C

High intensity Si and O peak observed (red peaks in Fig. 5.3 corresponds to Si and O). From the quantitative analysis high amount of O is noticed which may be come from glass substrate. Because, at high operating voltage, the electron beam penetrates the film and reaches the glass surface. This happens may be due to the fact that Fe and Zn has tendency to form their oxides. Moreover, the samples are annealed in non-inert atmosphere. So, the crystallinity increases along

with the oxidation. Thus, acute peak of O is observed and it's also lowering the amount of Zn, S and Fe as well.

Table 5.2: The EDX analysis of pure ZnS and ZnS:Fe thin films

Sample	Elements wt. %		
	Zn	S	Fe
Pure ZnS	96.308	3.692
5 wt. % ZnS:Fe	66.12	30.2	3.68
7 wt. % ZnS:Fe	62.41	30.06	7.53
9 wt. % ZnS:Fe	71.46	20.3	8.42
10 wt. % ZnS:Fe	75.515	19.175	5.309

5.3 Structural Analysis

The structural properties of pure and Fe doped ZnS thin films are investigated from X-ray diffraction pattern. The XRD pattern of pure and Fe doped ZnS thin films with different Fe doping percentages are shown in Fig. 5.4. The reflections 27.29° , 31.57° , 34.35° and 36.04° corresponding to the planes (111), (100), (002) and (101) found in the XRD patterns.

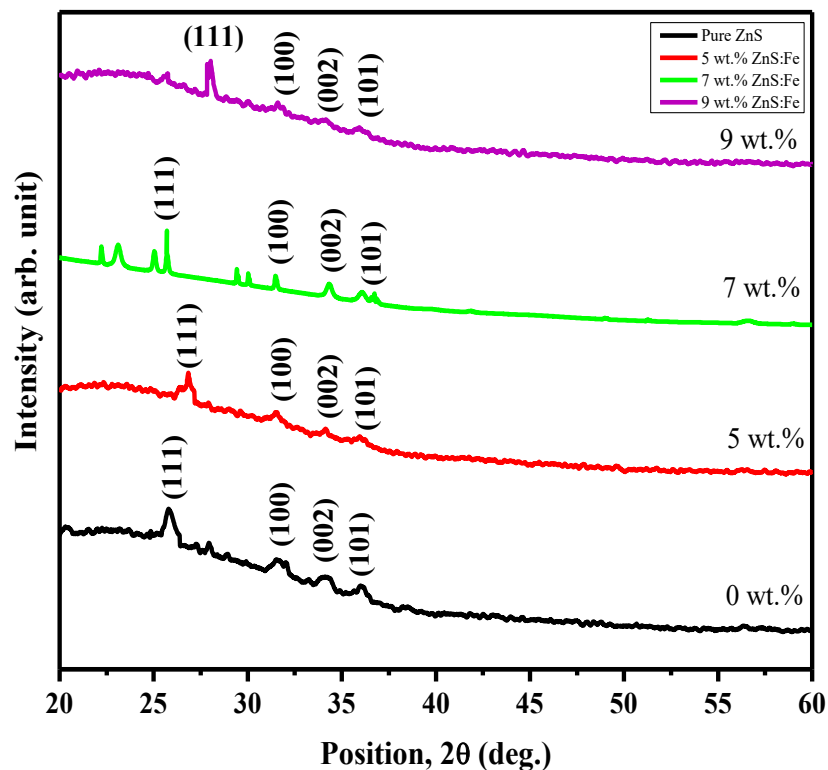


Figure 5.4: X-ray diffraction patterns of Pure ZnS and ZnS:Fe thin films (annealed at 550°C) XRD pattern of CBD deposited ZnS and ZnS:Fe thin films show polycrystalline mixed phases of cubic zinc blend type of crystal structure with preferential orientation along (111) plane. It is

noticed that (111) is well defined plane but (100), (002) and (101) planes are less intense. These planes are may be attributing the presence of ZnO or Zn(OH)₂ mixed phases. **Sanjay et al.** shows the mixed phases of the cubic phase of zinc sulfide and hexagonal zinc oxide which is very close to our XRD results [2]. For 7 wt. % Fe doped ZnS thin films some other peaks are observed at 25.05°, 29.43° and 29.9° which corresponds to the (100), (002) and (222) planes respectively and indicates that the wurtzite phase of ZnS is present [16]. The (111) peak can be considered as the preferential orientation. There is no extra peak observed for Fe impurity, that indicates Fe has substituted Zn from their lattice sites without changing its cubic structure. The ionic radius of Fe²⁺ (0.77Å) is close to that of ionic radius of Zn²⁺ (0.74Å), and therefore it is easy to penetrate Fe²⁺ into ZnS lattice or to substitute the Zn²⁺. The shift of diffraction peak corresponding to (111) plane is an evident of the effect of Fe incorporation in ZnS [3, 4]. The structural parameters like crystallite size (D), lattice parameter (a), dislocation density (δ) micro-strain (ε) and micro-stress (σ) are calculated for (111) plane using the equation (3.3), (3.4), (3.5), (3.6), and (3.7) respectively and is shown in the Table 5.3.

Table 5.3: Structural parameters of pure and Fe doped ZnS thin films

Composi-tion	Thickness (nm)	Position, 2θ (deg.)	(hkl)	Crystallite Size, (D) nm	Lattice Constant, (a) Å	Dislocation Density, (δ×10 ⁻³) Line/nm ²	Micro Strain, (ε×10 ⁻³)	Micro Stress, (σ×10 ⁻²) GPa
Pure ZnS	230	27.2964	(111)	29	5.654	1.14	1.17	4.4
5 wt. % ZnS:Fe	160	26.4114	(111)	31	5.28	1.04	1.19	4.2
7 wt. % ZnS:Fe	166	25.6989	(111)	35	5.294	0.7	0.9	3.6
9 wt. % ZnS:Fe	187	27.7362	(111)	28	5.317	1.2	1.22	1.4

From the Table 5.3 it is noticed that the average crystallite sizes varied from 28 to 35nm for pure ZnS and ZnS:Fe thin films. The maximum value of average crystallite size is 35 nm for 7 wt. % ZnS:Fe and minimum value of average crystallite size is about 28 nm for 9 wt. % ZnS:Fe. Lattice constant is decreased with the increase in Fe doping in ZnS. The dislocation density denotes the presence of defects in the deposited films. The dislocation density for pure ZnS and ZnS:Fe is very small and quite similar for all the films. So, the dislocation density indicates less defects on the films.

Micro-strain of any crystal causes the XRD peak broadening, lowering crystal size and indicates crystal defects. Besides, micro-stress is a physical quantity that express the internal force that the

neighboring particles of any continuous material exert on each other. A small amount of stress is observed from table 5.3 due to the slight difference in ionic radius of Fe^{2+} (0.77Å) and Zn^{2+} (0.74Å).

5.4 Optical analysis

5.4.1 Transmittance

Optical transmittance (T %) of pure ZnS and ZnS:Fe thin films are showed in Fig. 5.5. The transmittance of the thin film is strongly related to the thickness and surface condition observed in the film [5]. It is observed that the sharp transition of transmittance curve occur in the visible wavelength region for ZnS:Fe [6]. Optical transition spectra of pure ZnS and ZnS:Fe thin films in Fig. 5.5 showed that the films are transparent between the wavelength 400 nm to 1100 nm. Transmittance (T %) of pure ZnS thin film prepared at 3 hours deposition duration is observed to be the lowest. While the ZnS thin film deposited without any dopant are thicker, grain sizes are larger, which results in more scattering and lower transmittance without a sharp absorption edge.

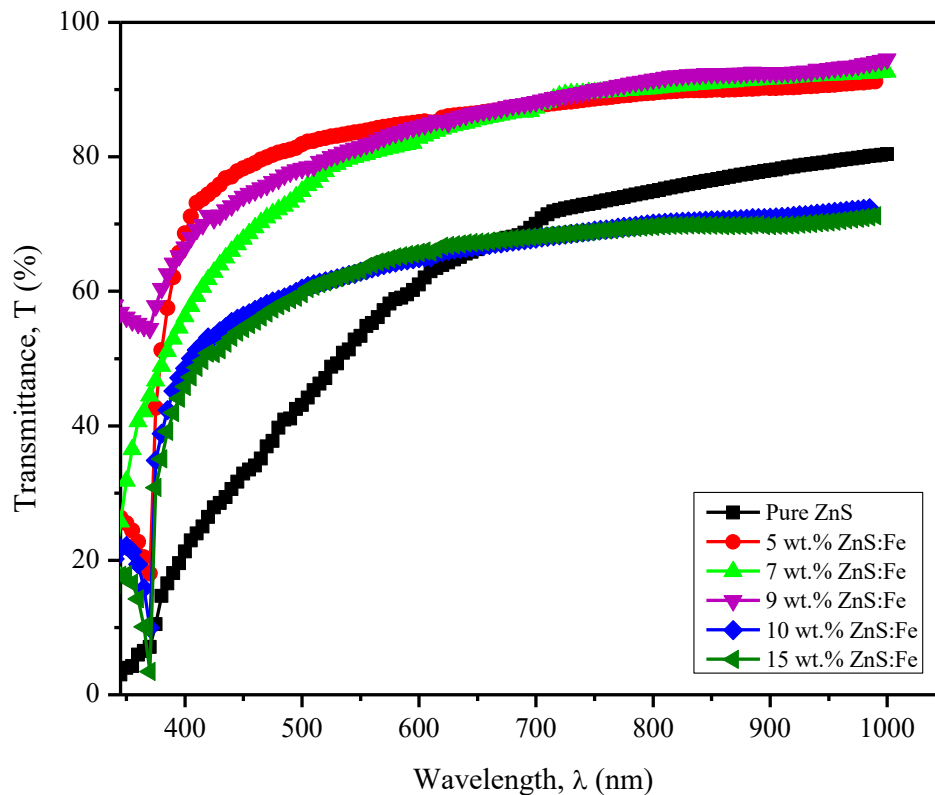


Figure 5.5: Variation of transmittance (T%) with wavelength for pure ZnS and ZnS:Fe thin films

The optical transmittance spectra of the films with different wt. % of Fe dopant showed higher transmittance compare to pure ZnS. 5 wt. % and 9 wt. % of ZnS:Fe thin films showed about 90 % transmittance in the visible region, the highest transmittance compared with other wt. % of dopant.

This may be attributed to better crystallinity, suitable grain size, smooth surface and good homogeneity of the thin film [7]. This higher value of T % is attributed to the decrease in free carrier absorption due to the elevated carrier mobility of the film [5]. T value drops for the ZnS:Fe thin films synthesized with 10 wt. % and 15 wt. % Fe dopant. It may be due to less uniformity, increase of surface roughness, larger grain size etc.

Increased Fe doping percentage causes an increase in the number of atoms on the thin film. Therefore, more photon absorption states are available. The free carrier absorption of photons also contributes to the reduction of optical transmittance. The increased scattering of photons by crystal defects created by doping. That may be the reason to decrease the transmittance at higher doping concentration.

5.4.2 Absorbance

The absorbance spectra of pure and Fe-doped ZnS thin films are shown in Fig. 5.6. From the spectra, it is observed that absorbance starts at a wavelength of ~350 nm.

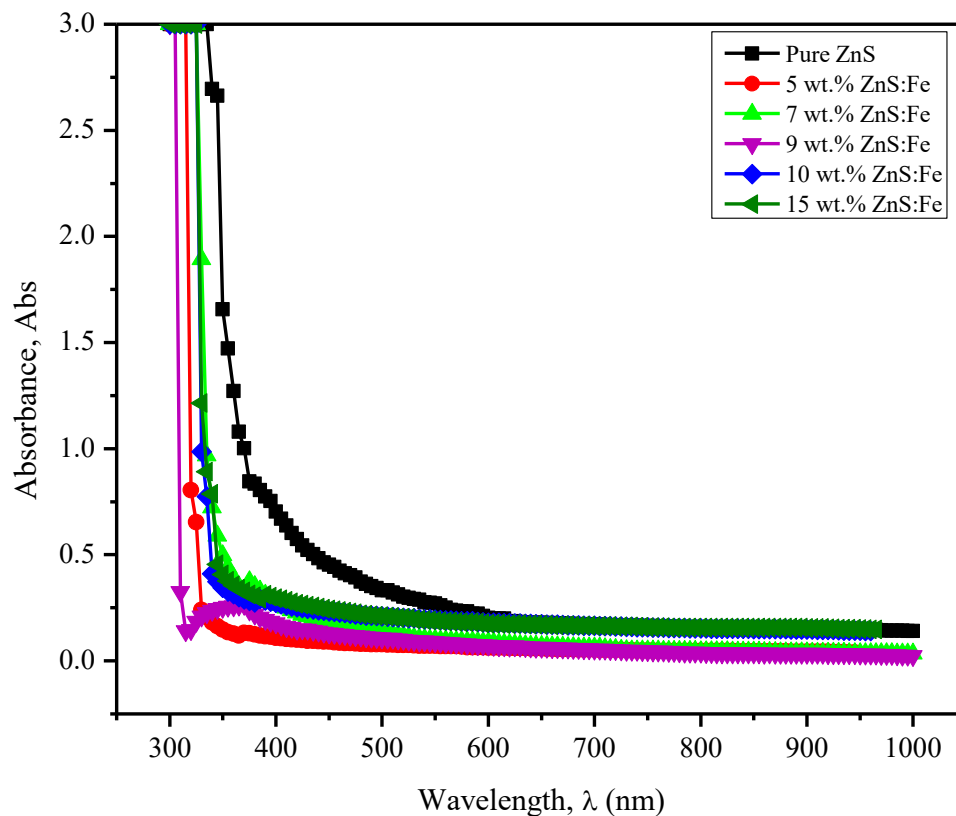


Figure 5.6: Variation of absorbance with wavelength for pure ZnS and ZnS:Fe thin films

The films have low absorbance in the visible and near infrared region, which reveals a good crystallinity and low defect density near the band edge [8]. From XRD analysis, a small value of dislocation density indicates fewer defects, which is consistent with the optical property. It is also

observed that absorbance is decreases for both pure and Fe doped ZnS thin films with the increase in wavelength. This decrease in absorption indicates the presence of optical band gap in the materials [9].

5.4.3 Absorption Coefficient

The absorption coefficient (α) of pure and Fe doped ZnS thin films are calculated using the equation (3.15) and plotted against photon energy ($h\nu$) in the Fig. 5.7. From the spectra lower absorption coefficient is observed in the visible region due to the higher transmittance of thin films in this region. The highest absorption coefficient is noticed for pure ZnS and lowest absorption coefficient is noticed for 5 wt. % ZnS:Fe thin film. Higher absorption coefficient is observed for higher carrier concentration in thin film [10].

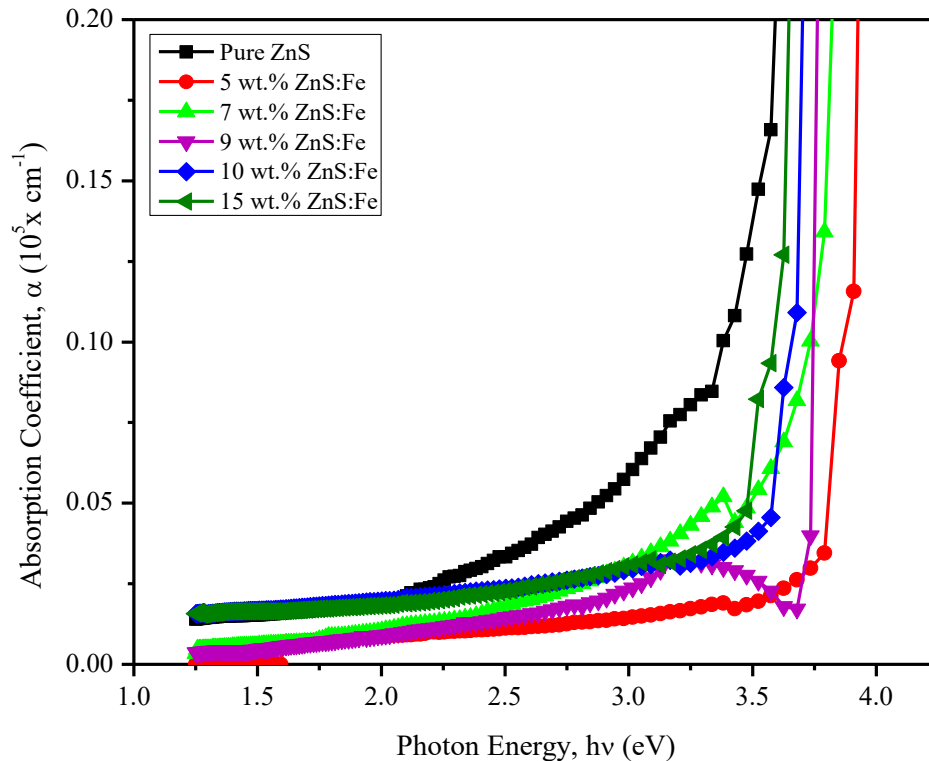


Figure 5.7: Variation of absorption coefficient with photon energy for pure ZnS and ZnS:Fe thin films

5.4.4 Optical Band Gap

The optical band gap of pure and Fe doped ZnS thin films are calculated from the **Tauc** relation represented in the equation (3.16). Fig. 5.8 shows the plot of $(\alpha h\nu)^2$ vs. $h\nu$ for pure and Fe doped ZnS thin films. The direct band gap energy of the films is determined from the intercept of the straight-line portion of the $(\alpha h\nu)^2$ versus $h\nu$ curve to the zero-absorption coefficient using a linear extrapolation technique. The energy gap in a semiconductor is responsible for the fundamental optical absorption edge [11,12].

The band gap value of pure and Fe doped ZnS thin films is found between 3.50 eV to 3.77 eV. The result obtained is similar with the result of **Kumar et al.** [4]. From the curve it is noticed that for 5 wt. % ZnS:Fe thin film bandgap energy is increased. Increase of bandgap energy is attributed to the Burstein-Moss (B-M) effect [13]. B-M effect state that in a heavily doped semiconductor the donor electrons inhabit energy level at the bottom of the conduction band. Pauli principle avoid energy states from being doubly employed and optical transitions are vertical.

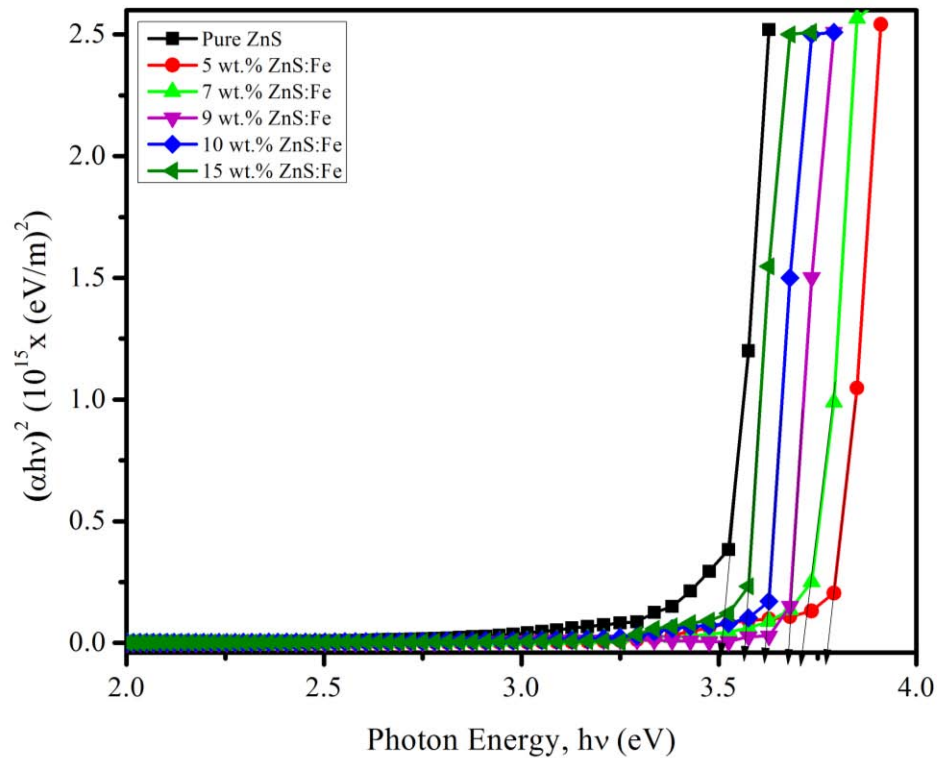


Figure 5.8: Variation of direct bandgap energy with photon energy for pure ZnS and ZnS:Fe thin films

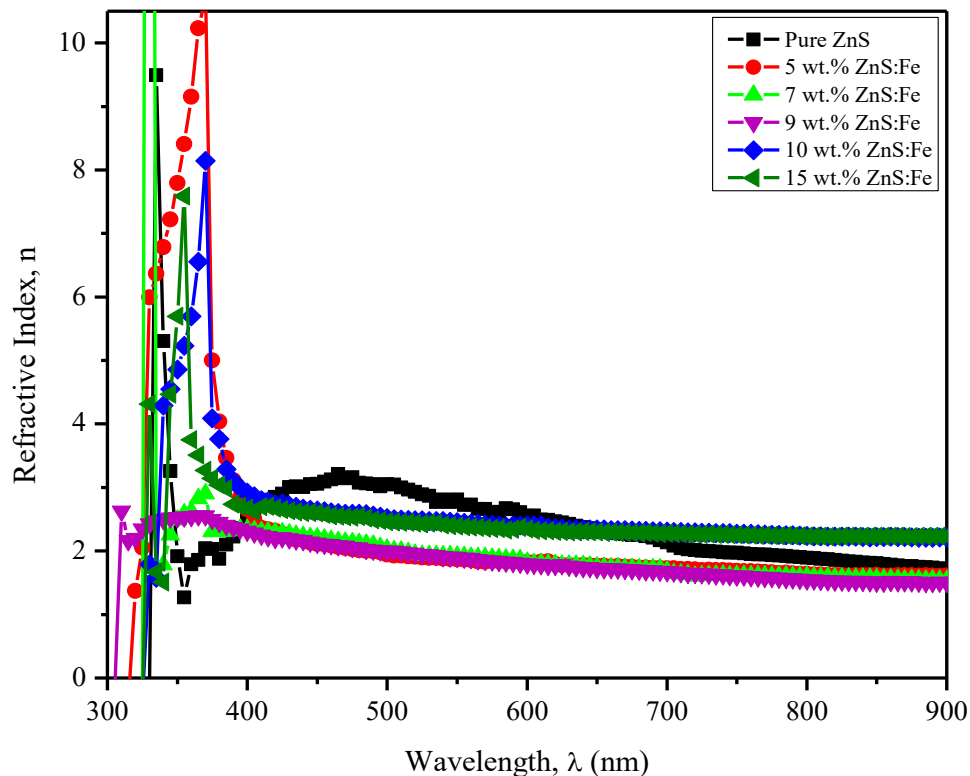
Thus, the valence electron needs an additional energy to be excited to the higher energy level in the conduction band to preserve linear momentum, as a result energy band is shifted. Further doping causes decrease in energy band, as shown in the Table 5.4. It happens may be due to the decrease in crystallite size and lattice parameter, which were confirmed through the XRD analysis. The minimum energy that must be given to valence electrons to become a conduction electron is the energy gap. So, the valence electrons get more bound by decreasing the interatomic distance, the more energy required to make them free in the conduction band. As a rule of thumb, the energy gap is inversely proportional to the inter atomic distance. According to the empirical relation between energy gap and lattice constant in cubic semiconductors by Richard Dalven is, the band gap energy is inversely proportional to the square of lattice constant [14].

Table 5.4: Band gap energy and refractive index of ZnS and ZnS:Fe thin films

Composition of the film	Band gap energy, E_g (eV)	Refractive index, n (at wavelength 500 nm)
Pure ZnS	3.50	3.05
5 wt. % ZnS:Fe	3.77	1.95
7 wt. % ZnS:Fe	3.71	2.03
9 wt. % ZnS:Fe	3.68	2.00
10 wt. % ZnS:Fe	3.62	2.52
15 wt. % ZnS:Fe	3.56	2.46

5.4.5 Refractive Index

The refractive index (n) of pure and Fe doped ZnS thin films is calculated through the equation (3.17) and plotted against wavelength presented in Fig. 5.9. It is observed that reflective index has higher value at UV region. In visible region n is increased for pure ZnS thin film and decreases for ZnS:Fe thin films. At higher wavelength region n is quite linear for all the films. As speed of light is inversely proportional to n , the higher value of n of a material indicates that light speed decreases when it passes through the material. The higher value of refractive index also causes for higher carrier concentration of the sample [10]. Lower reflective index happens due to successive internal reflections or due to the stuck photon inside the grain boundaries.

**Figure 5.9:** Variation of refractive index with wavelength for pure ZnS and ZnS:Fe thin films

5.4.6 Extinction Coefficient

Extinction coefficient (k) measures the attenuation of transmitted light through scattering and absorption while passing through a medium. k and absorption coefficient related by the equation (3.25). From the Fig. 5.10, it is noticed that the k has higher value in UV region for all the thin films. The sharp transition to lower k is occur at visible region. At higher wavelength region the extinction coefficient curve is linear. This change in extinction coefficient may happen due to the variation of absorbance.

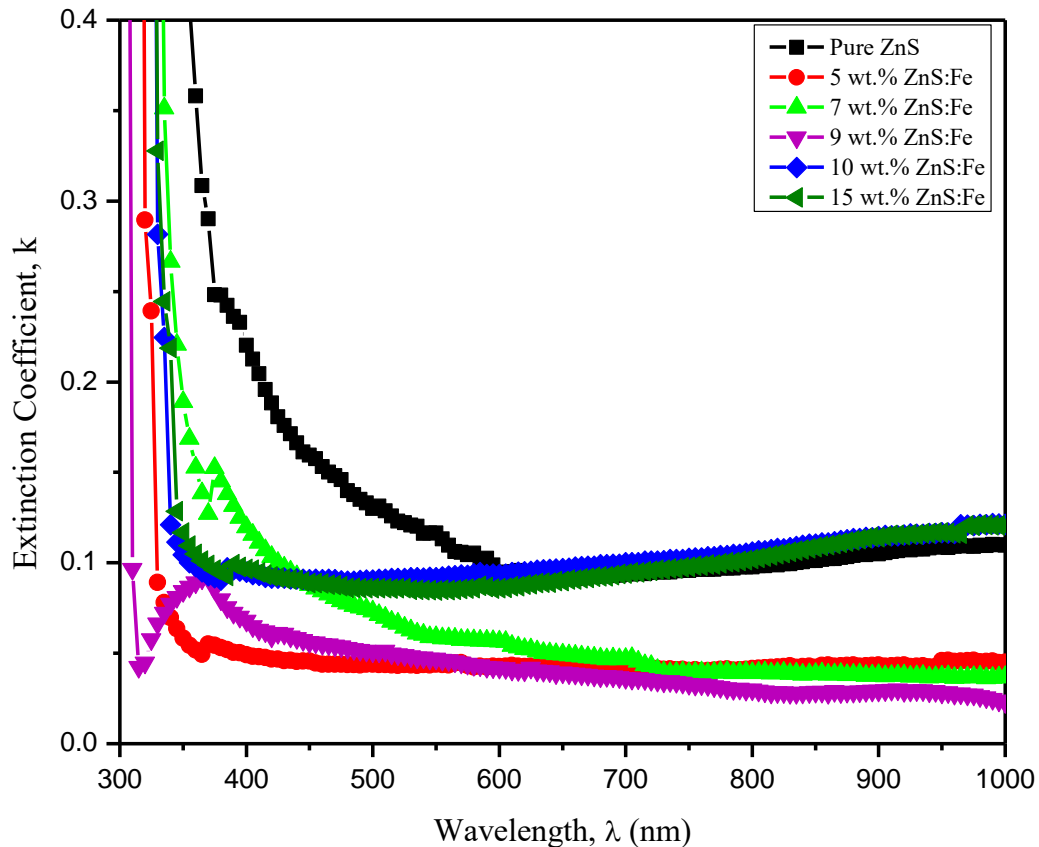


Figure 5.10: Variation of extinction coefficient with wavelength for pure ZnS and ZnS:Fe thin films

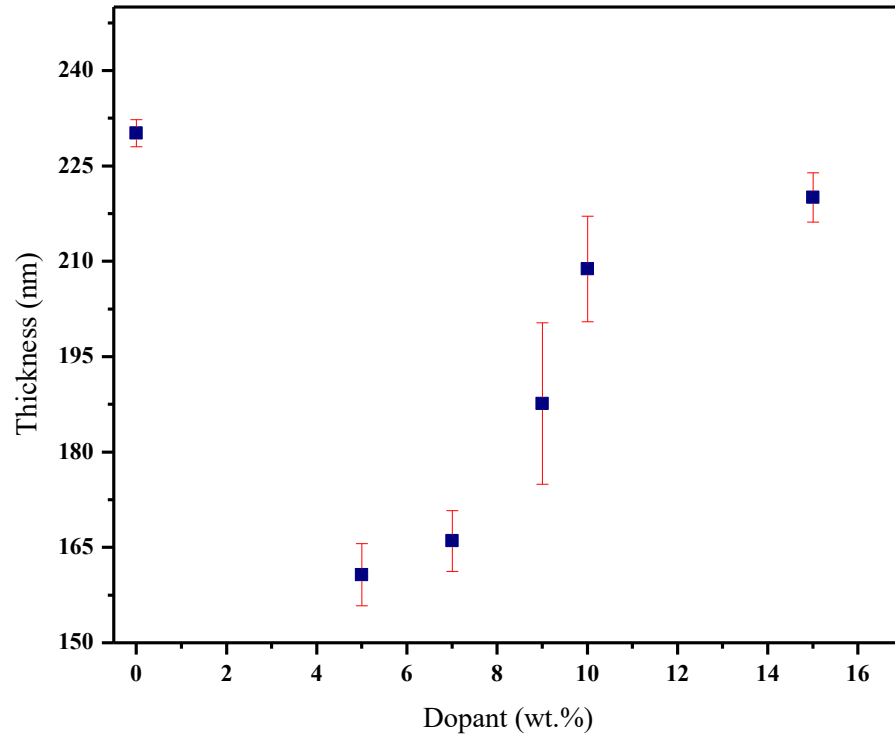
Higher k values may be corresponding to strong electronic absorption between the valance band and conduction band and a qualitative indication of roughness of the thin films [15].

5.5 Thickness Measurement

The variation of thickness as a function of doping percentage of pure and Fe doped ZnS thin films shown in the Fig. 5.11. Thickness of the films calculated using the equation (3.30) and showed in Table 5.5.

Table 5.5: Thickness of ZnS and ZnS:Fe thin films

Composition of the Film	Thickness (nm) ± 20
Pure ZnS	230
5 wt. % ZnS:Fe	160
7 wt. % ZnS:Fe	166
9 wt. % ZnS:Fe	187
10 wt. % ZnS:Fe	208
15 wt. % ZnS:Fe	220

**Figure 5.11:** Variation of thickness with different Fe doping percentage

It is noticed that pure ZnS thin film has maximum thickness. With the increase of Fe doping percentage thickness decreases. It happens may be due to the distraction between similar charges. In pure ZnS thin film present as Zn^{2+} ion and S^{2-} ion, so they attract each other. When Fe is doped on ZnS there are Zn^{2+} , S^{2-} and Fe^{+3} ions are present, so that same charges repulse each other and inter molecular distance increases. This increase in inter molecular distance causes the decrease in thickness of the thin films. [16]

5.6 Electrical property

5.6.1 I-V Characteristics

I-V characteristics curve of pure and Fe doped ZnS thin films is shown in Fig. 5.12. From the curve it is noticed that current is increased with the increase of voltage. The data for I-V measurement are taken for the voltages in the range of 0-20 Volt and the corresponding current (I) and voltage drops are measured. The nature of the curve is linear and the conduction process is ohmic [16]. It

is also observed that I is increased with the increase Fe doping percentage. It happens due to the fact that we measure the surface current of our thin films using four-point probe technique. ZnS is a semiconductor and after doping the surface has a lot of free Fe^{2+} charges as well. As a result, the semiconducting property enhanced [17].

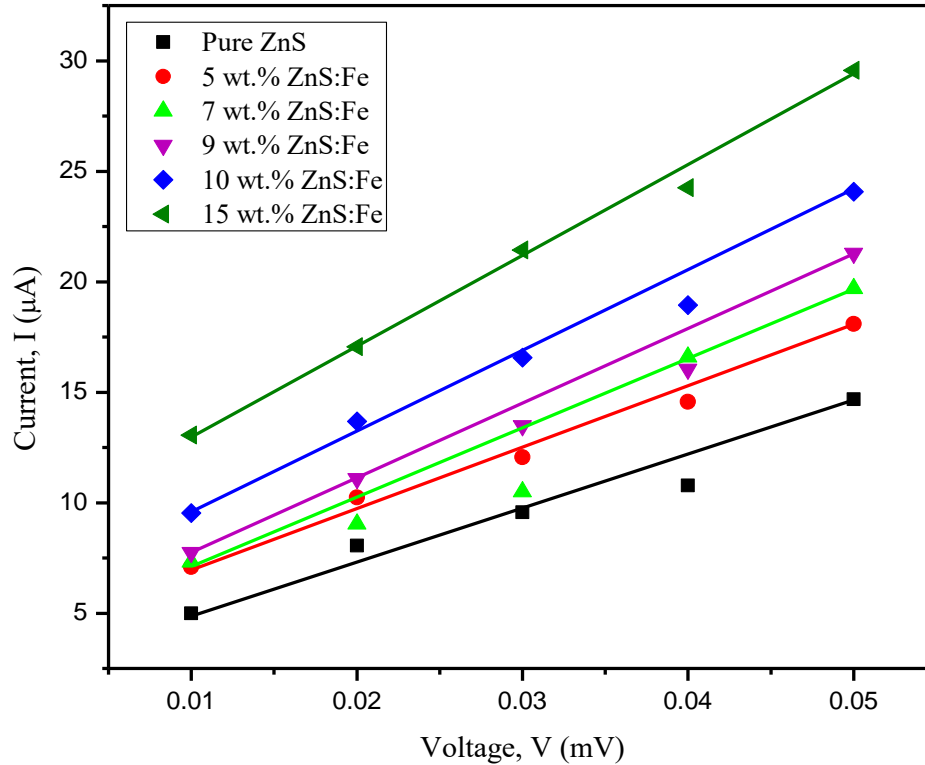


Figure 5.12: I-V characteristic curve of pure and Fe doped ZnS thin films

5.6.2 Resistivity and Conductivity

The distinction of average resistivity of pure and Fe doped ZnS thin films with different Fe doping percentages shown in Fig. 5.13. The average resistivity is calculated through the equation (3.37) for room temperature. From the curve it is noticed that the resistivity decreases with the increase in doping percentage. The average conductivity of pure and Fe doped ZnS thin films is calculated through the equation (3.26). Fig. 5.14 showed the distinction of average conductivity with different Fe doping percentages. The conductivity of the films increases with the increase in Fe doping percentages.

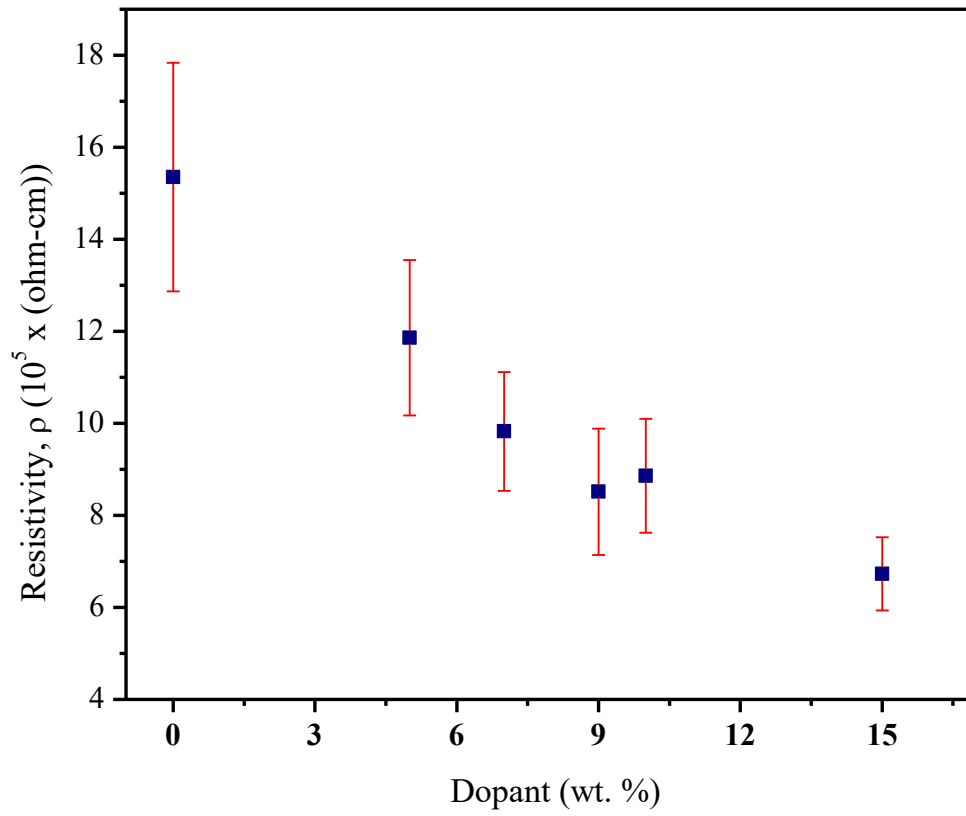


Figure 5.13: Variation of resistivity with Fe doping wt. %

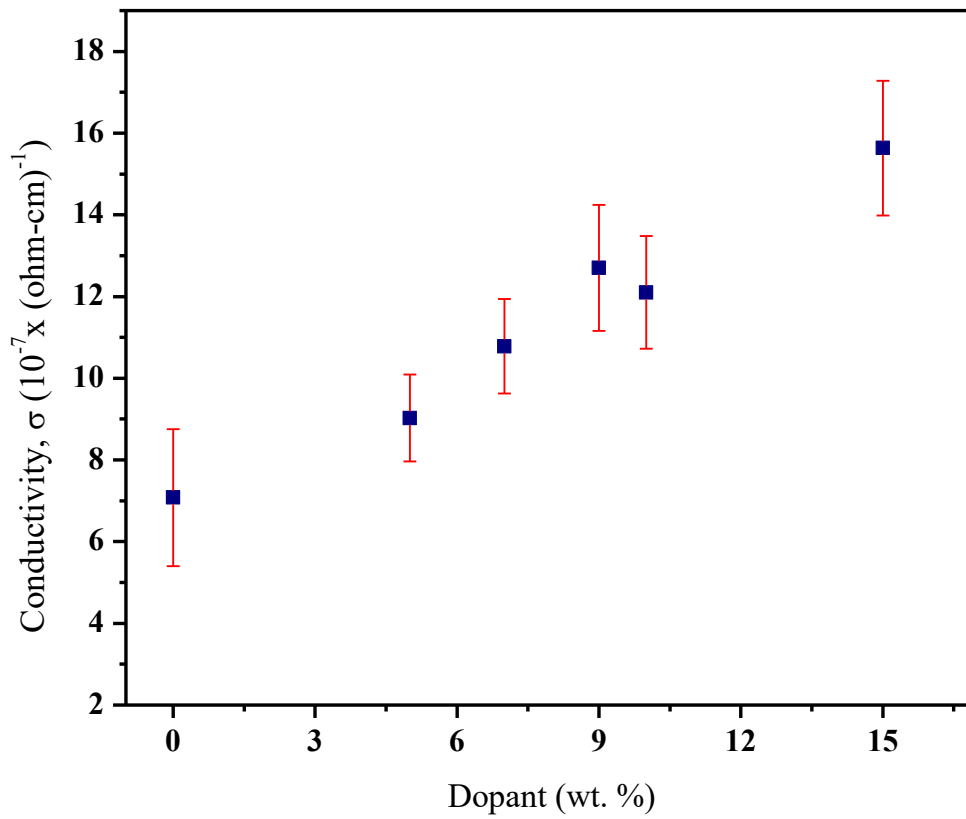


Figure 5.14: Variation of conductivity with Fe doping wt. %

It happens due to the presence of free charge carriers in the film. These free charge carriers rapidly increase with the increase in Fe percentage because every Fe atom provides one free electron to the ZnS thin films. This converted ZnS into a n-type semiconductor.

Table 5.6: Electrical measurements of ZnS and ZnS:Fe thin films

Composition of the film	Resistivity, ρ ($10^5 \times (\text{ohm-cm})$)	Conductivity, σ ($10^{-6} \times (\text{ohm-cm})^{-1}$)
Pure ZnS	(15.3±2.5)	(1.5 ±0.16)
5 wt. % ZnS:Fe	(11.8±1.6)	(1.21±0.13)
7 wt. % ZnS:Fe	(9.8±1.2)	(1.27±0.15)
9 wt. % ZnS:Fe	(8.5±1.3)	(1.078±0.11)
10 wt. % ZnS:Fe	(8.8±1.2)	(0.902±0.11)
15 wt. % ZnS:Fe	(6.7±0.7)	(0.708±0.16)

5.7 Magnetic Property

The magnetic properties of Fe doped ZnS thin films is carried out using vibrating sample magnetometer at room temperature. The M-H curve of different Fe doping percentages are shown in the Fig. 5.16.

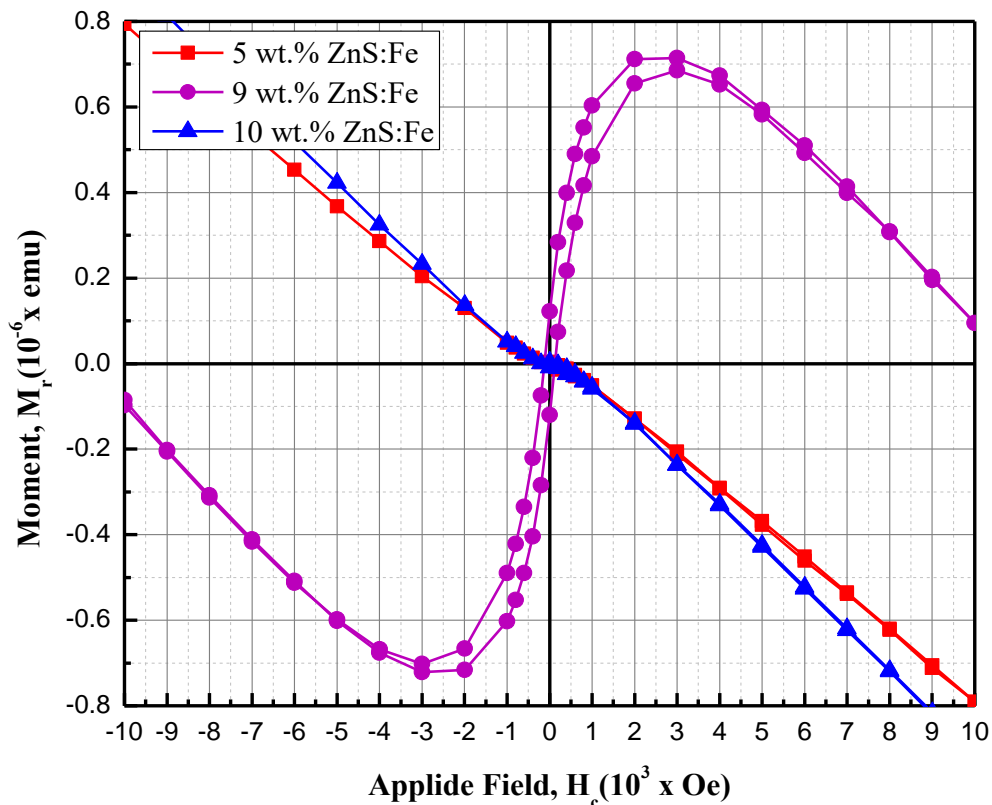


Figure 5.16: M-H curve for different Fe doping wt. %

From the hysteresis loop it is noticed that 5 wt. % and 10 wt. % ZnS:Fe thin films exhibit diamagnetic behavior but 9 wt. % ZnS:Fe thin film exhibits weak ferromagnetic behavior. ZnS is not a magnetic material but after doping Fe, it behaves like a weak ferromagnet [2,3]. For 9 wt. % Fe doping, the magnetization could not attain the saturation and at higher value of magnetic field the M-H curve looks linear with negative slope. This behavior of M-H curve at higher magnetization indicates the presence of diamagnetic contribution to the magnetization. The retentivity and coercivity are found to be 2.37×10^{-4} emu and 269 Oe. The hysteresis loop is a clear evidence of ferromagnetic soft character and huge diamagnetic property for higher magnetic field [18]. From the M-H loop spin injection into the semiconducting lattice is clear and describes spin polarized nanoclusters. It's may be happening due to the Fe defects which leads to pinning and makes the movement of the domains difficult [16].

References

- [1] Pavlovic, V. P., Nikolic, M. V., Pavlovic, V. B., Labus, N., Zivkovic., L., and Stojanovic, B. D., “Correlation Between Densification Rate and Microstructure Evolution of Mechanically Activated BaTiO₃”, *Ferroelectrics*, vol. 319, pp. 75–85, 2005.
- [2] Sanjay, K. A., Sunil, N. G., Sudhir, S. A., Bharat, B. K., Jin, O. B., Uttamrao, P. M., Sonali, D. N., Dinesh, P. A., and Suresh, W. G., “A novel template free, one pot large scale synthesis of cubic zinc sulfide nanotriangles and its functionality as an efficient photocatalyst for hydrogen production and dye degradation”, *J. Mater. Chem.*, vol. 21, pp. 19241-19248, 2011.
- [3] Akhtar, M. S., Malik, M. A., Alghamdi, Y. G., Ahmad, K. S., Riaz, S., and Naseem, S., “Chemical bath deposition of Fe-doped ZnS thin films: investigations of their ferromagnetic and half-metallic properties”, *Mater. Sci. Semicond. Process.*, vol. 39, pp. 283–291, 2015.
- [4] Kumar, S. and Verma, N. K., “Structural, optical and magnetic investigations on Fe doped ZnS nanoparticles”, *J. Mater. Sci.- Mater. Electron.*, vol. 26, pp. 2754–2759, 2015.
- [5] Prathap, P., Revathi, N., Subbaiah, Y. P. V., Reddy, K. T. R., and Miles, R. W., “Preparation and characterization of transparent conducting ZnS:Al films”, *Solid State Sci.*, vol. 11, pp. 224-232, 2009.
- [6] Babu P., Reddy V. R., Kondaiah S., Reddy, K. T. R. and Chinho, P., “Chemical bath deposition of Mn-doped ZnS thin films using greener complexing agents: effect of Mn-doping on the optical properties”, *Optic*, vol. 130, pp. 608-618, 2017.
- [7] Kim, Y. S., Yun, S. J., “Tin monosulfide thin films grown by atomic layer deposition using tin 2,4 pentandionate and hydrogen sulfide”, *Appl. Surf. Sci.*, vol. 229, pp. 105-111, 2004.
- [8] Hagiwara, Y., Nakada, T., and Kuniko, A., “Improved J(sc) in CIGS thin film solar cell using transparent conducting ZnO:B window layer”, *Sol. En. Mat. Sol. Cells.*, vol. 67(1-4), pp. 267-271, 2001.
- [9] Rejit, S. G., and Krishnan, C., “Optical characterization of Zn-doped nanoparticles”, *Scientia. Acta. Xaveriana*, vol. 4(1), pp. 91-98, 2013.
- [10] Liu, Q., Guobing, M., and Jianping, A., “Chemical bath-deposited ZnS thin films: preparation and characterization”, *Appl. Surf. Sci.*, vol. 254, pp. 5711-5714, 2008.

- [11] Torkaman, N. M., Ganjkhanalou, Y., Kazemzad, M., Babaghi, H. H., and Keyanpur-Red, M., “Crystallographic parameters and electro-optical constants in ITO thin films”, *Mater. Characterization*, vol. 61(3), pp. 362-370, 2010.
- [12] Park, Y., and Rhee, S., “Low temperature silicon dioxide deposited by remote plasma enhanced chemical vapor deposition: growth mechanism”, *J. Surf. Coat. Tech.*, vol. 179, pp. 229-236, 2004.
- [13] Burstein, E., “Anomalous optical absorption limit in InSb”, *Phys. Rev.*, vol. 93, pp. 632-633, 1954.
- [14] Richard, D., “Empirical relation between energy gap and lattice constant in cubic semiconductors”, *Phys. Rev. B*, vol. 8(12), 1973.
- [15] Bahsi, Z. B., and Oral, A. Y., “Effects of Mn and Cu doping on the microstructures and optical properties of sol-gel derived ZnO thin films”, *Optical Materials*, vol. 29, pp. 672–678, 2007.
- [16] Wael, Z. T., Farghali, A. A., Ahmed, M., Imam, N. G., and El-Dek, S. I., “Outstanding features of Cu-doped ZnS nanoclusters”, *Nanotechnology*, vol. 29, No. 21, 2018.
- [17] Matthew, E., Padmaja, G., Afef, J., Jemilia, P., Stephen E., and Michael C., “Dielectric surface currents and dielectric constant measurements of pure and multi-walled carbon nanotubes (MWCNT) doped polyvinyl alcohol thin films”, *Am. J. Mater. Sci.*, vol. 5(3A), pp. 1-7, 2015.
- [18] Saritas, S., Sakar, B. C., Kundakci, M., Yildirim, M., “The effect of Mg dopants on magnetic and structural properties of iron oxide and zinc ferrite thin films”, *Results Phys.*, vol. 9, pp. 416-423, 2018.

SUMMARY AND CONCLUSION

CHAPTER 6

SUMMARY AND CONCLUSION

6.1 Summary

In the present work, ZnS and ZnS:Fe thin films have been synthesized by chemical bath deposition technique using non-toxic complexing agents. The outcome of this investigation is summarized as follows:

- ❑ The X-ray diffraction (XRD) study revealed that pure ZnS and ZnS:Fe thin films showed polycrystalline cubic Zinc-blend type of crystal structure with preferential orientation along (111) plane. No peak corresponding to Fe impurity were found which indicates that Fe has substituted Zn from their lattice sites without changing the cubic structure. Average crystallite size varied between 28 to 35 nm.
- ❑ FESEM images showed that spherical nanostructured grains were uniformly distributed throughout the substrate surface for all the samples. More compact, homogeneous thin layer of films were observed for ZnS:Fe thin films.
- ❑ The EDX analysis confirmed the presence of Zn, S and Fe. Iron was successfully incorporated into the ZnS thin films.
- ❑ It is observed that the transmittance of the pure ZnS thin films was about 60% and increased up to 90 % for 5 to 9 wt. % Fe doped ZnS thin films in the visible region. The sharp absorption edge for ZnS:Fe thin films indicated good homogeneity in the shape and size of the grains and lower defects density near the band edge. Optical bandgap of pure ZnS and ZnS:Fe thin films were varied from 3.50 eV to 3.77 eV.
- ❑ Electrical resistivity of pure ZnS and ZnS:Fe thin films were varied from $8.5 \times 10^2 \Omega\text{-cm}$ to $3.7 \times 10^2 \Omega\text{-cm}$ at room temperature. The resistivity decreases for ZnS:Fe thin films.
- ❑ The hysteresis loop corresponding to 9 wt. % ZnS:Fe exhibited room temperature ferromagnetism.

6.2 Conclusion

Pure ZnS and ZnS:Fe thin films were synthesized successfully by locally fabricated modified chemical bath deposition setup. The influence of iron dopant on tuning optical bandgap was noteworthy. The increase in direct optical bandgap in a controlled manner may improve the performance of ZnS thin films as a non-toxic buffer layer in thin film solar cells. Also, the impurity induced room temperature ferromagnetism could enhance the photocatalytic activity for dye degradation and waste water remediation.

6.3 Scopes for future works

Till to date very few research works have been done on Fe doped ZnS thin films using non-toxic precursor solution as well as complexing agents, it is a very good opportunity to do more study on this composition. In order to improve the quality of the film of this material and for their characterization, more works are required. For example:

- ❑ Characterization of Fe doped ZnS thin films synthesizing by changing other deposition parameters.
- ❑ Investigation of the surface roughness and surface morphology by Atomic force microscopy and Transmission electron microscopy.
- ❑ Measurement of Hall Effect to observe the type of conductivity and transport phenomena.
- ❑ Study the annealing temperature effect in order to achieve better crystallinity.
- ❑ Investigation of photocatalytic activity specially for the sample that possesses room temperature ferromagnetism.